Wayne State University Dissertations

January 2022

Characterizing The Post-Translational Modifications Of The Pro-Oncogenic Type Ii Transmembrane Serine Protease Tmprss13

Carly Elizabeth Martin
Wayne State University

Follow this and additional works at: https://digitalcommons.wayne.edu/oa_dissertations

Part of the Biochemistry Commons, Biology Commons, and the Oncology Commons

Recommended Citation

CHARACTERIZING THE POST-TRANSLATIONAL MODIFICATIONS OF THE PRO-ONCOGENIC TYPE II TRANSMEMBRANE SERINE PROTEASE TMPRSS13

by

CARLY ELIZABETH MARTIN

DISSERTATION

Submitted to the Graduate School

of Wayne State University,

Detroit, Michigan

in partial fulfillment of the requirements

for the degree of

DOCTOR OF PHILOSOPHY

2022

MAJOR: CANCER BIOLOGY

Approved By:

_____
Advisor   Date

_____

_____

_____

_____

_____

DEDICATION

I would like to dedicate this dissertation to my husband Jake: thank you for all the years of support you have given me. This was a difficult process and I would not have come this far had it not been for your unwavering encouragement and your calmness to offset my lack thereof. Also, this dissertation is dedicated to my family (Mom, Dad, Amy, Danny, Ella, Helen, Brian and Edwin): thank you for always being a source of comfort. I would also like to dedicate this to my friends, who I can always count on to make me laugh until my stomach hurts. Finally, I would like to dedicate this to my cats, Tim and Jim. I hope I have made you all proud.

Additionally, I would like to acknowledge the List lab members, both past and present: Dr. Andrew Murray, Dr. Fausto Varela, TJ Hyland, Kimmie Sala-Hamrick, Jacob Mackinder, Victoria Foust, Evan Harrison, Michael Flynn, Joey Lundgren, and Hiwot Lessanework. It has been a privilege to work with some of the funniest, kindest, and smartest people that I have ever met. I have made friends for life in this lab.

TABLE OF CONTENTS

LIST OF FIGURES

CHAPTER 1: INTRODUCTION

Sections from this chapter (Chapter 1) were originally published in *Cancer and Metastasis Reviews*. Martin CE and List K. Cell surface-anchored serine proteases in cancer progression and metastasis. *Cancer Metastasis Rev*. 2019;38(3):357-387. doi:10.1007/s10555-019-09811-7. This dissertation will focus on the role of type II transmembrane serine proteases in colorectal and breast cancers, but for a comprehensive overview of serine proteases in additional cancer types, as well as serine protease inhibitors in cancer, please refer to the published review article (1).

1.1 Classes of proteases

Five mammalian classes of proteases have been identified based on their catalytic mechanism: cysteine, metalloproteases, aspartic, threonine, and serine (2,3). Metalloproteases and serine proteases are the largest protease classes, comprising roughly two thirds of the total amount of mammalian proteases. Cysteine proteases make up about a quarter of all mammalian proteases, while aspartic and threonine proteases are smaller classes which comprise the remainder of the proteases (2,3). Broadly, proteases are involved in the hydrolysis of peptide bonds, but the mechanism of catalysis differs between protease classes. For aspartic and metalloproteases, an activated water molecule is used as a nucleophile to attack the substrate peptide bond, while cysteine, serine, and threonine proteases utilize an amino acid residue (cysteine, serine, and threonine, respectively) in the enzyme active site as the nucleophile (2). Protease activity is tightly regulated through transcriptional control, post-translational modifications, zymogen activation, protease inhibitors, and epigenetic changes (2,4). This introduction will focus on the cysteine proteases, metalloproteases, and serine proteases, as they are the largest protease classes.

1.1.1 Cysteine proteases

There are two distinct superfamilies of cysteine proteases: the papain-like superfamily and the superfamily related to interleukin-1β converting enzyme (5). The papain-like proteases are

subdivided into family C1 (cathepsin B and cathepsin L-like) and family C2 (calpain-like) (6). The cysteine protease catalytic triad located in the substrate binding cleft is composed of cysteine-histidine-aspartic acid (6,7). Cysteine proteases catalyze peptide bond hydrolysis as their catalytic cystine thiol group acts as a nucleophile to attack the carbonyl of the peptide substrate (6,7).

The cathepsin and caspase families of cysteine proteases are well-studied and implicated in various biological and pathological processes. There are 11 cysteine cathepsins in humans which are mainly endopeptidases localized in endolysosomal vesicles, although several cathepsins including cathepsin K, B and L function both intra- and extracellularly (8). Many of the cysteine cathepsins have been implicated in oncogenic processes including tumor angiogenesis through the degradation of tissue inhibitors of matrix metalloproteases (TIMPs) and cell invasion through the cleavage of cell adhesion molecules such as E-cadherin (8-11). Caspases are typically associated with apoptotic cell death, but some family members play roles in inflammation and cell cycle regulation (12). Apoptotic caspases are separated into two functional categories: initiator caspases (caspases 8, 9, 10) and effector caspases (caspases 3, 6, 7) (12,13). Apoptosis is a multi-step process in which the initiator caspases undergo autocatalytic cleavage for activation and subsequently proteolytically activate the effector caspases, which cleave downstream molecules leading to cell death (14,15).

1.1.2 Metalloproteases

Metalloproteases are enzymes that depend on zinc ions to hydrolyze peptide bonds (16). These proteases are synthesized as zymogens in which the catalytic substrate cleft is covered by the prodomain by a zinc-thiol bond, which can either be cleaved by autolysis or a separate protease to allow for activation of the metalloprotease (17). After activation, metalloproteases can be inhibited by TIMPs which fold their N-termini to wedge into the metalloprotease active site (16).

The metzincin clan of metalloproteases includes matrix metalloproteases (MMPs), a disintegrin and metalloproteinases (ADAMs), and astacins (16,17). ADAM proteases and MMPs have been well studied in biological and pathological contexts. ADAM17 is one such ADAM

protease that has been shown to be involved in multiple biological processes and pathways including development, inflammation, and tumorigenesis (18). For example, ADAM17 is known to act as a sheddase for tumor necrosis factor (TNF) and to cleave epidermal growth factor receptor (EGFR) ligands, leading to EGFR activation and oncogenesis (18-20). MMPs are well-known proteases involved in the invasion and dissemination of tumor cells, as they degrade extracellular matrix proteins such as collagen and laminins (17,21). For this reason, MMP inhibitors (MMPIs) were tested in clinical trials in the 1990s and early 2000s, but they lacked efficacy and led to severe side effects due to their broad inhibition of MMPs and ADAMs (17,21). This broad inhibition caused abrogation of physiological ECM remodeling as well as inhibition of potentially anti-tumorigenic MMPs (21). Next generation MMPIs have the potential to be more efficacious in clinical trials, as they are more stable and selective. Additionally, more is now known about the potential off-target effects of inhibiting MMPs (22).

1.1.3 Serine proteases

The class of serine proteases contains 175 predicted members in humans of which the vast majority are secreted proteases (23). The name "serine protease" came from the observation that there is a nucleophilic serine residue located in the enzyme active site (24,25). This serine residue is a member of the catalytic triad of serine-histidine-aspartic acid (24,26). Generally, serine proteases catalyze the hydrolysis of peptide bonds by first causing an acylation reaction in which the nucleophilic serine residue attacks the peptide substrate carbonyl, leading to the formation of a tetrahedral intermediate stabilized by aspartic acid. Next, an acylenzyme is formed as the substrate N-terminus of the peptide is expelled, which is assisted by histidine acting as a general acid. A deacylation reaction then occurs when a water molecule attacks the acylenzyme to form a tetrahedral intermediate which then collapses to release the C-terminus of the cleaved peptide (25-27).

A subgroup of serine proteases is directly anchored to plasma membranes. These cell-surface anchored serine proteases are tethered to the plasma membrane either via a carboxy-

terminal transmembrane domain (Type I), an amino-terminal proximal signal anchor that functions as a transmembrane domain (Type II), or a carboxy-terminal hydrophobic region that functions as a signal for membrane attachment via a glycosyl-phosphatidylinositol linkage (GPI-anchored). The Type I transmembrane protease tryptase γ1 (also known as PRSS31, transmembrane tryptase and transmembrane protease γ-1) is expressed in cells of hematopoietic origin and has been studied most extensively in mast cells (28). The catalytic domain of all Type II membrane-anchored serine proteases belongs to the S1 family of serine proteases which includes the prototypic chymotrypsin and trypsin (29). One exception is fibroblast activation protein (FAP or seprase) which is a Type II transmembrane serine protease of the peptidase S9b family, a prolyl oligopeptidase subfamily, with post-proline dipeptidyl peptidase and endopeptidase enzymatic activity (for reviews see (30,31)). Though FAP has been implicated in cancer, we will focus on the S1 membrane anchored serine proteases, and from here on Type II transmembrane serine proteases (TTSPs) will refer to the S1 family members.

The type II transmembrane serine protease (TTSP) family encompasses 17 members in humans. TTSPs share a conserved N-terminal signal anchor that functions as the transmembrane domain, a "stem region" that is composed of a variable number of domains that belong to one of six conserved motifs, and a C-terminal serine protease domain (**Fig. 1A**). The serine protease domain has a histidine, aspartate, and serine triad of residues necessary for catalytic activity. TTSPs are divided into subfamilies based on the composition of the domains in the stem region, the phylogenetic relationship of the serine protease domain, and the chromosomal location of their genes (29,32-40) (**Fig. 1A**). TTSPs are synthesized as zymogens and require specific cleavage in a conserved activation loop resulting in a structural rearrangement leading to the formation of a fully functional protease. Several TTSPs, including matriptase (41), matriptase-2 (42), hepsin (43), TMPRSS2 (44), TMPRSS3 (45), TMPRSS4 (46), and TMPRSS13 (47) are

Figure 1: Membrane anchored serine proteases and protease inhibitors
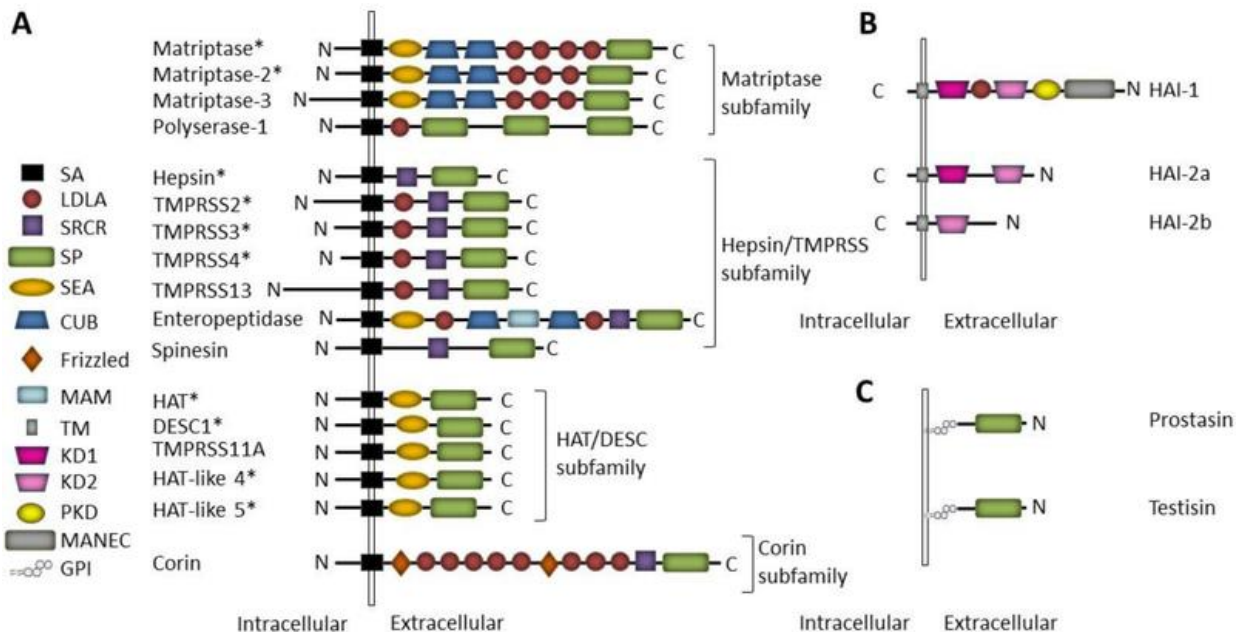
Figure 1: **A)** The type II transmembrane serine protease (TTSP) family members are attached to the membrane via a signal anchor (SA) located close to the N terminus. TTSPs are phylogenetically divided into four subfamilies: 1) matriptase, 2) hepsin/transmembrane protease, serine (TMPRSS), 3) human airway trypsin-like (HAT)/differentially expressed in squamous cell carcinoma gene (DESC), 4) corin. **B)** Hepatocyte growth factor activator inhibitor type 1 (HAI-1) and HAI-2 are type I transmembrane serine protease inhibitors. They have two extracellular Kunitz-type serine proteinase inhibitor domains (KD1 and KD2), a single-pass transmembrane domain near the carboxyl terminus, and a short intracytoplasmic domain. Two major splicing variants (isoforms a and b) of HAI-2 are known where the b isoform lacks KD1. HAI-2a is the predominant form in humans. **C)** Prostasin and testisin are composed of a single protease domain linked to a glycosylphosphatidylinositol (GPI) anchor that is added posttranslationally to the C terminus and attaches the proteases to the outer leaflet of the plasma membrane. Domains: SA=signal anchor, LDLA=low-density lipoprotein receptor class A, SRCR=group A scavenger receptor cysteine-rich, SP=serine protease, SEA= sea urchin sperm protein, enteropeptidase, agrin, CUB=Cls/Clr, urchin embryonic growth factor, bone morphogenetic protein-1, MAM= meprin, A5 antigen, receptor protein phosphatase μ. TM=transmembrane, KD1=Kunitz-type serine proteinase inhibitor domain 1, KD2=Kunitz-type serine proteinase inhibitor domain 2, PKD=polycystic kidney disease (PKD)-like, MANEC=motif at N terminus with eight cysteines, GPI=glycosylphosphatidylinositol anchor.

capable of auto-activation which is suggestive of a basal activity for their respective zymogens.

Indeed, the rat and human matriptase zymogens have been shown to harbor activity *in vitro* (48-

52). Furthermore, knock-in mice expressing only a non-cleavable form of matriptase (zymogen

locked) are viable, unlike matriptase null mice, suggesting that matriptase zymogen is biologically

active and capable of executing developmental and homeostatic functions of the protease (53).

Regulation of TTSP proteolytic activity is attributed to shedding of the protease from the cell surface upon complex formation with membrane associated or secreted serine protease inhibitors (Section 1.2.4 and **Fig. 1B**) or by internalization followed by lysosomal degradation (34).

Prostasin (PRSS8) is a serine protease with trypsin-like substrate specificity that was first isolated from seminal fluid (54). Later, it was reported that prostasin is GPI anchored to the cell surface and is released from the cell upon GPI-anchor cleavage by phospholipase C (**Fig. 1C**) (55). The Kunitz-type inhibitor HAI-1 was also found to form stable inhibitor complexes with prostasin (56-58). Testisin (PRSS21) was first cloned and characterized in human eosinophils (59) and characterized as a new human serine proteinase in the testis (60). It was later demonstrated that testisin is tethered to the cell surface via a GPI-anchor (**Fig. 1C**) (61). Both testisin and prostasin expression are epigenetically regulated by gene methylation (62,63).

1.2 The type II transmembrane serine proteases in development and physiology

1.2.1 Matriptase subfamily: Matriptase and Matriptase-2

Matriptase (Matriptase-1, MT-SP1, ST14, TADG15, SNC19, CAP3) is one of the most studied members of the TTSP family in both normal physiology as well as in diseases, including cancer. Matriptase was first described in 1993 as a new cancer-associated protease with gelatinolytic activity expressed by cultured human breast cancer cells (64). Subsequently, matriptase was cloned from human prostate cancer cells, ovarian cancer cells, and breast cancer cells by three different groups, and a mouse ortholog (epithin) was cloned from thymic cells (39,65-67). Matriptase expression localizes to the epithelial component of a wide variety of organs, as well as in monocytes and macrophages of the immune system (35,68-70). Matriptase regulation and signaling has been studied most extensively in the epidermis, where it has been shown to have pleiotropic effects on differentiation, homeostasis, and pathology. Mice lacking matriptase expression develop full term *in utero*, but are born with dry, wrinkled, and shiny skin, along with defects in vibrissae hair growth (71). The pups only survive up to 48 hours post-birth

(71), with this early post-natal death being attributed to accelerated loss of water through the epidermis, a consequence of a defective epidermal barrier (71). Studies in conditional matriptase knock-out mice revealed that matriptase is required for normal function of several epithelia including colonic epithelium and salivary gland epithelium (72). A mutation in the *ST14* gene encoding matriptase causes the human condition Autosomal Recessive Ichthyosis with Hypotrichosis (ARIH) which is characterized by scaly thickened skin and brittle, curly, and sparse hair (73). A matriptase hypomorphic mouse model phenocopying ARIH syndrome in humans was developed by *ST14* gene trapping causing severely attenuated matriptase expression with approximately 1% matriptase transcript retained in the epidermis of hypomorphic mice compared to control mice (72). These matriptase hypomorphic mice present with scaly dry skin and brittle, sparse hair (72,74). Unlike matriptase null mice, matriptase hypomorphic mice survive the neonatal period, mature to adulthood, and have normal fertility as adults (72). This model, in addition to conditional knock-out models, has enabled long-term studies of the impact of matriptase reduction for tissue homeostasis and cancer progression (see Section 2). Substrates for matriptase have been identified *in vitro* and/or *in vivo* and include the pro-form of the urokinase plasminogen activator (uPA) (41,75-77), platelet derived growth factor D (PGDF-D) (78), macrophage-stimulating protein 1 (MSP-1) (68), protease-activated receptor 2 (PAR-2) (41,79,80), and the pro-form of hepatocyte growth factor (HGF) (75,76,81-83).

Matriptase-2 (TMPRSS6) was identified and cloned in 2001 from fetal liver (84). In normal adult human and mouse tissues, the primary sites of matriptase-2 expression are liver, kidney, and uterus (84-86). Matriptase-2 has been established to be essential in iron homeostasis based on the phenotypes of iron-refractory iron deficiency anemia identified in mouse models as well as in human patients with mutations in *TMPRSS6* (*Tmprss6* in mice), the gene encoding matriptase-2 (86-94). The only known physiological substrate of matriptase-2 is hemojuvelin. It has been reported that matriptase-2 cleaves the extracellular domain of human epidermal growth factor

receptor 4 (HER4), the insulin receptor (INSR), and platelet-derived growth factor receptors (PDGFRs) α and β *in vitro* (95).

1.2.2 Hepsin/TMPRSS subfamily: Hepsin, TMPRSS2, TMPRSS3, TMPRSS4 and TMPRSS13

Hepsin (Transmembrane protease, serine 1, TMPRSS1) was the first serine protease characterized to contain a transmembrane domain, and was named based on its original identification in hepatocytes (96). Hepsin displays a broad range of expression in multiple organs including kidney, liver, stomach, thymus, thyroid, pituitary gland, prostate, and pancreas (97-99). Hepsin was also found to be important for normal hearing. The cochleae of hepsin null mice display a deformed and hypertrophic tectorial membrane, as well as defects of nerve fiber compaction in the spiral ganglia and reduced expression of myelination genes (100). Additionally, hepsin null mice produce significantly less thyroxine, a thyroid hormone, than wild-type (WT) littermates (100). As thyroxine is required for the development of the inner ear, the impaired hearing may be secondary to a defect in thyroid hormone metabolism. Candidate proteolytic substrates for hepsin include the pro-forms of HGF, uPA, and MSP-1, and zymogens of matriptase and prostasin (80,101-105).

TMPRSS2 was first identified in basal cells of the prostate epithelium (106) and later in the epithelial compartment of a number of other tissues, including kidney tubules, airway epithelium, colonic epithelium, bile duct, and ovaries (40). Expression of the *TMPRSS2* gene in the prostate is androgen and androgen receptor-dependent and it is widely accepted that the major implication of TMPRSS2 in cancer results from genetic fusion of the TMPRSS2 promoter with members of the erythroblast transformation specific (ETS) transcription factors (107-110). The physiological function of TMPRSS2 is unclear, as TMPRSS2 null mice do not present with an obvious phenotype (111). Recent studies have demonstrated that TMPRSS2 cleaves and activates viral hemagglutinin (112-114) and that Tmprss2 null mice are resistant to H10 influenza A virus pathogenesis (115). Mammalian TMPRSS2 substrates include PAR-2, matriptase, pro-HGF, laminin β1, and nidogen-1 (116-118).

TMPRSS3 (TADG-12) was originally isolated as a protease that was overexpressed in ovarian cancer (119). In normal tissue, TMPRSS3 is expressed in colon, heart, kidney, liver, lung, pancreas, prostate, stomach, testis, thymus, small intestine, spleen, tonsil, and inner ear (45). Mutations in the human *TMPRSS3* gene were identified as a cause of congenital and childhood onset autosomal recessive deafness (45,120). Mice carrying a protein-truncating nonsense mutation in *Tmprss3* exhibit severe deafness and display degeneration of the organ of Corti (121). Cochlear hair cell degeneration starts at the onset of hearing, postnatal day 12, in the basal turn cochlear and progresses very rapidly toward the apex, reaching completion within 2 days (121). The epithelial sodium channel (ENaC) is activated by TMPRSS3 (45).

TMPRSS4 (CAP2, previously termed TMPRSS3) was cloned as a gene overexpressed in pancreatic cancer (122). TMPRSS4 is expressed in various tissues, including skin, lung, kidney and gastrointestinal tract (123). Experiments in *Xenopus laevis* oocytes demonstrated that TMPRSS4 activates ENaC-mediated sodium transport (123,124), however, studies in TMPRSS4 null mice showed that the protease is not required for ENaC activation *in vivo* (125). Thus, mice deficient in TMPRSS4 challenged with sodium-deficient diet did not develop any impairment in renal sodium handling as evidenced by normal plasma and urinary sodium and potassium electrolytes, as well as normal aldosterone levels. The physiological function of TMPRSS4 is not clear and null mice are viable, fertile, and without any obvious histological abnormalities (125). A role of TMPRSS4 in influenza virus infection mediated through proteolytic cleavage of the viral protein hemagglutinin was proposed (123) and later confirmed using *Tmprss2/Tmprss4* double-knock-out mice that showed a reduced H3N2 Influenza A virus spread and lung pathology, in addition to reduced body weight loss and mortality (126). Neither of the two single protease knock-out models displayed significant protection from H3N2 Influenza A infection (126).

TMPRSS13 (MSPL, mosaic serine protease large-form) was first identified from a human lung cDNA library (127). Further, Southern blot and RT-PCR analysis showed TMPRSS13 expression in human lung, placenta, pancreas, prostate, thymus, spleen, brain, and colon tissues,

as well as peripheral blood lymphocytes (127,128). A mouse model to study TMPRSS13 expression and function in development was generated by insertion of a promoterless β-galactosidase-neomycin fusion gene into the endogenous *Tmprss13* locus, causing a partial deletion of exon 9 and full deletion of exon 10, but allowing detection of gene expression *in situ* by staining with X-gal (129). Strong staining was observed in multi-layered squamous epithelium, including epidermis, upper digestive tract, and cornea. TMPRSS13-deficient newborn mice had a significant reduction in epidermal stratum corneum thickness which was coupled with increased rate of fluid loss across the epidermis (129). Interestingly, the increased trans-epidermal fluid loss did not cause a decrease in postnatal survival, unlike what was observed from matriptase-deficient newborn mice (71,129). Three mammalian substrates of TMPRSS13 have been identified: prostasin, HGF and ENaC (130-132). Additionally, TMPRSS13 plays a role in viral infections by cleaving hemagglutinin of influenza viruses and by activating the SARS-CoV-2 spike protein (133-137).

1.2.3 HAT/DESC subfamily: HAT, HATL-4, HATL-5, and DESC1

HAT (human airway trypsin-like protease) protein was first isolated in 1997 from the sputum of patients with chronic airway diseases and cloned the following year from human trachea cDNA (138,139). HAT is highly expressed in respiratory epithelium, tongue, skin, esophagus, and cervix (140,141). It has been shown that HAT increases mucin gene expression in airway epithelial cells (142,143). In addition, it has been demonstrated that HAT supports proteolytic activation of influenza A and B viruses and the SARS coronavirus *in vitro* (112,113). Therefore, HAT may play a role in activation and spread of different respiratory viruses in the human airways (112,113). Additional candidate substrates identified for HAT include the uPA receptor (uPAR) and PAR-2 (143,144) (145) (146). A recent study demonstrated that HAT deficient mice did not display any overt phenotypes in the absence of external challenges or additional genetic deficits (140).

Human airway trypsin-like protease 4 (HATL-4, TMPRSS11F) was cloned from human megakaryoblasts (147) and is expressed in epithelial cells and exocrine glands in tissues including skin, esophagus, trachea, tongue, eye, bladder, testis, and uterus. In the skin, HATL-4 expression is expressed in keratinocytes and sebaceous glands (147). HATL-4 null mice are viable and fertile, and display no apparent physical or histological abnormalities. Functionally, newborn null mice display significantly increased transepidermal body fluid loss indicative of a role for HATL-4 in the formation of a functional epidermal barrier (147).

Human airway trypsin-like protease 5 (HATL-5, TMPRSS11b) was cloned from a human esophagus cDNA library and it was demonstrated that it encodes a glycosylated, cell-surface localized, and catalytically active protease (148). HATL-5 displays a relatively restricted tissue expression profile with both transcript and protein present in the cervix, esophagus, and oral cavity. HATL-5 protein localizes on the cell surface of differentiated epithelial cells in the stratified squamous epithelia of all three of these tissues (148).

Differentially expressed in squamous cell carcinoma 1 (DESC1, TMPRSS11E) was cloned from primary squamous cell carcinoma tissue and expression in normal tissue was detected in skin, oral mucosa, prostate, testis, and lung (140,149,150). The physiological function of DESC1 is not known; however, a role in pathophysiology has been proposed because DESC1 activates influenza and coronaviruses in cell culture (150).

1.2.4 Cognate inhibitors of the type II transmembrane serine proteases

The two cell surface Kunitz-type serine protease inhibitors hepatocyte growth factor activator inhibitor-1 (HAI-1; SPINT1) and HAI-2 (SPINT2) were initially identified in a human gastric cancer cell line, and cDNA cloning revealed that they are both type I transmembrane proteins (151,152). They have two extracellular Kunitz-type serine proteinase inhibitor domains (KD1 and KD2), a single-pass transmembrane domain near the carboxyl terminus, and a short intracytoplasmic domain. In addition, the amino-terminus of HAI-1 has a motif at N terminus with seven cysteines (MANEC) domain and a polycystic kidney disease (PKD)-like domain, as well as

a low-density lipoprotein (LDL)-receptor class A domain between KD1 and KD2 (153) (**Fig. 1B**). Two major splicing variants (isoforms a and b) are known for HAI-2 where the b isoform lacks KD1 (153).

HAI-1 and HAI-2 have been identified as physiological inhibitors of matriptase. Complexes between matriptase and HAI-1 and HAI-2, respectively, can be detected in human milk (154,155) and the general co-localization of matriptase, HAI-1, and HAI-2 in epithelia suggests a global regulation of matriptase by these two inhibitors (56,156,157) . The physiological roles of the inhibitors were studied in mice with a null deletion in the *Spint1* or *Spint2* gene which demonstrated that HAIs are essential for placental development and embryonic survival in mice (158-161). All developmental defects in HAI-1- and HAI-2-deficient embryos, however, are rescued in whole or in part by simultaneous matriptase-deficiency, thus demonstrating that a matriptase-dependent proteolytic pathway is a critical morphogenic target for both protease inhibitors (158,159). Additional matriptase inhibitors include the secreted serpins antithrombin III, alpha1-antitrypsin, and alpha2-antiplasmin that form inhibitory complexes with matriptase in human milk (154). Matriptase-2, hepsin, HATL-5, and TMPRSS13 are also inhibited by HAI-1 and HAI-2 (47,102,130,148,162,163).

1.3 The type II transmembrane serine proteases in colorectal cancer

1.3.1 Matriptase

A 2006 study demonstrated that the ratio of matriptase:HAI-1 mRNA is higher in colorectal cancer adenomas and carcinomas than corresponding tissue from control individuals (164). Additionally, a 2007 study that investigated the ratio of matriptase to HAI-1 via immunohistochemistry (IHC) analysis showed that the matriptase: HAI-1 ratio is higher in more differentiated colon adenocarcinoma and decreases in poorly and moderately differentiated cancers (165). These studies indicate that the matriptase: HAI-1 ratio is important for CRC tumor development, and that the ratio is dependent on the grade/differentiation of the tumor. Silencing of matriptase expression with siRNA or inhibition of matriptase activity using small-molecule

inhibitors in the CRC cell line DLD-1 led to decreased activation of pro-HGF and decreased cell invasion through an extracellular matrix *in vitro* (76).

Similarly to matriptase null mice, which have severe epidermal barrier defects (71), mice with matriptase ablation specifically in the intestinal epithelium (*villin-Cre$^{+/0}$;St14$^{LoxP/-}$*) display intestinal epithelial barrier defects due to decreased tight junction formation (166). These mice also form colonic adenocarcinomas that resemble CRC that arise from inflammatory bowel disease. Loss of matriptase in the colon therefore leads to dysregulated epithelial barrier function, which allows for intestinal microbes and resident immune cells to cause chronic intestinal inflammation that eventually leads to adenocarcinoma formation (166). Thus, inflammation-associated colon carcinogenesis can be initiated and promoted solely by an intrinsic intestinal permeability barrier perturbation, and in this context matriptase acts as a tumor suppressor by supporting normal barrier function. The intestinal barrier defect in this matriptase loss-of-function model limits interpretation pertaining to the contribution of matriptase in CRC, since conclusions cannot be drawn regarding matriptase loss in the context of an intact intestinal barrier. Additional studies using alternative models, such as orthotopic xenografts assessing growth of matriptase-deficient CRC cells implanted in a normal intestinal background, would be informative.

1.3.2 TMPRSS4

TMPRSS4 mRNA and protein expression are significantly increased in CRC tissue samples compared to normal colon mucosa, and the expression of TMPRSS4 correlates with both the tumor grade as well as the presence of lymph node metastases (167,168). RNAi-mediated silencing of TMPRSS4 in the CRC cell line HCT116 demonstrated decreased cell proliferation, invasion and migration, as well as a reduction in the cancer stem cell (CSC) markers CD44 and CD133 (167). Thus, TMPRSS4 expression may be linked to the ability of CRC cells to self-renew.

1.3.3 TMPRSS13

Our group has recently shown that TMPRSS13 is significantly upregulated at the mRNA level in colon adenocarcinoma as compared to normal colon tissue. Similarly, there is a significant increase in TMPRSS13 protein expression in colon adenocarcinoma tissue samples as compared to normal colon, as well as a correlation between TMPRSS13 IHC staining and CRC grade (169). RNAi-mediated TMPRSS13 silencing in CRC cell lines caused a reduction in cell proliferation and an increase in apoptosis. TMPRSS13 was also shown to mediate chemoresistance of CRC cell lines, as TMPRSS13 silencing in combination with chemotherapy treatment led to a drastic increase in apoptosis, while overexpression of TMPRSS13 reduced chemotherapy-induced cell death (169). Additionally, TMPRSS13 silencing also led to a significant reduction in the invasive capacity of DLD1 colorectal cancer cells (169).

1.4 The type II transmembrane serine proteases in breast cancer

1.4.1 Matriptase

Matriptase was first described in 1993 as a new cancer-associated protease with gelatinolytic activity expressed by cultured human breast cancer cells (64). In breast carcinomas, increased matriptase expression correlates with tumor grade and stage and a high matriptase expression is predictive of poor survival (156,170-172). The cognate matriptase inhibitors HAI-1 and HAI-2 are expressed at a significantly lower level in poorly differentiated breast tumors, and HAI-2 expression is inversely correlated with nodal involvement and tumor dissemination (173). Interestingly, in a long-term survival study of node-negative breast cancer patients, 30-year survival data demonstrated that high expression of both matriptase and c-Met, the receptor for HGF, were significantly associated with poorer disease-free survival (171). Using genetic mouse models, it was demonstrated that matriptase is critically involved in mammary carcinogenesis and that one of the molecular mechanisms through which matriptase exerts its pro-carcinogenic effects is activation of pro-HGF on the cancer cell surface, leading to initiation of the c-Met signaling pathway and elicitation of mitogenic and invasive responses in breast cancer (83).

Matriptase hypomorphic mice that displayed an approximate 75% reduction in matriptase protein levels in mammary glands were used (83). When crossed into the mouse mammary tumor virus (MMTV) Polyomavirus middle T (PymT) antigen genetic mammary tumor model, matriptase hypomorphic mice displayed a significant delay in tumor onset, as well as a decreased tumor burden caused by abrogation of tumor cell proliferation (83). For mechanistic studies, primary mammary carcinoma cells with genetic disruption of the matriptase encoding gene by tamoxifen-inducible Cre-loxP recombination were generated. Matriptase null cells displayed an impaired ability to initiate activation of the c-Met signaling pathway in response to fibroblast-secreted pro-HGF (83). The matriptase/c-Met signaling axis also mediates proliferation and invasion in human inflammatory breast cancer (IBC) cell lines and in non-IBC human triple-negative ductal carcinoma cell lines (82,83).

Platelet-derived growth factor-C (PDGF-C) is another substrate of matriptase that contributes to breast cancer cell migration and survival *in vitro* (174). MCF-7 luminal breast cancer cells engineered to overexpress PDGF-C produced proteases capable of cleaving PDGF-C to its active form. Increased PDGF-C expression enhanced cell proliferation, anchorage-independent cell growth, and tumor cell motility by autocrine signaling. Matriptase was identified as the major protease responsible for processing of PDGF-C in MCF-7 cells (174).

1.4.2 Matriptase-2

Matriptase-2 (TMPRSS6) is highly expressed in normal mammary tissue and mainly confined to the epithelial cells (175). In breast carcinomas, matriptase-2 protein levels decreased with increasing tumor grade with very low matriptase-2 levels observed in undifferentiated ductal or lobular tumors. Reduced matriptase-2 levels in breast cancer tissues correlated with an overall poor prognosis (89,175). When matriptase-2 was stably expressed in the highly invasive breast cancer cell line MDA-MB-231, which do not endogenously express matriptase-2, reduced cell invasion and migration was observed *in vitro*. Furthermore, matriptase-2 expressing cells implanted subcutaneously into nude mice displayed significantly impaired tumor growth (175).

Thirteen single nucleotide polymorphisms (SNPs) in the *TMPRSS6* gene were investigated in triple-negative breast cancer and four variants were associated with reduced matriptase-2 expression and poor survival (89).

1.4.3 Hepsin

Hepsin is overexpressed in breast cancer tissues as compared to adjacent non-malignant breast tissue (162,176). Hepsin expression also positively correlated with the tumor stage and lymph node metastases (176). The overexpression of hepsin in mammary epithelial organoids was associated with a downregulation of HAI-1 and augmented HGF/c-Met signaling which caused deterioration of desmosomes and hemidesmosomes (162,176). Hepsin facilitates the invasive potential of breast cancer cells through remodeling of the basement membrane by cleavage of laminin-332, a component of the hemidesmosome at cell-cell junctions (177). Decreasing hepsin activity with a selective inhibitor or its expression with siRNA-mediated silencing reduced desmosome cleavage and impaired the proliferation and invasiveness of cultured breast cancer cells (177,178).

1.4.4 TMPRSS3

In an IHC study comparing breast cancer patient tissue samples to adjacent healthy breast tissue, a significantly higher expression of TMPRSS3 in cancerous tissue was demonstrated (179). The expression level of TMPRSS3 also correlated with disease stage, lymph node positivity, and proliferation of the cancer cells. Consequently, high expression of TMPRSS3 led to lower disease-free and overall survival (179). Additionally, TMPRSS3 was found to positively associate with distant organ metastasis in breast cancer (180). In one study the expression of TMPRSS3 in breast cancer samples was described to be low in poorly differentiated tumors, and low TMPRSS3 expression was significantly associated with reduced overall survival (181). The expression levels and the clinical significance of TMPRSS3 in breast cancer therefore remain unclear.

1.4.5 TMPRSS13

Recent work from our group has demonstrated a significant increase in TMPRSS13 transcript levels in invasive ductal carcinoma (IDC) samples as compared to normal breast tissue. IHC staining also showed a significant increase in TMPRSS13 protein expression in IDC as compared to normal breast tissue or benign lesions (132). In a genetic mouse model of mammary carcinoma (MMTV-PymT), genetic ablation of TMPRSS13 expression (129) led to significantly increased tumor-free survival, as well as significantly reduced tumor burden and growth rate (132). Mammary tumors harvested from TMPRSS13-deficient mice showed decreased proliferation and increased apoptosis. This effect was mirrored *in vitro*, as RNAi-mediated decrease in TMPRSS13 expression in breast cancer cell lines increased apoptosis and decreased cell proliferation and invasion (132).

CHAPTER 2: EXAMINING THE BIOCHEMICAL CHARACTERISTICS AND PRO-ONCOGENIC ACTIVITY OF TMPRSS13: BACKGROUND AND SPECIFIC AIMS

2.1 Background: Biochemical characteristics of TMPRSS13

TMPRSS13, like other TTSP family members, harbors an intracellular N-terminus, an extracellular C-terminal catalytic serine protease (SP) domain, and an extracellular stem region. The stem region of TMPRSS13 is comprised of a low-density lipoprotein receptor class A domain and a scavenger receptor cysteine rich (SRCR) domain (47,127,128). There are five potential sites of N-linked glycosylation in the extracellular domain of TMPRSS13 based on the N-X-S/T sequence motif, but only four are predicted to be glycosylated based on the surrounding amino acid context: two in the SRCR domain and two in the SP domain (47,128). The intracellular domain of TMPRSS13 is a long and highly phosphorylated intrinsically disordered region. Notably, TMPRSS13 is highly phosphorylated in the context of inactivation, either by mutagenesis of the catalytic serine or zymogen activation site or by co-expression with endogenous inhibitors, the hepatocyte growth factor activator inhibitors (HAI)-1 or HAI-2. Phosphorylated TMPRSS13 is the predominant form localized on the cell surface, as observed in cell surface biotinylation assays and immunofluorescent cell staining (47). The role that various post-translational modifications play in the function and trafficking of TMPRSS13 are examined in Specific Aim 1.

2.2 Background: The role of TMPRSS13 in breast and colorectal cancers

As detailed in Chapter 1, TMPRSS13 has recently been shown to be upregulated at the transcript and protein levels in both breast and colorectal cancers (132,169). TMPRSS13 plays a pro-oncogenic role in both cancer types, as overexpression leads to an increase in chemoresistance and genetic silencing of TMPRSS13 sensitizes cells to chemotherapy and reduces cell invasion (132,169). In a genetic model of mammary carcinoma, loss of TMPRSS13 reduces tumor burden and growth rate and significantly improves tumor-free survival (132). The potential pro-oncogenic signaling pathways to which TMPRSS13 belongs, as well as determining the role of phosphorylation in the activity and localization of TMPRSS13, are examined in Aim 2.

Hypothesis: Post-translational modifications of TMPRSS13 by N-linked glycosylation, non-zymogen activation cleavage, and phosphorylation are critical for its tumor-promoting properties by regulation of zymogen activation and trafficking to the cell surface.

2.3 Specific Aims

AIM 1) To biochemically characterize the mechanisms of activity, trafficking, and shedding of TMPRSS13.

I have found that N-linked glycosylation of the serine protease SP domain of TMPRSS13 is critical for its ability to autoactivate, cleave a protein substrate, and localize to the cell surface. In the absence of SP domain glycosylation, TMPRSS13 remains localized in the endoplasmic reticulum. Further, phosphorylation of TMPRSS13 (shown in cancer cells that endogenously express TMPRSS13 and by exogenous expression in HEK293T cells) is abrogated in the absence of N-linked glycosylation. This study also led to the discovery of an additional site of cleavage in the stem region of TMPRSS13 that is located prior to the first glycosylated residue. Cleavage at this additional site is important for TMPRSS13 autoactivation and catalytic activity, shedding into conditioned media, phosphorylation, and cell surface localization. Data from Aim 1 is summarized in Chapters 3 and 4.

AIM 2) To determine the impact of intracellular phosphorylation of TMPRSS13 in breast and colorectal cancer cell lines.

TMPRSS13 has a long, intrinsically disordered intracellular domain. It is the only TTSP known to be phosphorylated in this region, and prior studies have indicated that phosphorylation is coupled with catalytic activity and cell surface localization. Using site-directed mutagenesis to delete portions of the intracellular domain as well as to selectively mutate phosphorylated serine/threonine residues, I have found that loss of phosphorylation does not affect the autoactivation or proteolytic activity of TMPRSS13. Combined with data from Aim 1, this further informs the life-cycle of TMPRSS13, as TMPRSS13 glycosylation, additional cleavage, and cleavage for zymogen activation all occur prior to cell surface localization, at which point TMPRSS13 becomes phosphorylated. The kinases responsible for TMPRSS13 phosphorylation

have yet to be identified, but as there are at least 14 phosphorylated serine/threonine residues across the entire intracellular domain of TMPRSS13, there are likely several kinases responsible for this phosphorylation, potentially including CDK5 and ERK1/2. With our collaborators at the University of Sherbrooke, we have also performed preliminary mass spectrometry studies that indicate that phosphorylated TMPRSS13 interacts with the E-cadherin/beta catenin signaling axis on the cell surface. These results may provide insight into the oncogenic activity of TMPRSS13. Data from Aim 2 is summarized in Chapter 5.

CHAPTER 3: N-LINKED GLYCOSYLATION OF TMPRSS13

Sections of this research (Chapter 3) were originally published in the *Journal of Biological Chemistry*. Martin CE, Murray AS, Sala-Hamrick KE, Mackinder JR, Harrison EC, Lundgren JG, Varela FA, List K. Posttranslational modifications of serine protease TMPRSS13 regulate zymogen activation, proteolytic activity, and cell surface localization. *J Biol Chem*. 2021 Oct;297(4):101227. doi: 10.1016/j.jbc.2021.101227. (182).

3.1 Abstract

TMPRSS13, a member of the type II transmembrane serine protease (TTSP) family, harbors four N-linked glycosylation sites in its extracellular domain. Two of the glycosylated residues are located in the scavenger receptor cysteine-rich (SRCR) protein domain, while the remaining two sites are in the catalytic serine protease (SP) domain. In this study, we examined the role of N-linked glycosylation in the proteolytic activity, autoactivation, and cellular localization of TMPRSS13. Individual and combinatory site-directed mutagenesis of the glycosylated asparagine residues indicated that glycosylation of the SP domain is critical for TMPRSS13 autoactivation and catalytic activity toward one of its protein substrates, the prostasin zymogen. Additionally, SP domain glycosylation-deficient TMPRSS13 displayed impaired trafficking of TMPRSS13 to the cell surface, which correlated with increased retention in the endoplasmic reticulum. Importantly, we showed that N-linked glycosylation was a critical determinant for subsequent phosphorylation of endogenous TMPRSS13. Taken together, we conclude that glycosylation plays an important role in regulating TMPRSS13 activation and activity, phosphorylation, and cell surface localization.

3.2 N-linked glycosylation of TMPRSS13 – Introduction

The type II transmembrane serine proteases (TTSPs) are a family of 17 cell surface-anchored proteases, divided into four different subfamilies: HAT/DESC, hepsin/TMPRSS, matriptase, and corin (34,37,40,183). TTSPs are synthesized as inactive zymogens that require cleavage at an arginine or lysine residue for activation, and, upon zymogen activation, the

catalytic serine protease (SP) domain remains tethered to the remainder of the protease by a disulfide bridge (33,34). The dysregulation of many TTSP family members has been implicated in the development and progression of various cancers (1,29,38,39,89,118,141,148,162,166,175,181,184-190). Transmembrane Protease, Serine 13 (TMPRSS13, also known as Mosaic Serine Protease Large-Form (MSPL)), a TTSP that belongs to the hepsin/TMPRSS subfamily, has recently been implicated as a pro-oncogenic protease in both breast and colorectal cancers (132,169).

TMPRSS13 is distinct from the rest of the TTSPs due to its long, intrinsically disordered and highly phosphorylated intracellular domain (34,47). TMPRSS13 was first cloned from human lung in 2001 (127), and since then its expression has been identified on epithelial cells in various tissues, such as the epidermis and respiratory epithelia (127-129,150,191); TMPRSS13-deficient neonatal mice exhibit mild epidermal barrier defects that subside as they reach adulthood (129). TMPRSS13 is able to cleave and activate pro-hepatocyte growth factor (HGF) *in vitro* (130). In cancer, TMPRSS13 plays a promotional role by supporting primary tumor growth and metastasis *in vivo* (132). Furthermore, TMPRSS13 promotes cell survival, invasion, and resistance to drug-induced apoptosis in cancer cells (132,169). TMPRSS13 also plays a role in cleavage of viral hemagglutinin to increase pathogenicity of influenza viruses (133,136), and it cleaves and activates SARS-CoV-2 spike protein to promote viral entry and replication (134,135,137). Therefore, TMPRSS13 has emerged as a novel target for the design and discovery of drugs for treating cancer and viral infections. At the biochemical and cellular levels, however, TMPRSS13 has not been extensively characterized. We have previously shown that TMPRSS13 is modified by glycosylation (47), but the functional role of this post-translational modification has not been determined. Glycosylation can affect catalytic activity and the recognition, specificity and binding affinity of substrates/inhibitors which are important parameters to consider for drug development strategies. To determine the role of glycosylation for TMPRSS13 function, we performed a comprehensive study using multiple biochemical and cellular approaches.

Asparagine (N)-linked protein glycosylation is a process that entails the stepwise addition of carbohydrates onto a lipid molecule and the subsequent transfer of the oligosaccharide group onto an asparagine residue of a newly-formed protein in the endoplasmic reticulum (ER) (192,193). The consensus sequence motif for N-linked glycosylation is N-X-S/T, where X is any non-proline amino acid (192). N-linked glycans serve various functional roles, including assisting in proper polypeptide folding, protein quality control, and protein solubility (192,194,195). Several TTSP family members are known to be glycosylated, including hepsin (196,197), enteropeptidase (198,199), matriptase (48,200), matriptase-2 (42), corin (195,199,201,202), TMPRSS11a (203), and TMPRSS3 (122), where glycosylation is important for one or more processes including zymogen activation, catalytic activity, stability, trafficking to the cell surface, and shedding. The function of post-translational modifications for individual proteases, while frequently modulating similar processes, cannot be predicted since there is currently no known general pattern, and glycosylation can have differential effects on catalytic activity and cellular properties.

This study is the first to investigate the role of N-linked glycosylation for the autoactivation, proteolytic activity, cellular localization, and phosphorylation of TMPRSS13.

3.3 N-linked glycosylation of TMPRSS13 – Results

3.3.1 N-linked glycosylation of the serine protease domain is critical for TMPRSS13 autoactivation

TMPRSS13 has four predicted sites of N-linked glycosylation in its extracellular domain, based on both the N-X-S/T consensus sequence and the surrounding amino acid context (47,204). To investigate the role of N-linked glycosylation for TMPRSS13 functions, site-directed mutagenesis was performed to selectively mutate these four putatively glycosylated asparagine residues (N250, N287, N400, N440) into glutamine residues. N250 and N287 are both located in the scavenger receptor cysteine rich (SRCR) region of TMPRSS13, while N400 and N440 are located in the SP domain (**Fig. 2A**). The lipoprotein receptor class A domain (L) domain does not contain predicted glycosylation sites. The resulting plasmids encode the full-length V5-tagged

human TMPRSS13 variants: N250Q-T13-V5, N287Q-T13-V5, N400Q-T13-V5, N440Q-T13-V5, and N400Q/N440Q-T13-V5, the latter of which has both N-glycosylation sites in the SP domain mutated.

HEK293T cells were transfected with wild-type (WT) TMPRSS13, S506A (catalytically dead; the serine residue in the catalytic triad is mutated to alanine (47)) TMPRSS13, R320Q (zymogen locked; the zymogen activation site is mutated to glutamine (47)) TMPRSS13, and the five N-linked glycosylation mutant plasmids. As described previously, WT-TMPRSS13 is capable of autoactivation by zymogen cleavage at R320 which releases its proteolytically active SP domain under reducing SDS-PAGE conditions (47). S506A and R320Q TMPRSS13 mutants serve as negative controls for proteolytic activity and activation/autoactivation, respectively (47). 48 hours after transfection, cells were lysed and treated with Peptide:N-glycosidase F (PNGase F), an enzyme that removes most types of N-linked glycosylation including high mannose, hybrid, and complex oligosaccharides (205-207).

Whole cell lysates with or without PNGase F treatment were separated by SDS-PAGE under reducing conditions, which disrupts the disulfide bond that tethers the SP domain to the stem region of TMPRSS13, thereby allowing visualization of the released active SP domain by western blotting. Western blots were probed with two antibodies directed against different epitopes of TMPRSS13: one that recognizes amino acids 195-562 on the extracellular portion of the protease (α-extra-TMPRSS13) and one that recognizes the first 60 amino acids of the protease (α-intra-TMPRSS13); antigens are indicated in **Fig. 2A panel II**.

Detection of WT-TMPRSS13 using the α-extra-TMPRSS13 antibody (**Fig. 2B**) shows that full-length non-phosphorylated TMPRSS13 migrates in accordance with its predicted molecular weight of ~61 kDa plus the addition of a ~5 kDa V5 tag (~66 kDa total) upon treatment with PNGase F compared to the glycosylated form of TMPRSS13 at ~80 kDa without PNGase F treatment (**Band #2**) indicating that PNGase F is removing N-linked glycans from full-length TMPRSS13. The released SP domain migrates as a ~36 kDa band without PNGase F treatment

Figure 2: N-linked glycosylation of TMPRSS13 is important for autoactivation
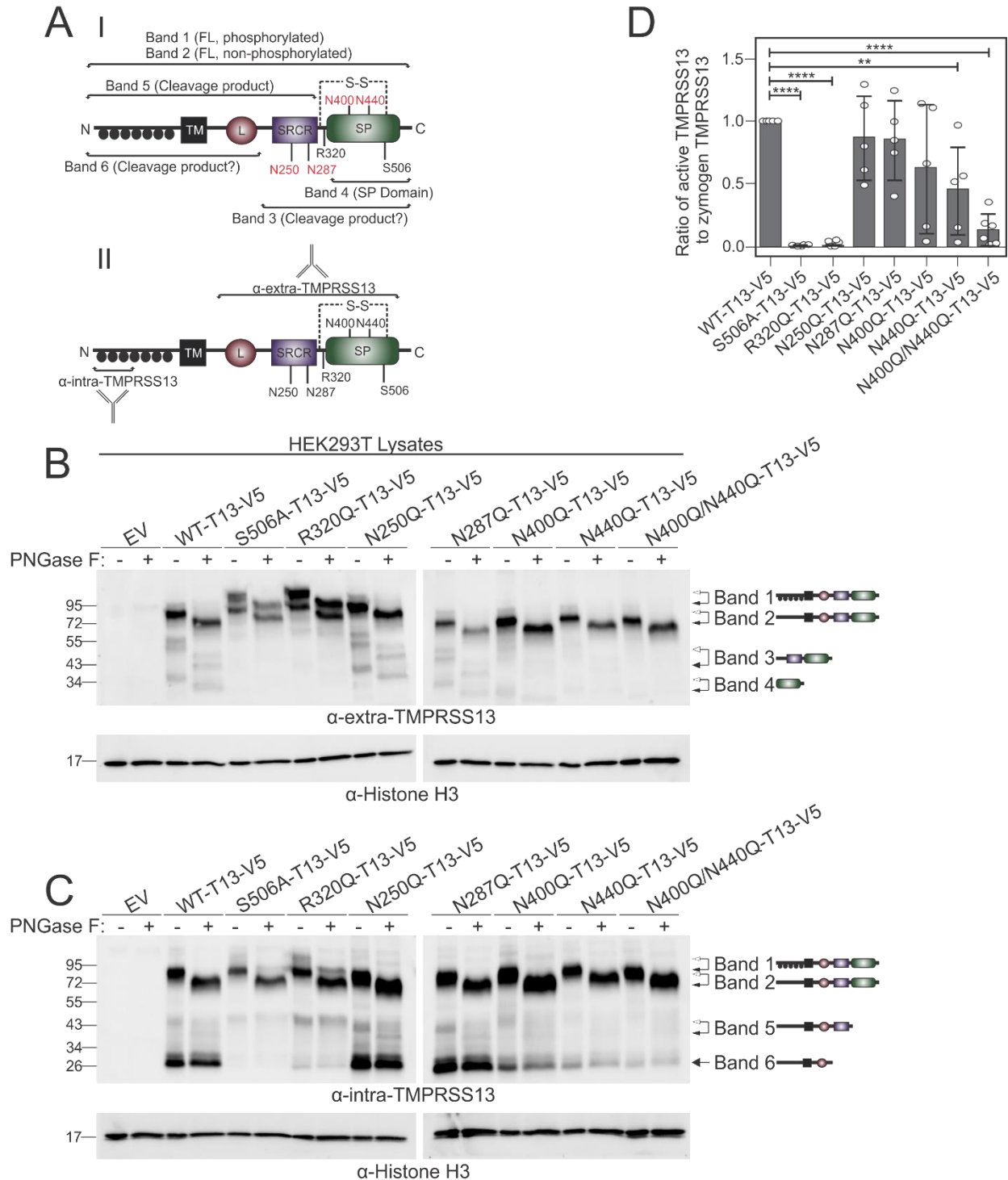
Figure 2: **A)** Schematic representation of TMPRSS13 showing full-length TMPRSS13 and cleavage fragments (I) and epitopes for anti-intra-TMPRSS13 and anti-extra-TMPRSS13 antibodies (II). FL, full-length TMPRSS13; TM, transmembrane domain; L, lipoprotein receptor class A domain; SRCR, group A scavenger receptor cysteine rich domain; SP, serine protease domain. The activation cleavage site is located at R320, the catalytic serine residue is located at

S506, and the four sites of N-linked glycosylation are N250, N287, N400, and N440 (in red text). The disulfide bridge tethering the SP domain to the stem region is denoted with "S-S" and a dashed line. Phosphorylation of the intracellular domain is indicated by filled black circles. **B-C)**, HEK293T cells were transfected with TMPRSS13 constructs and proteins from cell lysates were separated by SDS-PAGE under reducing conditions using 10% gels and analyzed by western blotting. Lanes with protein extracts treated with PNGase F prior to SDS-PAGE are indicated by "+" and those that received no PNGase F are indicated by "-". Proteins were detected using anti-extra-TMPRSS13 **(B)**, anti-intra-TMPRSS13 **(C)** or anti-histone H3 antibodies. Arrows to the right of the western blots indicate TMPRSS13 bands defined in *A* (white arrowheads; TMPRSS13 form prior to PNGase F treatment) and their representative schematics (black arrowheads; TMPRSS13 form after PNGase F treatment). **D)** Bar graph showing the ratio of the released SP-domain to the full-length TMPRSS13 protein, normalized to WT-TMPRSS13. Error bars are representative of standard deviation. One-way ANOVA with Dunnett's multiple comparisons post-hoc test was used to determine significance of SP-domain release compared to WT-TMPRSS13. Results for at least five biological replicates are shown. **p≤0.01, ****p≤0.0001.

(**Band #4**), representing the catalytically active protease domain, as we have previously

demonstrated by α2-macroglobulin capture (47). This band also migrates as a lower molecular

weight species upon PNGase F treatment, further confirming that the SP domain is glycosylated.

Notably, we have shown that the S506A and R320Q mutants are highly phosphorylated

in their intracellular domains and display a phosphorylated high molecular weight (HMW) form by

western blotting, and phosphorylation of WT-TMPRSS13 is also observed upon co-expression

with the cognate inhibitor hepatocyte growth factor activator inhibitor (HAI)-2 (47). For the S506A

and R320Q mutants, the HMW band ~95 kDa (**Band #1**) is detected, indicative of phosphorylation

of the intracellular domain (as detailed in (47)). The phosphorylated form shifts downward upon

PNGase F treatment indicating that this form, like non-phosphorylated full-length TMPRSSS13,

is also glycosylated in agreement with our previously published observations (47). The S506A

and R320Q mutants are rendered enzymatically inactive or are zymogen activation deficient,

respectively; no autoactivation leading to released SP domain is detected in either mutant.

In the N250Q and N287Q single mutants, the released SP domain is readily detected,

suggesting that abrogating glycosylation in the SRCR domain does not significantly impede the

ability of TMPRSS13 to autoactivate (quantitation of released SP domain relative to full-length

TMPRSS13 for all constructs is shown in Fig. 2D). However, there is a reduced ratio of the SP

domain compared to the full-length TMPRSS13 protein in the N440Q single mutant, indicative of

a role for this site in its autoactivation (**Fig. 2D**). The N400Q/N440Q double mutant is detected as a full-length, non-phosphorylated protein with little to no detectable release of its SP domain. Thus, the mutation of both glycosylation sites in the SP domain of TMPRSS13 significantly decreases activation of the TMPRSS13 protein, indicating that N-linked glycosylation at both sites in the SP domain is critical for efficient autoactivation (**Fig. 2D**).

WT, N250Q and N287Q TMPRSS13 also display a ~55 kDa band (**Band #3**) that, based on its molecular weight and the fact that it shifts to a lower molecular weight form upon treatment with PNGase F, may represent a cleavage product resulting from a cleavage site between the transmembrane (TM) and SRCR domains (**Band #3**). Since this form is not observed in the S506A and R320Q mutants, and it is detected at reduced levels in the N400Q/N440Q single and double mutants, it may represent an autocleavage fragment (see **Fig. 2C, Band #6** for detection of the potential other half of cleaved TMPRSS13 using the intracellular TMPRSS13 antibody). Additionally, it is noteworthy that while the N400Q/N440Q double mutant has a significant reduction in autoactivation, similar to S506A and R320Q, it does not show a detectable phosphorylated form. This implies that phosphorylation of TMPRSS13 is not solely a consequence of reduced catalytic activity of the protease.

When parallel western blots were probed with the α-intra-TMPRSS13 antibody that is directed against the intracellular portion of TMPRSS13, the full-length non-phosphorylated TMPRSS13 and HMW phosphorylated forms are detected similarly to the α-extra-TMPRSS13 blot (**Fig. 2C**) with a shift to lower molecular weight forms upon PNGase F treatment. Two additional forms are visible in WT-TMPRSS13: one at ~43 kDa (**Band #5**) and one at ~26 kDa (**Band #6**). Based on the molecular weight of Band #5, and because it shifts to a lower molecular weight form upon PNGase F treatment, this form likely represents the intracellular portion of TMPRSS13 following cleavage at R320, the canonical activation site. We hypothesize that Band #6 represents the intracellular fragment of TMPRSS13 following cleavage at an additional cleavage site (extracellular fragment, **Band #3** in **Fig. 2B**) between the transmembrane (TM)-

domain and SRCR domain. This prediction is based on its molecular weight and the observation that it does not shift downward upon PNGase F treatment, indicating that it represents a cleaved form without glycosylation sites (fragment including the intracellular domain, the TM domain, and potentially the L domain, see Fig 2A). As Band #6 is not detected in the S506A mutant, and is observed at reduced levels in the R320Q mutant, it is plausible that this cleavage product is generated by TMPRSS13 autocleavage as mentioned above. In comparison to WT-TMPRSS13, N400Q and N440Q single mutants show greatly reduced levels of Band #5 and Band #6, and the level is further reduced in the N400Q/N440Q double mutant suggesting that mutations of N-glycosylation sites in the SP domain impair the proposed autocleavage of TMPRSS13.

To investigate whether endogenously expressed TMPRSS13 is also N-linked glycosylated, we employed two different methods to assess its glycosylation in human cancer cells: 1) Tunicamycin-mediated inhibition of N-linked glycosylation in live cells (208,209), and 2) Assessment of glycosylation status by PNGase F treatment of whole cancer cell lysates. For tunicamycin treatment, four cell lines were used: triple-negative breast cancer lines BT-20, HCC1937, and MDA-MB-468, and DLD1 colorectal cancer cells. Upon treatment of live cancer cells with tunicamycin for 48 hours, whole cell lysates were analyzed by reducing SDS-PAGE and western blotting using the α-intra-TMPRSS13 antibody. We have previously shown that this antibody can detect endogenous TMPRSS13 in cancer cells, using siRNA-mediated TMPRSS13 silencing to confirm specificity (47,132,169). In untreated cells, glycosylated full-length

TMPRSS13 was observed, in both the phosphorylated and non-phosphorylated forms, whereas only one band at ~60 kDa was detected in tunicamycin-treated cells indicating that tunicamycin blocked N-linked glycosylation and phosphorylation of endogenous TMPRSS13 (**Fig. 3A**). In parallel experiments, PNGase F was used to remove N-linked glycans from endogenous TMPRSS13 in whole cell lysates from DLD-1 and BT-20 cancer cells (**Fig. 3B-C**). A similar shift in full-length TMPRSS13 migration was observed indicating the removal of endogenous N-linked glycans from the protease. Together these observations suggest that endogenous TMPRSS13 is

Figure 3: TMPRSS13 is endogenously glycosylated
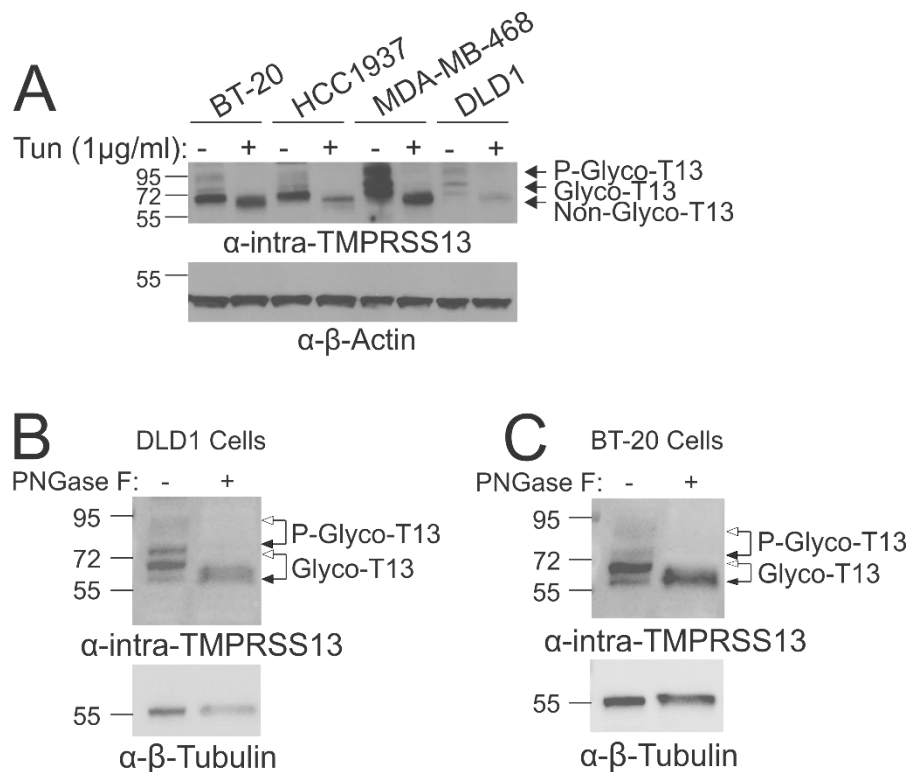
Figure 3. **A)** Breast cancer (BT-20, HCC1937, MDA-MB-468) and colorectal cancer (DLD1) cell lines were treated for 48 hours with 1 µg/ml Tunicamycin (indicated with "+") or vehicle control (DMSO, indicated with "-"). Proteins in whole cell lysates were separated by SDS-PAGE under reducing conditions using a 10% gel and detected by western blotting using anti-intra-TMPRSS13 and anti-β-actin antibodies. **B-C)** Proteins from **(B)** DLD1 or **(C)** BT-20 cell lysates were separated by SDS-PAGE under reducing conditions using 10% gels. Lanes with protein extracts treated with PNGase F prior to SDS-PAGE are indicated by "+" and those that received no treatment are indicated by "-". Proteins were detected by western blotting using anti-intra-TMPRSS13 and anti-β-tubulin antibodies. The white arrowheads connected to black arrowheads indicate the mobility shift upon PNGase F treatment. P-glyco-T13, phosphorylated and glycosylated TMPRSS13; Glyco-T13, glycosylated TMPRSS13; Non-glyco-T13, non-glycosylated TMPRSS13.

glycosylated and that the glycosylation phenotype observed in the HEK293T cell exogenous expression model reflects a biologically relevant post-translational modification.

3.3.2 The ability of TMPRSS13 to cleave and activate its protein substrate prostasin is regulated by N-linked glycosylation

Due to the impact of N-linked glycosylation on the autoactivation of TMPRSS13, the next step was to determine if N-linked glycosylation affects the ability of TMPRSS13 to proteolytically cleave a different protein substrate. We have previously shown that endogenous TMPRSS13 levels affect endogenous prostasin protein levels in breast cancer cells, and that recombinant

TMPRSS13 cleaves and activates the pro-form of prostasin in HEK293T cells (132). Prostasin is a glycophosphatidylinositol (GPI)-anchored serine protease that, unlike TMPRSS13, is incapable of autoactivation and the zymogen form requires cleavage at Arg44 by another protease in order to become proteolytically active (210). This requirement can be exploited to assess the proteolytic capability of TMPRSS13 mutants to cleave and activate prostasin zymogen.

HEK293T cells were transfected with WT-TMPRSS13-V5 and mutant expression plasmids plus full-length human prostasin, and cells were treated with phosphatidylinositol-specific phospholipase C (PI-PLC) to release prostasin into the supernatant. Subsequently, protease nexin (PN)-1, an endogenous inhibitor of prostasin that forms an SDS-stable complex with active prostasin (211), was added to the prostasin-containing supernatants. In western blot analysis, the detection of a band at ~95 kDa corresponding to the active prostasin/PN-1 complex reflects that prostasin has been cleaved and activated by TMPRSS13 (**Fig. 4A**). In this assay, WT-TMPRSS13 is used as a positive control for prostasin activation, while S506A and R320Q mutants are used as negative controls. N250Q and N287Q mutations did not appear to affect the catalytic ability of TMPRSS13 to activate prostasin zymogen. N400Q and N440Q mutations decreased the ability of TMPRSS13 to activate prostasin, while the double mutant N400Q/N440Q showed the most significant decrease in TMPRSS13-mediated prostasin activation among the glycosylation mutants (**Fig. 4B**). These results, coupled with those from Fig. 2, indicate that glycosylation in the SP domain of TMPRSS13 is critical for efficient catalytic activity for both autoactivation and cleavage/activation of a different protein substrate.

3.3.3 Glycosylation-deficient TMPRSS13 displays impaired localization to the cell surface and is retained in the endoplasmic reticulum

We have previously shown that WT-TMPRSS13 does not localize to the surface of HEK293T cells unless co-transfected with one of its cognate inhibitors, the Kunitz domain-containing hepatocyte growth factor activator inhibitor (HAI)-1 or HAI-2 (47). The S506A and

Figure 4: Lack of N-linked glycosylation impairs TMPRSS13-mediated activation of prostasin
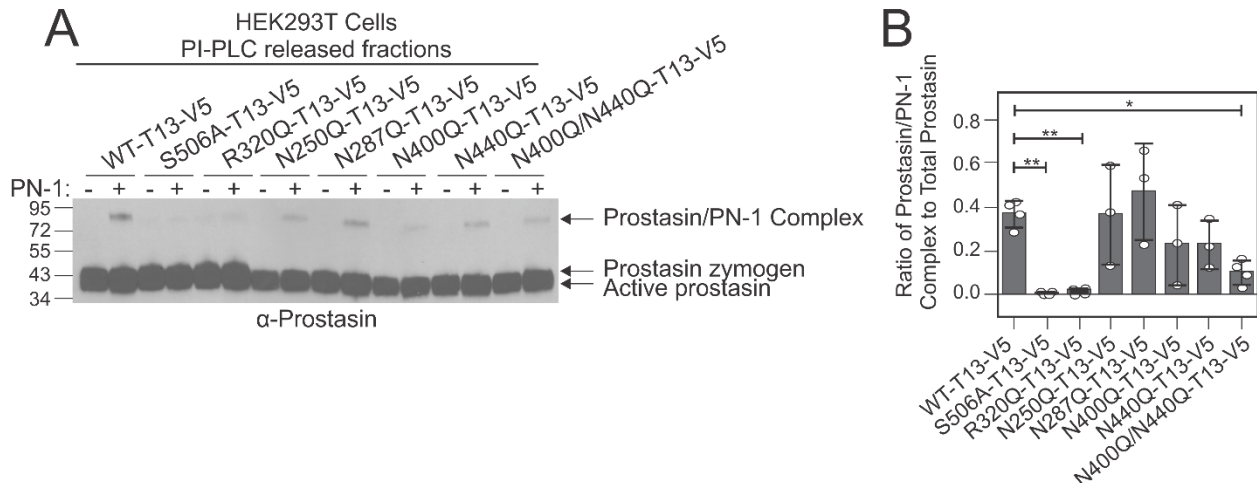
Figure 4. A) HEK293T cells were co-transfected with plasmids encoding TMPRSS13 variants and human full-length prostasin. Phosphatidylinositol-specific phospholipase C (PI-PLC) was added to cleave the glycophosphatidylinositol anchor from prostasin and release it into the supernatant. Protease nexin-1 (PN-1) was added (indicated by "+") to form SDS-stable complexes with active prostasin. Proteins were separated by SDS-PAGE under reducing conditions using a 4-15% gel and proteins were detected on western blots using an anti-prostasin antibody. The prostasin zymogen and active forms, as well as the active prostasin/PN-1 complex are indicated with arrows. **B)** Bar graph showing the ratio of the prostasin/PN-1 complex to total prostasin levels. Error bars are representative of standard deviation. One-way ANOVA with Dunnett's multiple comparisons post-hoc test was used to determine significance of prostasin activation compared to WT-TMPRSS13. Results from at least four biological replicates are shown. *$p \le 0.05$, ** $p \le 0.01$.

R320Q mutants, however, readily localize to the cell surface without concomitant expression of HAIs (47). When TMPRSS13 is expressed with either HAI-1 or HAI-2, efficient cell-surface localization occurs suggesting that the cognate inhibitors facilitate TMPRSS13 localization while preventing intracellular activation (47).

To assess the role of glycosylation for TMPRSS13 cellular trafficking, immunofluorescence cell staining was performed. HEK293T cells were transfected with WT-TMPRSS13, S506A-TMPRSS13, or N400Q/N440Q-TMPRSS13, in the presence or absence of HAI-2. Cells were fixed and left non-permeabilized to visualize cell surface staining (**Fig. 5**) or were permeabilized to visualize intracellular TMPRSS13 as well as endogenous KDEL, an ER marker (**Fig. 6**) As expected, in non-permeabilized cells WT-TMPRSS13 was not detected on the cell surface when expressed alone (**Fig. 5A**). When WT-TMPRSS13 was co-expressed with HAI-

Figure 5: Lack of catalytic domain glycosylation impairs TMPRSS13 cell surface localization
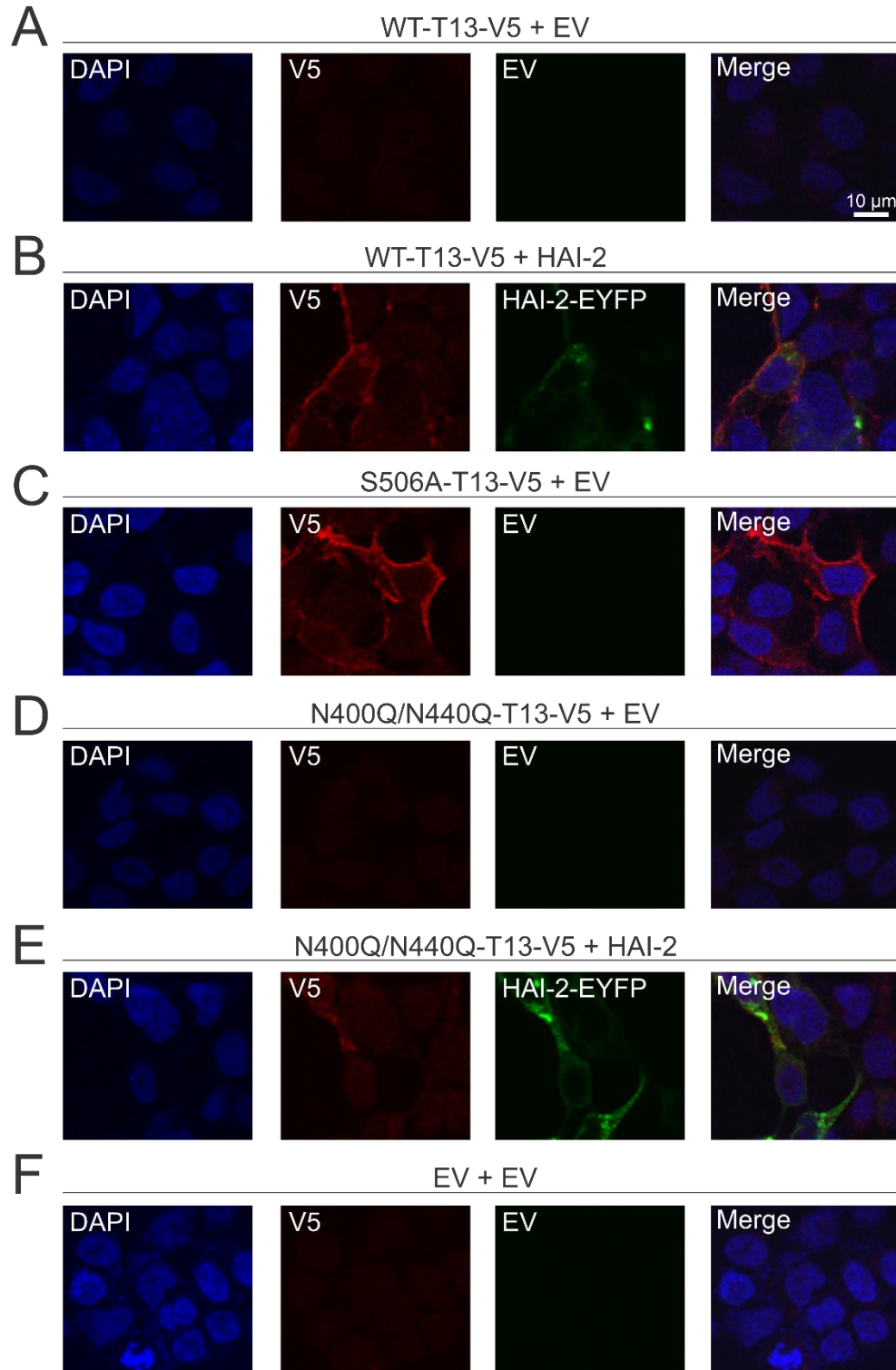
Figure 5: 24 hours after seeding onto glass coverslips, HEK293T cells were transfected for 48 hours with **(A)** WT-TMPRSS13 (T13)-V5 plus empty vector (EV), **(B)** WT-TMPRSS13-V5 plus HAI-2-EYFP, **(C)** S506A-TMPRSS13-V5 plus EV, **(D)** N400Q/N440Q-TMPRSS13-V5 plus EV,

(E) N400Q/N440Q-TMPRSS13-V5 plus HAI-2-EYFP, or **(F)** EV plus EV. Cells were fixed (no permeabilization), incubated overnight with anti-V5 antibody, and analyzed by confocal microscopy. Nuclei (DAPI) (*blue, A-F*), TMPRSS13-V5 (*red, A-F*), HAI-2 (*green, B and E*). Merged images are shown in panels on the right. Scale bar measures 10 μm.

Figure 6: Glycosylation deficiency causes ER retention of TMPRSS13
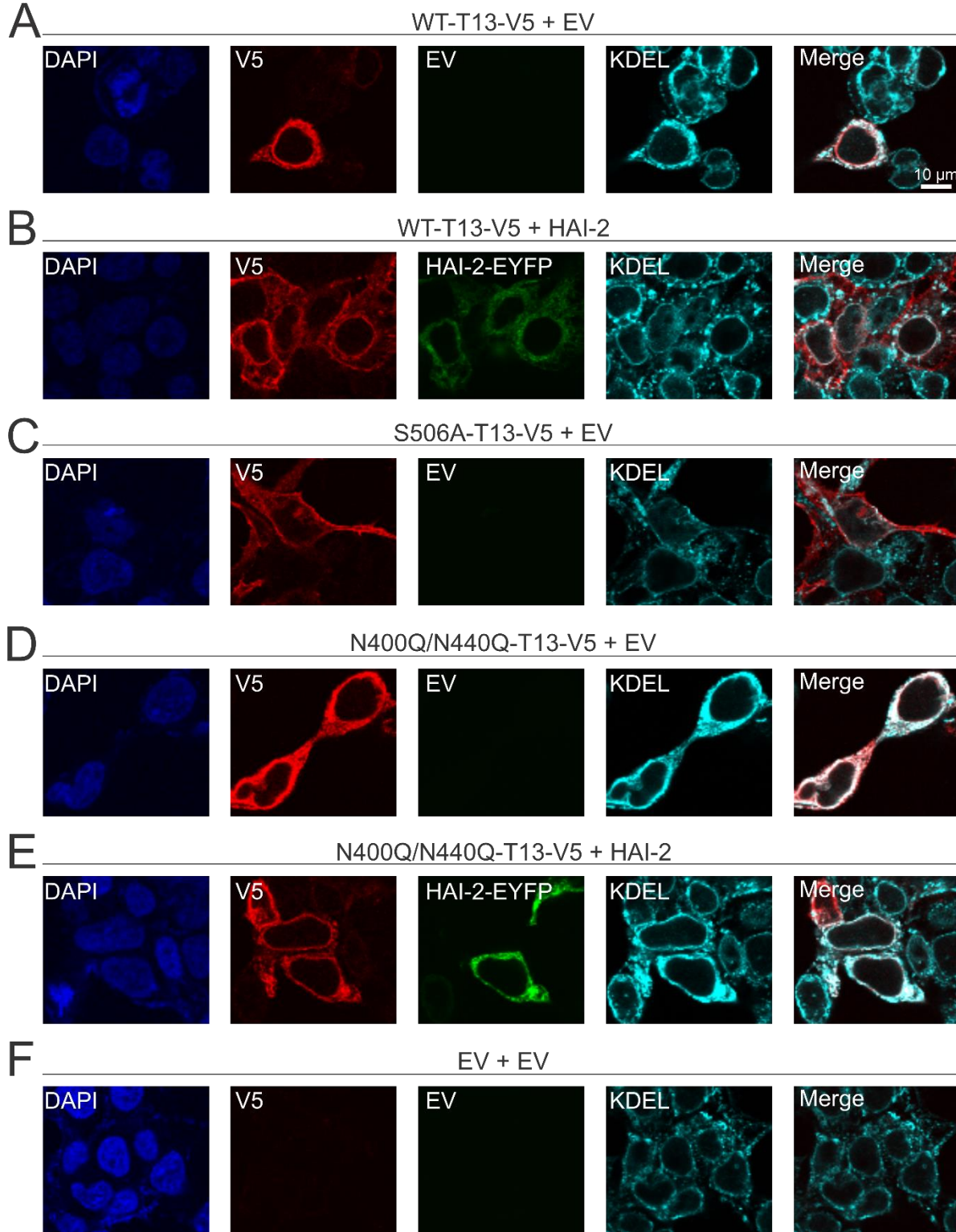
Figure 6: 24 hours after seeding onto glass coverslips, HEK293T cells were transfected for 48 hours with **(A)** WT-TMPRSS13 (T13)-V5 plus empty vector (EV), **(B)** WT-TMPRSS13-V5 plus HAI-2-EYFP, **(C)** S506A-TMPRSS13-V5 plus EV, **(D)** N400Q/N440Q-TMPRSS13-V5 plus EV,

(E) N400Q/N440Q-TMPRSS13-V5 plus HAI-2-EYFP, or **(F)** EV plus EV. Cells were fixed, permeabilized, and incubated overnight with anti-V5 to detect TMPRSS13 or anti-KDEL to detect endogenous KDEL. Nuclei (DAPI) (*blue, A-F*), TMPRSS13-V5 (*red, A-F*), HAI-2 (*green, B and E*), KDEL (*cyan, A-F*). Merged images of TMPRSS13/KDEL are shown in panels on the right. Scale bar measures 10 μm.

2, cell surface TMPRSS13 was observed (**Fig. 5B**). S506A-TMPRSS13 localizes readily to the cell surface without requiring co-transfection with HAI-2 (**Fig. 5C**). In contrast, N400Q/N440Q-TMPRSS13 was not detected at the cell surface either in the absence or presence of HAI-2, indicating impaired cellular trafficking in this glycosylation-deficient form of TMPRSS13. To further examine the cellular fate of N400Q/N440Q, staining of permeabilized cells was performed. N400Q/N440Q was detected intracellularly and co-localized with KDEL in the absence (**Fig. 6D**) or presence (**Fig. 6E**) of HAI-2 suggesting that lack of glycosylation in the SP domain of TMPRSS13 limits the ability of TMPRSS13 to exit the ER and localize to the cell surface. The glycosylated WT-TMPRSS13, when unopposed by simultaneous transfection with HAI-2 was also retained in the ER (**Fig. 6A**) while co-transfection with HAI-2 increased cell surface localization (**Fig. 6B**).

Catalytically inactive, glycosylated S506A-TMPRSS13 efficiently localized to the surface without HAI-2 (**Fig. 6C**), suggesting that the activity status of glycosylated TMPRSS13 is an important determinant for cell surface localization. If proteolytic activity status is the only determinant for proper trafficking, it would be expected that the activity-impaired glycosylation-deficient N400Q/N440Q-TMPRSS13 would be capable of reaching the cell surface. Based on the observation that N400Q/N440Q-TMPRSS13 displays cell surface trafficking deficiency, which unlike WT-TMPRSS13 is not rescued by concomitant expression of HAI-2, we propose that glycosylation is critical for proper TMPRSS13 trafficking independent of its proteolytic activity and presence of cognate inhibitors. We considered the possibility that impaired binding of HAI-2 to N400Q/N440Q-TMPRSS13 might contribute to the lack of a rescuing effect of HAI-2. However, immunoprecipitation experiments did not reveal a significant difference between HAI-2 levels co-precipitated with WT-TMPRSS13-V5 or N400Q/N440Q-TMPRSS13-V5 (**Fig. 7A-B**). It is possible

Figure 7: Lack of SP-domain glycosylation does not affect TMPRSS13 interaction with HAI-2
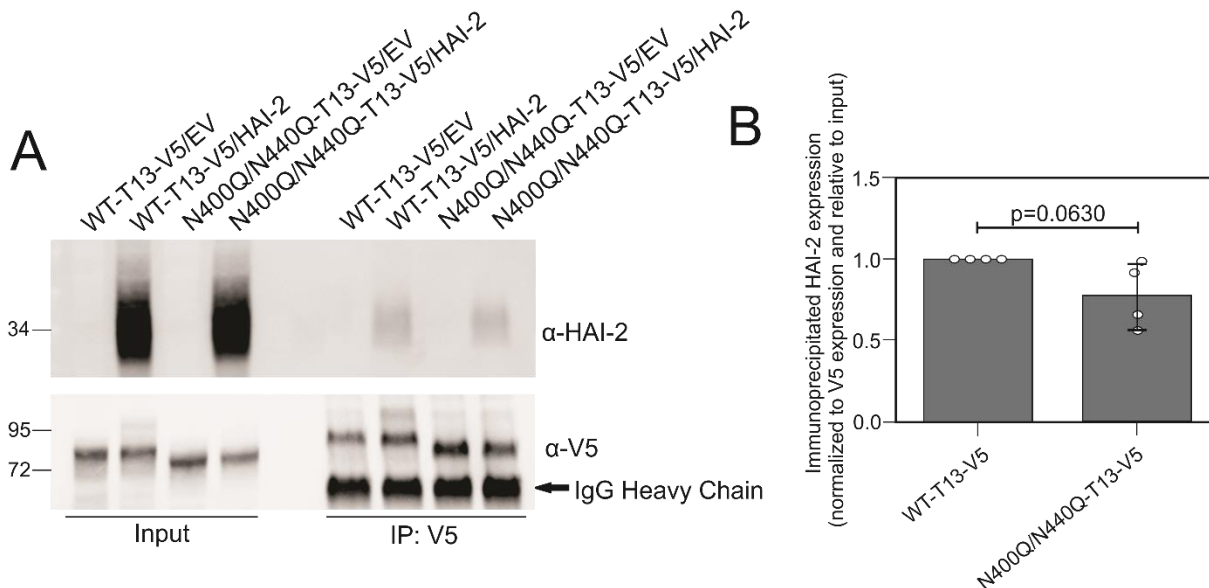
Figure 7: **A)** HEK293T cells transfected with WT-TMPRSS13 (T13) + empty vector (EV), WT-TMPRSS13+HAI-2, N400Q/N440Q-TMPRSS13+EV, or N400Q/N440Q+HAI-2 were immunoprecipitated with anti-V5 antibody and separated by SDS-PAGE under reducing conditions using a 10% gel. Whole cell lysates were included to verify protein expression prior to immunoprecipitation (*input*). Proteins were detected by western blotting using anti-V5 and anti-HAI-2 antibodies. **B)** Quantification of HAI-2 interaction with WT-TMPRSS13-V5 or N400Q/N440Q-TMPRSS13-V5, normalized to V5 expression. Error bar is representative of standard deviation. Student's t-test was used to evaluate the difference in TMPRSS13/HAI-2 interaction. Results for four biological replicates are shown.

though, that the lack of N-linked glycans in the SP domain of TMPRSS13 changes interactions

with ER chaperone proteins causing accumulation of N400Q/N440Q-TMPRSS13-V5 in the ER.

To further validate the immunocytochemistry findings using a biochemical approach, we

analyzed lysates from cells expressing WT or mutant TMPRSS13 in combination with cell-surface

biotinylation analysis using a membrane-impermeable biotinylation reagent. HEK293T cells were

transfected with WT-TMPRSS13 or mutant plasmids, in the presence or absence of HAI-2. Cell-

surface proteins were biotin-labeled and pulled down using streptavidin-agarose beads and

samples were subsequently analyzed by SDS-PAGE and western blotting (**Fig. 8**). As expected,

there is a predominance of the HMW (phosphorylated) form of TMPRSS13 at the cell surface, as

previously seen with WT-TMPRSS13 co-expressed with HAI-2 and with the S506A and R320Q

mutants co-transfected with empty vector (EV) (47). In addition, the "wash" fractions containing

Figure 8: Impairment of phosphorylation and cell surface localization in glycosylation deficient TMPRSS13
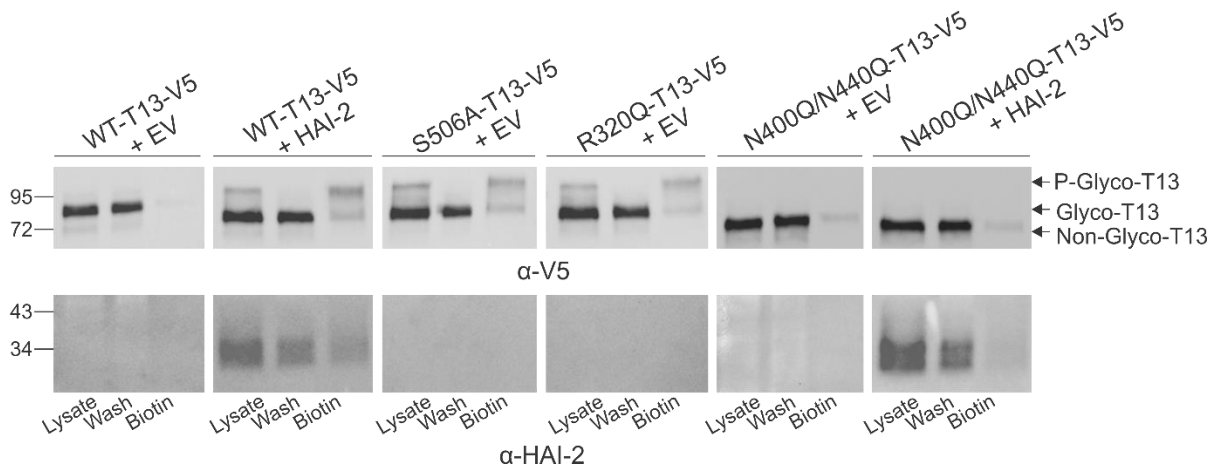
Figure 8: HEK293T cells were transfected with WT-TMPRSS13 (T13)-V5, S506A-TMPRSS13-V5, R320Q-TMPRSS13 (T13)-V5 and N400Q/N440Q-TMPRSS13-V5 plasmids plus empty vector (EV) or in combination with HAI-2. Cell-surface proteins were biotin-labeled at room temperature for 30 min. Biotin-labeled proteins were precipitated with streptavidin-agarose beads for 1 hour at 4°C. Beads were pelleted and supernatants containing non-biotinylated proteins were collected (*wash*). Beads were washed five times in PBS, then biotin-labeled proteins were eluted from beads by treatment with Laemmli buffer with 5% 2-mercaptoethanol. Whole cell lysate input (*lysate*), non-biotinylated proteins (*wash*), and biotin-labeled proteins (*biotin*) were separated by SDS-PAGE under reducing conditions using 10% gels. Proteins were detected by western blotting using anti-V5 (TMPRSS13) and anti-HAI-2 antibodies. P-glyco-T13, phosphorylated and glycosylated TMPRSS13; Glyco-T13, glycosylated TMPRSS13; Non-glyco-T13, non-glycosylated TMPRSS13.

non-biotinylated proteins show minimal or no phosphorylated TMPRSS13, indicating that the majority of phosphorylated TMPRSS13 is localized to the cell surface. WT-TMPRSS13 shows minimal cell surface localization when unopposed by HAI-2 while cell-surface TMPRSS13 is readily detected upon co-expression with HAI-2. No discernable differences between WT-TMPRSS13 (with or without HAI-2) and SRCR domain glycosylation site mutants (N250Q and N287Q) were observed (data not shown). Importantly, for N400Q/N440Q-TMPRSS13 a cell-surface phosphorylated form is undetectable in both the presence and absence of HAI-2. These data, in combination with the immunofluorescent cell staining, indicate that ER retention of glycosylation-deficient TMPRSS13 causes impairment of trafficking to the cell surface, independent of inhibitor expression.

3.3.4 Endogenous TMPRSS13 is modified by N-linked glycosylation and phosphorylation

To investigate the role of glycosylation for endogenous TMPRSS13 turnover and phosphorylation status, BT-20 and DLD1 cells were treated with cycloheximide and/or tunicamycin followed by western blot analysis of whole-cell lysates. HAI-1 and HAI-2 are endogenously expressed in both cell lines (47). Importantly, both cell lines express a full-length, glycosylated TMPRSS13 form (denoted as Glyco-T13 in Fig. 9) and a lower molecular weight TMPRSS13 form (non-Glyco-T13) that are detected prior to treatment with cycloheximide (**Fig. 9A-D left panels, vehicle, 0 h cycloheximide; Fig. 3B-C**) or tunicamycin (**Fig. 9A-D right panels, vehicle, 0 h cycloheximide; Fig. 3A**). We infer that this lower molecular weight variant represents a hypo- or non-glycosylated form of TMPRSS13, which is supported by the findings that only this form is detected upon PNGase F treatment (**Fig. 9C-D**) or tunicamycin treatment (**Fig. 9A-D right panels, tunicamycin).** The HMW phosphorylated form of TMPRSS13 (P-Glyco-T13) appears to be glycosylated as demonstrated by its absence (non-detectable) in tunicamycin treated cells and a shift in mobility upon PNGase F treatment (**Fig. 9C-D).** Detection of endogenous full-length glycosylated TMPRSS13 (Glyco-T13) rapidly decreases within the first 4 hours of cycloheximide treatment (**Fig. 9A-D)**, while non-glycosylated TMPRSS13 (Non-Glyco-T13) is detectable for up to 30 hours (**Fig. 9A-B**). The persistent detection of non-glycosylated TMPRSS13 may reflect increased ER retention, as observed with the N400Q/N440Q-TMPRSS13 mutant in Figure 4. Interestingly, the HMW phosphorylated and glycosylated form of TMPRSS13 (P-Glyco-T13) also appears to have increased stability compared to the non-phosphorylated glycosylated form and can be detected for up to 30 hours in DLD1 cells and 12 hours in BT20 cells (**Fig. 9A-B**). Additionally, tunicamycin treatment eliminates detection of the phosphorylated form of TMPRSS13 (**Fig. 9A-D**; **Fig. 3A**). The fast turnover of Glyco-T13 may reflect conversion to P-Glyco-T13 with subsequent transport to the secretory pathway and cell surface. Cycloheximide likely abrogates generation of new Glyco-T13 as it has been shown that N-

Figure 9: N-linked glycosylation determines cellular stability and phosphorylation status of endogenous TMPRSS13
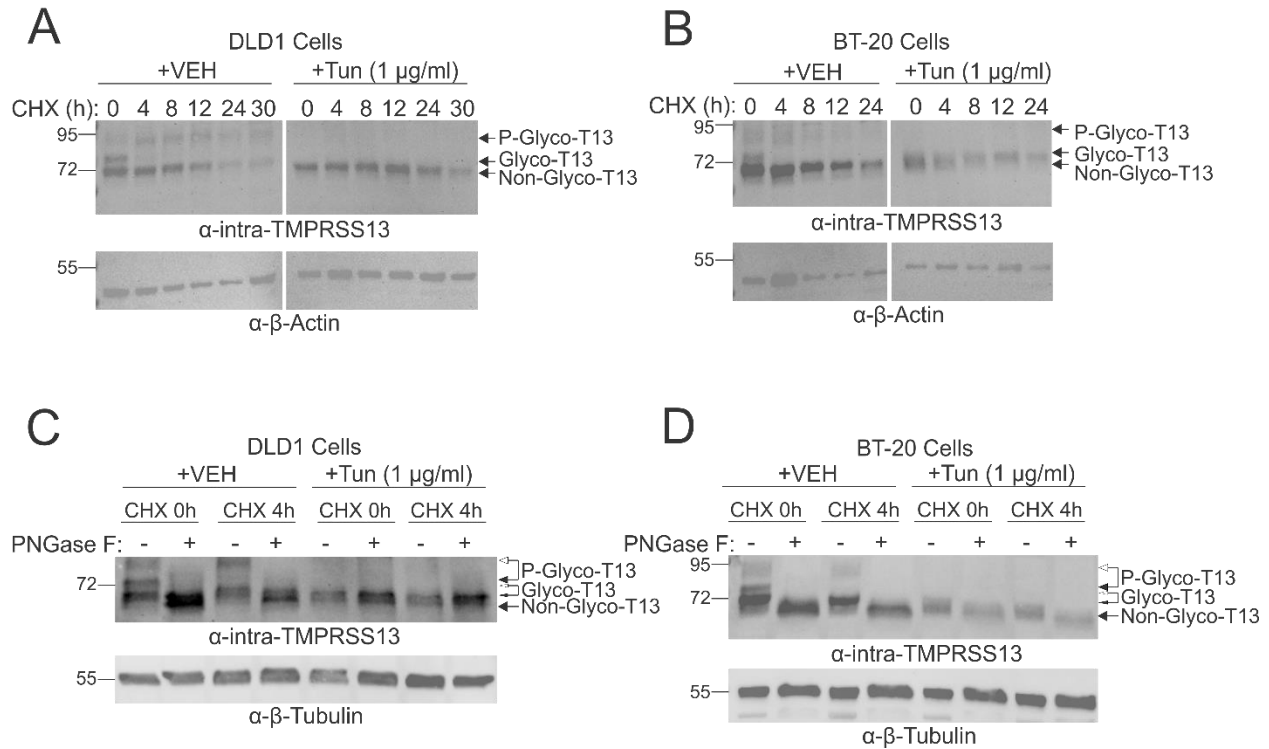
Figure 9: **A)** DLD1 colorectal cancer cells or **(B)** BT-20 breast cancer cells were treated with 1 µg/ml Tunicamycin (Tun) or vehicle control (VEH; DMSO) for 24 hours, then cycloheximide (CHX) was added for (*A*) 0-30 or (*B*) 0-24 hours. Proteins in whole cell lysates were separated by SDS-PAGE under reducing conditions using 10% gels and detected on western blots using anti-intra-TMPRSS13 and anti-β-actin antibodies. Whole cell lysates from **(C)** DLD1 or **(D)** BT-20 cells treated with tunicamycin or vehicle control and cycloheximide for 0-4 hours were subsequently treated with PNGase F prior to SDS-PAGE under reducing conditions (indicated by "+") using 10% gels. Lanes with lysates without PNGase F treatment are indicated by "-". Proteins were detected by western blotting using anti-intra-TMPRSS13 and anti-β-tubulin antibodies. P-glyco-T13, phosphorylated and glycosylated TMPRSS13; Glyco-T13, glycosylated TMPRSS13; Non-glyco-T13, non-glycosylated TMPRSS13. The white arrowheads connected to black arrowheads indicate the mobility shift upon PNGase F treatment.

glycosylation is inhibited by cycloheximide within approximately 30 minutes due to a lack of newly synthesized acceptor polypeptides (212).

Together the results indicate that proper glycosylation of endogenous TMPRSS13 is necessary for its phosphorylation and possibly localization to the cell surface.

3.4 N-linked glycosylation of TMPRSS13 – Discussion

In this study we determined that the N-linked glycosylation of TMPRSS13 in its catalytic SP domain plays an important role in its cell surface localization as well as its function as an enzyme. The process of N-linked glycosylation is highly conserved and occurs on the majority of eukaryotic proteins that are translated across the rough ER (192,213). The functional roles of N-linked glycans are plentiful, including contributions to proper protein folding, protein quality control, intracellular trafficking, and protein stability (213,214). Proteins that are unfolded or misfolded due to a lack of glycosylation are often recognized by ER chaperones and degraded by the ER-associated degradation system (ERAD) (215).

Several TTSP family members are known to harbor N-linked glycosylation sites that are important for their zymogen activation and cellular localization (42,197,199,201). Mutation of N-linked glycosylation sites in the catalytic domain of TMPRSS13 significantly reduces its proteolytic activity, demonstrated by a lack of autoactivation and a decrease in TMPRSS13-mediated prostasin activation cleavage. Furthermore, we show that glycosylation in the SP domain is essential for phosphorylation and cell surface localization. In contrast, mutation of glycosylation sites in the SRCR-domain did not have any significant effects on TMPRSS13 activity and trafficking. This reliance on N-linked glycans for adequate zymogen activation/catalytic activity and cell trafficking has been shown in other TTSPs including corin, hepsin, matriptase, and matriptase-2 (42,197,200,201). Human corin harbors 19 N-glycosylation sites in its extracellular region (216). Corin does not autoactivate; however, N-glycosylation at Asn1022 (N1022), the only N-glycosylation site in the protease domain of human corin, is critical for zymogen activation by proprotein convertase subtilisin/kexin-6 (PCSK6) (201,202,217-219). Abolishing N-glycosylation at N1022 also reduces the cell surface expression of corin (201). Matriptase-2 has seven N-glycosylation sites, but unlike TMPRSS13 and corin, none of these are located in the SP domain (42). Matriptase-2 is capable of autoactivation and mutation of N216Q, N453Q, and N518Q, but not the other mutants, caused impaired zymogen activation. All three of these N-glycosylation

sites are located away from the activation cleavage site. Mutations at two separate N-glycosylation sites in the closely related TTSP, matriptase, one in the CUB domain and another in the SP domain, also impaired matriptase activation (48,200). It was proposed that N-glycans, at least in some cases, do not directly affect substrate binding but may be important for maintenance of a proper protein conformation required for the autoactivation of these TTSPs (48). To this end, the TTSP hepsin, like matriptase-2, has no glycosylation sites in the SP-domain and harbors a single N-glycosylation site at Asn112 in the SRCR domain (197), yet mutation of the SRCR domain site leads to impaired hepsin zymogen activation, intracellular trafficking, and cell surface expression (197).

The requirement of N-glycosylation of a particular protease may depend on its expression level and specific cell environments including presence of cognate inhibitors and/or ER chaperones. Glycosylation in the SP domain of TMPRSS13 is critical for autoactivation, however the precise mechanism is still unknown. For matriptase, it has been proposed to be a transactivation process initiated by interaction between zymogen forms which leads to activation of the protease and that HAI-1 and HAI-2 regulate this trans(auto)-activation (48,220). In HEK293T cells where endogenous TMPRSS13, HAI-1 or HAI-2 proteins ((47) and data in this study) are not detected, autoactivation of recombinant TMPRSS13 and activation of the protein substrate, prostasin, is observed without concomitant expression of HAI-1/HAI-2. Importantly, HAIs are essential for WT-TMPRSS13 trafficking to the cell surface ((47) and data in this study). The impaired N400Q/N440Q-TMPRSS13 transport to the cell surface accompanied by ER/Golgi accumulation was not rescued by co-expression with HAI-2, as shown by both immunocytochemistry and cell surface biotinylation assays. However, no significant impairment of the mutant's ability to bind HAI-2 was detected. It can be speculated that one or more additional binding partners are involved in proper TMPRSS13 trafficking and that binding to these partners is affected by lack of glycans in the SP domain. An example of this was observed in studies of corin where the SP domain N1022Q mutant displayed impaired cell surface localization (199).

Increased binding of the N1022Q mutant to calnexin, a chaperone that specifically acts to retain unfolded or unassembled N-linked glycoproteins in the ER, was observed and it was proposed that N-glycosylation in the protease domain mediates calnexin-assisted protein folding with subsequent ER exiting and transport to the cell surface (199). Studies are underway to identify TMPRSS13 binding partners critical for cellular trafficking.

Importantly, our observations from exogenously-expressed TMPRSS13 in HEK293T cells extend to endogenous forms of TMPRSS13 in cancer cell lines. We detected glycosylated forms of endogenous TMPRSS13 in human cancer cells using tunicamycin inhibition of the N-glycosylation process and PNGase F-mediated removal of N-glycans. These studies revealed the presence of three major forms in total cell lysates which represent non-glycosylated, glycosylated, and glycosylated/phosphorylated TMPRSS13. The observation that the phosphorylated form of TMPRSS13 is not detected upon tunicamycin treatment suggests that N-glycosylation is critical for phosphorylation. The detection of different endogenous glycosylation variants of TMPRSS13 with differential stability and phosphorylation status in breast and colorectal cancer cells is interesting because proteomic/glycomic studies have demonstrated that some cancer-associated proteases exhibit altered glycosylation patterns with functional implications in malignancies. These studies include the secreted kallikrein-related peptidases (KLKs), a family of serine proteases (221,222). For example, changes in KLK3 glycosylation patterns were observed in samples from patients with prostate cancer compared to benign prostatic hyperplasia (223). Furthermore, glycosylation of KLK2 has a significant effect on protease activity against small synthetic substrates (224). Studies of matriptase proposed that the pro-metastatic effect of the cancer-associated glycosyltransferase *N*-Acetylglucosaminyltransferase V (GnT-V) in gastric cancer cells was mediated by modification and stabilization of active matriptase upon addition of β1–6 GlcNAc branching (225). In a follow-up study, analysis of matriptase and GnT-V in thyroid cancer tissues suggested that post-translational modification by GnT-V contributes to regulation of matriptase levels (226). It is plausible that glycosylation of TMPRSS13 is critical for its

demonstrated pro-oncogenic properties (132,169) by modulation of activity, stability, and cell-surface localization and therefore warrants further studies.

TMPRSS13 is unique among the TTSP family members by harboring a long cytoplasmatic tail that is highly disordered and phosphorylated (47). The intracellular domain of TMPRSS13 contains a total of 30 serine residues, 12 threonine residues, and 1 tyrosine residue (47) of which at least 14 are phosphorylated (Martin and List, unpublished data). On the cell surface, the phosphorylated form is the most prevalent, and co-expression of HAI-1 or HAI-2 with WT-TMPRSS13 promotes TMPRSS13 phosphorylation and cell-surface localization (47). It is not yet known whether phosphorylation is required for cell-surface localization or whether phosphorylation exclusively takes place on cell-surface localized TMPRSS13. Therefore, the lack of phosphorylated TMPRSS13 upon tunicamycin treatment may reflect an indirect effect by impairing transport of TMPRSS13 to the cellular compartment where phosphorylation takes place, possibly at the cell-surface. Though posttranslational modification of TMPRSS13 by N-glycosylation occurs in its extracellular region while phosphorylation occurs in its intracellular region, a direct effect of glycosylation on phosphorylation cannot entirely be ruled out. The role that phosphorylation plays in the activity and trafficking of TMPRSS13 is currently under investigation.

Recently, it has been shown that TMPRSS13 has anti-apoptotic properties (132,169) and that the protease promotes cancer progression *in vivo* (132). Furthermore, TTSPs including TMPRSS13 have garnered significant attention in virology because they can enhance viral entry driven by the spike proteins of the highly virulent MERS-CoV, SARS-CoV, and SARS-CoV-2 (137). The active form of TMPRSS13 is expressed in human lung as well as nasal tissue, and siRNA mediated-knockdown of TMPRSS13 in Calu-3 human lung cancer cells resulted in a significant reduction in SARS-CoV-2 replication (137). Therefore, TMPRSS13 with its accessibility on the cell surface represents a candidate target for the development of inhibitors for treating cancer and viral infections.

In summary, this study identifies that the N-linked glycosylation status of the SP domain of TMPRSS13 is critical for its zymogen autoactivation, proteolytic activity towards the protein substrate prostasin, phosphorylation, and cellular localization. These new insights lay the groundwork for future functional and mechanistic studies defining the role of post-translational modifications of TMPRSS13 under various pathophysiological conditions.

3.5 Materials and Methods

3.5.1 Cell lines and culture conditions

HEK293T, COS7, and MDA-MB-468 cells (all from ATCC, Manassas, VA) were cultured in Dulbecco's modified eagle media (Gibco/Thermo Fisher Scientific) supplemented with 10% fetal bovine serum (FBS) (Atlanta Biologicals, Lawrenceville, GA), 10 units/mL Penicillin and 10 µg/mL streptomycin (Gibco, Life Technologies, Grand Island, NY). HCC1937 cells (ATCC) were cultured in RPMI + L-GLUT media (RPMI-1640 media with 2 mM L-glutamine) supplemented with 1.5 g/L sodium bicarbonate, 4.5 g/L glucose, 10 mM HEPES, 1 mM sodium pyruvate, 10% FBS, and 10 units/mL Penicillin and 10 µg/mL streptomycin. BT-20 cells (ATCC) were cultured in Eagle's + NEAA media (Eagle's minimal essential medium with 2 mM L-glutamine and Earle's balanced salt solution adjusted to contain 1.5 g/L sodium bicarbonate, 0.1 mM non-essential amino acids, 1 mM sodium pyruvate, and 10% FBS). DLD1 cells (ATCC) were grown in RPMI 1640 media + L-GLUT media adjusted to contain 10% FBS).

3.5.2 Western blotting

Cultured human cells were washed 3 times with ice-cold PBS and lysed in-well using ice-cold RIPA buffer (150 mM NaCl; 50 mM Tris/HCl, pH 7.4, 0.1% SDS; 1% NP-40) with protease inhibitor cocktail (Sigma Aldrich, St. Louis, MO) and phosphatase inhibitor cocktail (Sigma Aldrich), and cleared by centrifugation at 12,000 x g at 4°C. Protein concentrations were determined using a Pierce BCA Protein Assay Kit (Thermo Fisher Scientific, Waltham, MA). Proteins were separated by SDS-PAGE under reducing conditions using 10% or 4-15% Mini-Protean® gels or Criterion™ TGX midi gels (Bio-Rad) and blotted onto PVDF membranes.

Membranes were blocked with 5% (w/v) dry milk powder in TBS-T (Tris-buffered saline, 0.1% Tween-20) for 1 hour at room temperature and subsequently incubated overnight at 4°C in primary antibodies diluted in 5% dry milk powder/TBS-T. Primary antibodies used for western blotting included rabbit anti-TMPRSS13 raised against a recombinant protein fragment corresponding to a region within amino acids 195 and 562 of human TMPRSS13 (anti-extra-TMPRSS13) (PA5-30935, Thermo Fisher Scientific and Life Technologies, Inc); rabbit anti-TMPRSS13 raised against an epitope within the first 60 amino acids of human TMPRSS13 (anti-intra-TMPRSS13) (ab59862, Abcam, Cambridge, MA); mouse-anti-V5 (R960-25, Thermo Fisher Scientific and Life Technologies, Inc); goat anti-HAI-2 (AF1106, R&D Systems Inc., Minneapolis, MN); mouse anti-prostasin (612173, BD Biosciences, San Jose, CA), rabbit anti-Histone H3 (D1H2, Cell Signaling Technology, Danvers, MA), mouse anti-beta-tubulin (E7-c, Developmental Studies Hybridoma Bank) and mouse anti-beta-actin (NB600-501, Novus Biologicals, Littleton, CO). Secondary antibodies included goat anti-rabbit (12-348, Millipore, Billerica, MA), goat anti-mouse (AP181P, Millipore), and rabbit anti-goat (31403, Thermo Fisher Scientific) HRP-conjugated antibodies. Detection of antibodies was performed using ECL Western Blotting substrate or Super-Signal West Femto Chemiluminescent Substrate (Pierce, Thermo Fisher Scientific). After detection, PVDF membranes were stripped using Restore™ Western Blot Stripping Buffer (Thermo Fisher Scientific) for 15 minutes at room temperature prior to re-probing with a different primary antibody.

3.5.3 Cloning of full-length TMPRSS13 plasmid constructs

WT-TMPRSS13-V5, S506A-TMPRSS13-V5, R320Q-TMPRSS13-V5, and untagged WT-TMPRSS13 and S506A-TMPRSS13 constructs were generated as previously described (47). Point mutations using WT-TMPRSS13-V5 as a template for N250Q-TMPRSS13-V5, N287Q-TMPRSS13-V5, N400Q-TMPRSS13-V5 and N440Q-TMPRSS13-V5 were generated using the Q5® Site-Directed Mutagenesis Kit (New England Biolabs, Ipswich, MA). The N400Q/N440Q-TMPRSS13-V5 mutant plasmid was synthesized by the GenScript company (Piscataway, NJ).

Primers used for N250Q mutagenesis were 5'-CAGCAACTGGCAAGACTCCTACTC-3' and 5'-CTACAGATGGGAAGCCAC-3'. Primers used for N287Q mutagenesis were 5'-CTTGAGATACCAATCCACCATCCAG-3' and 5'- ATTGAGAAGCTGTTGGCAAAATC-3'. Primers used for N400Q mutagenesis were 5'-CATCAACAGCCAATACACCGATGAG-3' and 5'-ATGATCTCGGCAATGGAG-3'. Primers used for N440Q mutagenesis were 5'-CTTTAGCCTCCAAGAGACCTGCTGG-3' and 5'-GTCTGTCCATGCATGGGG-3'. For untagged N400Q/N440Q-TMPRSS13 construct, point mutations were made using WT-TMPRSS13 as a template and primers for N400Q and N440Q mutagenesis. Transformation of all vectors was performed in NEB 5-alpha Competent E. *coli* cells (New England Biolabs) and positive clones were isolated and amplified using standard techniques.

3.5.4 Transient transfections with TMPRSS13 expression vectors

Transfections of HEK293T cells were performed using Lipofectamine® LTX reagent with PLUS™ reagent according to the manufacturer's instructions (Invitrogen, Life Technologies, Inc.). Transfection was performed with 500 ng of plasmid DNA for single transfections or 1 µg of DNA total for co-transfections. Vectors included in transfections were pcDNA3.1-TMPRSS13 vectors, empty vector pcDNA3.1, and pcDNA3.1-HAI-2 (227). The HAI-2 vector was kindly provided by Dr. Stine Friis, University of Copenhagen.

3.5.5 Prostasin/PN-1 complex formation assay

Forward transfection of the mammalian expression vector pIRES2-EGFP containing full-length human prostasin cDNA and TMPRSS13 plasmids (WT, S506A, R320Q, N250Q, N287Q, N400Q, N440Q, N400Q/N440Q) was performed in HEK293T cells. Transfection was performed with 1 µg of total plasmid DNA for co-transfections per well using Lipofectamine® LTX reagent with PLUS™ reagent according to the manufacturer's instructions (Invitrogen, Life Technologies, Inc.). For phosphatidylinositol-specific phospholipase C (PI-PLC) treatment, washed cells were mechanically lifted from the plates by gentle pipetting, incubated with 1 unit/ml PI-PLC (Sigma-Aldrich) in PBS for 4 h at 4°C, then centrifuged for 10 min at 1000 x *g*, and the supernatant

containing the PI-PLC-released proteins was collected. For complex formation, PN-1 derived from murine sperm (described in (211)) was added for 1 h at 37°C in 50 mM Tris, 100 nM NaCl pH 8.5. Proteins were analyzed by reducing SDS-PAGE and western blot analysis.

3.5.6 Tunicamycin and cycloheximide treatment

Tunicamycin (T7765, Sigma Aldrich) was reconstituted in DMSO to a concentration of 10 mg/ml. Cancer cell lines were plated and allowed to adhere to plates and reach ~80% confluence. Cells were subsequently treated with tunicamycin at a final concentration of 1 µg/ml for 48 hours. Vehicle-treated cells received an equivalent volume of DMSO. When tunicamycin treatment was performed with cycloheximide treatment, DLD1 and BT-20 cells were treated for 24 hours with tunicamycin prior to treatment with 75 µg/ml of cycloheximide (C-1189, AG Scientific) for up to 30 hours. Following treatment, cells were washed three times in PBS and lysed in-well using RIPA buffer.

3.5.7 Deglycosylation of TMPRSS13

Proteins in lysates prepared as indicated above were deglycosylated using the PNGase F deglycosylation kit according to the manufacturer's instructions (New England Biolabs).

3.5.8 Biotin labeling of cell surface proteins

48 hours post-transfection, HEK293T cells expressing TMPRSS13, empty vector (EV), and/or HAI-2 constructs were washed three times with PBS. Cells were then gently detached and resuspended in 1.0 mL of PBS, and EZ-Link Sulfo-NHS-SS-Biotin (Thermo Scientific, Waltham, MA) was added for a final concentration of 800 µM. Cells were biotin-labeled for 30 min at room temperature. After biotin labeling, cells were pelleted and the biotinylation reaction was quenched by washing the cells three times with PBS containing 100 mM glycine. Cells were then lysed in RIPA buffer supplemented with protease inhibitor mixture (Sigma), and protein concentrations were quantitated. 120 µg of protein was added to 40 µl of streptavidin-agarose (Sigma) in a final reaction volume of 200 µl and rotated at 4°C for 60 min. Beads were pelleted by centrifugation at 800 × g, and supernatant containing non-biotinylated proteins was collected (wash). Beads were

washed five times with cold PBS and subsequently treated with 60 µl of Laemmli sample buffer with 5% 2-mercaptoethanol and boiled for 5 minutes prior to SDS-PAGE.

3.5.9 Immunoprecipitation

48 hours post-transfection, HEK293T cells expressing TMPRSS13, empty vector (EV), and/or HAI-2 were lysed with RIPA lysis buffer with protease inhibitor mixture. 1 µl of primary mouse anti-V5 (R960-25, Thermo Fisher Scientific) was added to 150 µg of protein lysates, and lysis buffer was added for a total reaction volume of 250 µl. Lysates were then rotated at 4°C for 60 minutes. After immunoprecipitation, 30 µl of EZview™ Red Protein A affinity gel (Sigma) were added to the reaction per the manufacturer's protocol. Samples were then rotated at 4°C for 60 minutes, then beads were pelleted at 4°C and washed five times with cold PBS, pH 7.5. After the final wash, 60 µl of 2x Laemmli buffer with 5% 2-mercaptoethanol was added, and samples were analyzed by SDS-PAGE and western blotting.

3.5.10 Immunocytochemistry

Cell imaging was performed using HEK293T cells transfected with human full-length TMPRSS13 vectors, empty vector pcDNA3.1, or HAI-2-EYFP (enhanced yellow fluorescent protein) (228). Cells were seeded on coverslips and allowed to adhere and grow overnight. Cells were transiently transfected, and 48 h post transfection, media was removed and cells were fixed in Z-Fix (ANATECH LTD, Battle Creek, MI) for 15 min at room temperature. For permeabilized samples, cells were treated with 0.05% Triton X-100 in PBS for 15 min on ice. Cells were then blocked in 5% BSA in PBS for 1 h prior to addition of primary antibodies. TMPRSS13-V5 was detected using a monoclonal anti-V5 antibody (Invitrogen, Life Technologies, Inc.) or an isotype control antibody. KDEL was detected using a monoclonal anti-KDEL antibody (PA1-013, Invitrogen, Life Technologies, Inc.) or an isotype control antibody. After incubation with primary antibodies overnight at 4°C, cells were washed in PBS and secondary Texas Red-conjugated goat anti-mouse and AlexaFluor-647-conjugated goat anti-rabbit antibodies (Invitrogen, Life Technologies, Inc.) were used to detect TMPRSS13-V5 or KDEL. Cells were washed with PBS

and mounted with ProLong™ Diamond Antifade Mountant with DAPI (Invitrogen). Confocal images were acquired on the Leica SP5 scope at the Microscopy Imaging and Cytometry Resources Core at Wayne State University School of Medicine. Acquired permeabilized images were pseudo-colored and merged using ImageJ image analysis (229).

3.5.11 Statistical analyses

GraphPad Prism software was used for all statistical analyses. For statistical comparisons between three or more groups, one-way ANOVA was used with Dunnett's post hoc analysis. For statistical comparisons between two groups, student's T-test was used. All statistical analyses are representative of at least three biological replicates.

CHAPTER 4: STEM DOMAIN CLEAVAGE OF TMPRSS13

A manuscript containing this research (Chapter 4) has been submitted for publication.

4.1 Abstract

TMPRSS13 is a member of the type II transmembrane serine protease (TTSP) family comprised of seventeen family members in humans. We have previously shown that TMPRSS13 is capable of autoactivation, and that glycosylation plays a critical role in regulation of TMPRSS13 activity, phosphorylation, and cell surface localization. Here we characterize a novel post-translational mechanism important for TMPRSS13 function: proteolytic cleavage within the extracellular TMPRSS13 stem region located between the transmembrane domain and the first site of N-linked glycosylation at asparagine (N)-250 in the scavenger receptor cysteine rich (SRCR) domain. Importantly, the catalytic competence of TMPRSS13 is essential for stem region cleavage, suggesting an autonomous mechanism of action. Site-directed mutagenesis of the ten basic amino acids (four arginine and six lysine residues) in this region abrogated zymogen activation and catalytic activity of TMPRSS13, as well as phosphorylation, cell surface expression, and shedding. Mutation analysis of individual arginine residues identified R223, a residue located between the low-density lipoprotein receptor class A domain and the SRCR domain, as important for stem region cleavage. Mutation of R223 causes a reduction in the aforementioned functional processing steps of TMPRSS13. These data provide further insight into the roles of different post-translational modifications as regulators of the function and localization of TMPRSS13. Additionally, the data suggest the presence of complex interconnected regulatory mechanisms that may serve to ensure the proper levels of cell-surface and pericellular TMPRSS13-mediated proteolysis under homeostatic conditions.

4.2 Stem domain cleavage of TMPRSS13 – Introduction

The type II transmembrane serine proteases (TTSPs) are single-pass transmembrane proteins with an intracellular N-terminus and an extracellular C-terminal catalytic serine protease (SP)-domain, which are synthesized as zymogens requiring cleavage at a canonical site for

activation (29,33,34,37,40,183,230). TTSPs also harbor an extracellular stem region between the transmembrane domain and the SP-domain composed of various types and combinations of protein domains. TTSPs are divided into four subfamilies, based on phylogenetic analyses of their SP- domains and the domain structure of their extracellular stem regions (1,29,33,34,37-40,183,230). TMPRSS13 (for Transmembrane Protease, Serine 13, also known as Mosaic Serine Protease Large-Form (MSPL) (127,128)) belongs to the hepsin/TMPRSS subfamily. The stem region in TMPRSS13 contains a group A scavenger receptor cysteine-rich (SRCR) domain, preceded by a single low-density lipoprotein receptor class A (LDLA) domain (47,128,182). Studies of TMPRSS13-deficient mice have demonstrated its importance for proper formation of the cornified layer of the skin, for epidermal barrier function, and hair growth (129). In malignancies, TMPRSS13 transcript and protein levels are significantly elevated in colorectal and breast cancer (132,169). Furthermore, loss of TMPRSS13 expression in a genetic model of mouse mammary carcinoma led to a significant delay in detectable tumor formation, a reduction in tumor burden, and increased overall survival (132). TMPRSS13 has also been implicated in the promotion of viral infections, including highly pathogenic avian influenza (HPAI) viruses, influenza A and B (IAV and IBV), and SARS-CoV-2 (134-137,231). In HPAI, TMPRSS13 cleaves viral hemagglutinin (HA) and in SARS-CoV-2, TMPRSS13 can activate the spike protein to facilitate viral entry (134,135,137,231). TMPRSS13 is also capable of cleaving IAV H3 and IBV HA (136).

We have previously shown that TMPRSS13 is post-translationally modified via three different mechanisms affecting function: 1) N-linked glycosylation of the SRCR-domain and the SP-domain, 2) proteolytic autoactivation of the zymogen form, and 3) phosphorylation in the intracellular domain (47,182). In this study, a novel modulatory *mechanism* of TMPRSS13 function executed by proteolytic cleavage within its stem region was identified using site-directed mutagenesis. A comprehensive characterization of its effects on TMPRSS13 zymogen activation,

activity, intracellular phosphorylation, cell-surface trafficking, and shedding into the extracellular space was performed.

4.3 Stem domain cleavage of TMPRSS13 – Results

4.3.1 TMPRSS13 is cleaved in its extracellular stem region in a manner dependent on its own catalytic competence

In two previously published studies, we observed a low molecular weight (LMW) form of TMPRSS13 that, based on its molecular weight and glycosylation mapping analyses, was predicted to represent an N-terminal fragment of the protease following proteolytic cleavage at a site between the transmembrane (TM) domain and the first N-glycosylated residue (N250 in the SRCR-domain) (47,182). Importantly, the LMW form was not detected in the catalytically dead TMPRSS13 (S506A-TMPRSS13) mutant which pointed to *the possibility* that the LMW form was generated by autocleavage (47,182). To validate the identity of this LMW form and to identify the functional importance of cleavage in the extracellular stem region of TMPRSS13, site-directed mutagenesis of human full-length TMPRSS13 was used followed by expression in HEK293T cells and western blot analysis. Previous amidolytic studies of TMPRSS13 substrate preferences using recombinant soluble TMPRSS13 indicated that peptides harboring arginine or lysine at position P1 can be cleaved, but cleavage after arginine is more efficient (128). The canonical zymogen auto-activation site for TMPRSS13 has an arginine residue in the P1 position as do published protein substrates of TMPRSS13. These include the mammalian pro-forms of the prostasin serine protease and hepatocyte growth factor, as well as HA in influenza viruses (130,132,231,232). Based on this information, we individually mutated the four arginine residues located between the TM and SRCR domains to glutamine (R191Q, R196Q, R205Q, R223Q) (**Fig. 10A**). In addition, a ten-site TMPRSS13 mutant (denoted "RK-TMPRSS13") was also constructed, which has the four previously indicated arginine residues mutated to glutamine as well as the six additional lysine residues within the predicted stem region cleavage sequence (K193Q, K201Q, K213Q, K215Q, K228Q, K232Q) (**Fig. 10A, panel II**). Finally, a reverse-mutant was generated with one arginine

residue restored at position 223 (Q223R) in the RK-TMPRSS13 ten-site mutant, as the R223Q single-mutant displayed diminished stem region cleavage and functional phenotypes (**Fig. 10A, panel III**). The V5-tagged mutants were transfected into HEK293T cells, alongside empty vector PCDNA3.1 (EV), WT-TMPRSS13-V5 (standard for TMPRSS13 zymogen-activation and stem region cleavage), S506A-TMPRSS13-V5 (catalytically dead; the serine residue in the catalytic triad is mutated to alanine (47)), and R320Q-TMPRSS13-V5 (zymogen locked; the zymogen activation site is mutated to glutamine (47)). Whole cell lysates (**Fig. 10**) and conditioned media (**Fig. 11**) were collected from these transfected cells and proteins were separated by SDS-PAGE under reducing conditions. These conditions caused the disulfide bond that links the cleaved SP-domain to the TMPRSS13 stem region to be disrupted, allowing for the released, active SP-domain to be detectable by western blotting. As previously detailed, TMPRSS13 was detected with two antibodies directed against different TMPRSS13 epitopes: one that recognizes amino acids 195-562 (extracellular; α-extra-TMPRSS13), and one that recognizes amino acids 1-60 (intracellular; α-intra-TMPRSS13) (47,182) (**Fig. 10A, panel I**). Using these two different antibodies, activation status of WT-TMPRSS13 and mutants can be assessed, resulting from cleavage at the R320 zymogen activation site concomitantly with stem region cleavage (N-terminal and C-terminal fragments are recognized with α-intra-TMPRSS13 and α-extra-TMPRSS13, respectively).

As we have described previously (47,182), S506A- and R320Q-TMPRSS13 are highly phosphorylated, represented by a band ~95 kDa when detected with α-intra-TMPRSS13 (**Fig. 10B, Band 1**). This high molecular weight (HMW) band is undetectable (or at very low levels) in WT-TMPRSS13 and in the stem region cleavage site mutants. We have shown that phosphorylation of WT-TMPRSS13 is increased upon co-expression with the cognate inhibitor hepatocyte growth factor activator inhibitors (HAI)-1 or HAI-2 (47,182). For HAI-2 co-expression analyses of TMPRSS13 mutants see Fig. 13.

Full-length, non-phosphorylated TMPRSS13 at ~72 kDa is observed (**Fig. 10B, Band 2**) in all TMPRSS13 constructs. A band at ~43 kDa is observed in WT-TMPRSS13 and is proposed to represent the intracellular portion of the protease following cleavage at R320 for zymogen activation and SP domain release (**Band 3**), which is in accordance with our previous published study (182). This form is also readily detected in the R191Q, R196Q, and R205Q single mutants. The LMW species ~26 kDa, proposed to be the intracellular portion of TMPRSS13 following cleavage at the stem region cleavage site, is also observed in WT-TMPRSS13 as well as in R191Q, R196Q, R205Q indicating that mutation in any single of these three arginine residues does not lead to significant impediment of LMW generation. In accordance with our previous observations (47,182), the catalytic activity of TMPRSS13 is important for the generation of the LMW form since decreased detection of the LMW form in catalytically dead S506A-TMPRSS13 expressing cells compared to WT-TMPRSS13 was consistently observed (**Fig. 10B-C**). Importantly, the R320Q mutation caused a reduction in the level of the LMW and 43 kDa forms compared to WT-TMPRSS13 (**Fig. 10B-C**). In the RK-TMPRSS13 ten-site mutant, the levels of detected LMW and the 43 kDa form were negligible (at a level comparable to that observed in S506A-TMPRPRSS13 mutant). To further validate that R223 is important for stem region cleavage, the reverse mutant Q223R in the ten-site mutant was included (**Fig. 10B**). Both the 43 kDa form and the LMW form are detected, which indicates a partial rescue of zymogen- and stem region cleavage when this site is intact. Another interesting observation was that the zymogen-locked (R320Q) mutant of TMPRSS13 displayed higher levels of LMW than the catalytically dead form (S506A) (**Fig. 10B**). It has been shown that the zymogen form of matriptase is biologically active (having an apparent catalytic activity of ~3% of that of activated matriptase) and is able to autoactivate (51,220,233). It is plausible that TMPRSS13 zymogen too displays a low level of catalytic activity, however this hypothesis awaits further study.

When parallel western blots were probed with the α-extra-TMPRSS13 antibody (**Fig. 10D**), HMW phosphorylated forms (**Band 1**) and the and non-phosphorylated full-length

Figure 10: TMPRSS13 harbors a cleavage site in its extracellular domain
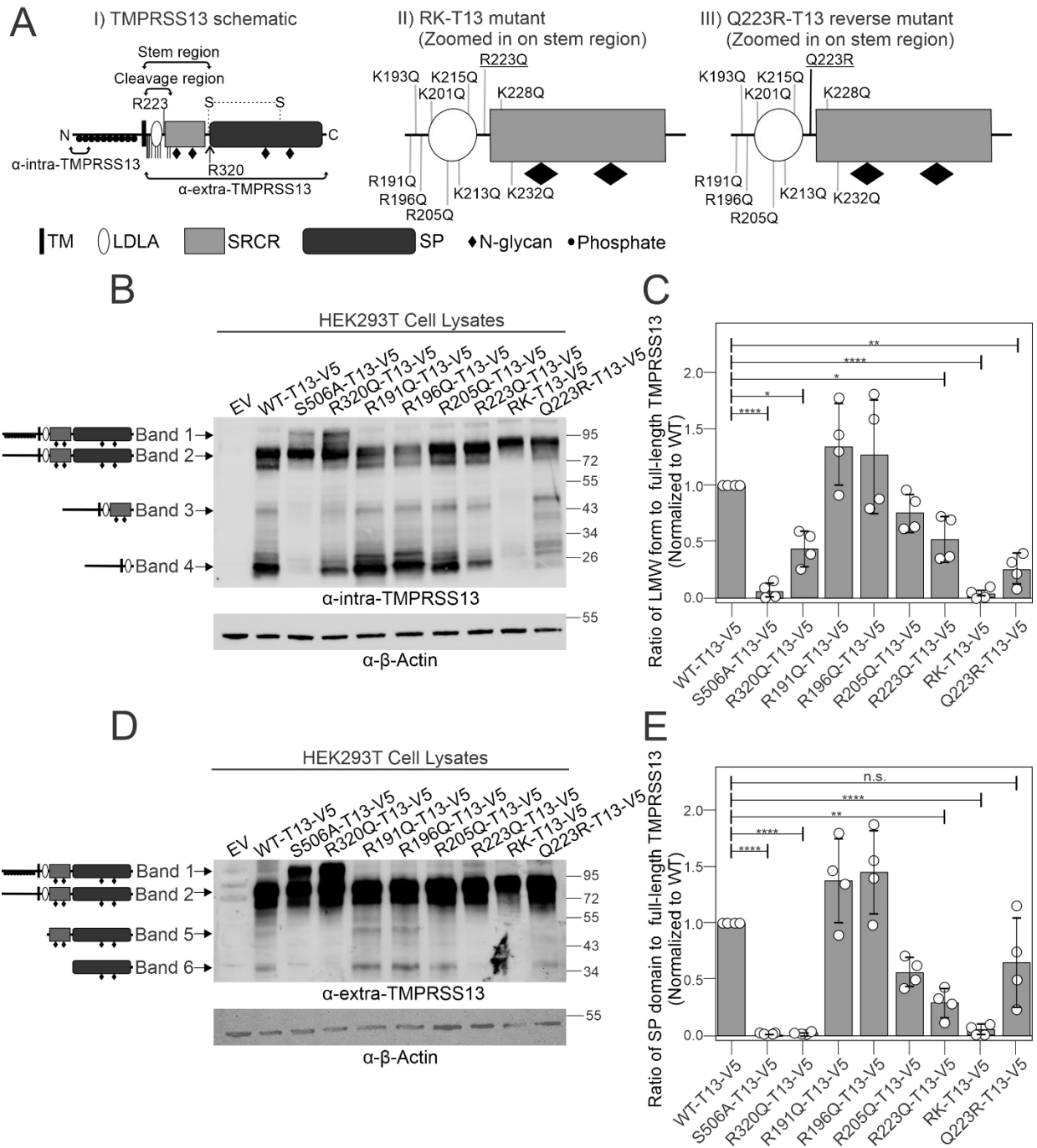
Figure 10. A) Schematics of TMPRSS13. I) Epitopes for anti-intra-TMPRSS13 and anti-extra-TMPRSS13 antibodies. Filled circles indicate phosphorylated residues in the intracellular domain. Filled diamonds indicate sites of N-linked glycosylation. Black vertical lines indicate wild-type arginine/lysine residues between the TM domain and the first glycosylated residue, N250. The zymogen activation site R320 is denoted with an arrow. Dotted lines indicate the disulfide bridge linking the SP domain to the stem region. II) Schematic of the RK-TMPRSS13 mutant, zoomed in to expand the stem region between the TM and LDLA domains. Gray vertical lines indicate ten

arginine/lysine residues that have been mutated to glutamine. R223Q is underlined. III) Schematic of the Q223R-TMPRSS13 reverse mutant, zoomed in to expand the stem region between the TM and LDLA domains. Gray vertical lines indicate nine arginine/lysine residues that have been mutated to glutamine and the black vertical line indicates wild-type R223. Q223R is underlined. TM, transmembrane domain; LDLA, low-density lipoprotein receptor class A domain; SRCR, group A scavenger receptor cysteine-rich domain; SP, serine protease domain. **B and D)** HEK293T cells were transfected for 48 hours with empty vector (EV) PCDNA3.1, WT-TMPRSS13 (T13)-V5, S506A-T13-V5, R320Q-T13-V5, R191Q-T13-V5, R196Q-T13-V5, R205Q-T13-V5, R223Q-T13-V5, RK-T13-V5 and Q223R-T13-V5. Proteins in whole cell lysates were separated by SDS-PAGE under reducing conditions using 10% gels and analyzed by western blotting. Proteins were detected using **(A)** anti-intra-TMPRSS13, **(D)** anti-extra-TMPRSS13, or anti-beta-actin antibodies. Arrows and schematics to the left of the western blots define the TMPRSS13 form that is detailed in the text. **C)** Bar graph showing the ratio of expression of the LMW form to full-length TMPRSS13 protein, normalized to WT-TMPRSS13. Error bars represent standard deviation. One way ANOVA with Dunnett's multiple comparisons post hoc test was used to determine the significance of the released SP-domain as compared with WT-TMPRSS13. Results for four biological replicates are shown. LMW, low-molecular weight. **E)** Bar graph showing the ratio of released SP-domain to full-length TMPRSS13 protein, normalized to WT-TMPRSS13. Error bars represent standard deviation. One way ANOVA with Dunnett's multiple comparisons post hoc test was used to determine the significance of the released SP-domain as compared with WT-TMPRSS13. Results for four biological replicates are shown.   * $p \leq 0.05$, **$p \leq 0.01$, ****$p \leq 0.0001$, n.s. not significant.

TMPRSS13 form (**Band 2**) were both observed similarly to the α-intra-TMPRSS13 blot (**Fig. 10B**).

The form detected at ~55 kDa in WT, R191Q, R196Q, and R205Q TMPRSS13 (**Band 5**) is

predicted to be the extracellular C-terminal fragment of TMPRSS13 following cleavage at R223

in the stem region. Importantly, the released SP-domain, indicative of active site cleavage, is

significantly reduced in R223Q relative to full-length TMPRSS13 when compared to WT-

TMPRSS13 (**Fig. 10D and 10E**). In the reverse Q223R mutant, the level of SP-domain release is

rescued to a level that is not statistically different from WT-TMPRSS13. To verify that the SP-

domain represents a catalytically active form of TMPRSS13, an amidolytic assay was performed

using the conditioned media from WT and mutant TMPRSS13 (see section below and Figure 2).

These data indicate that mutation of the ten arginine/lysine residues between the TM-

domain and N250 impedes activation-cleavage of TMPRSS13 to a level comparable to

catalytically dead (S506A) TMPRSS13. Reversal of just one residue, Q223, into wild-type arginine

in the RK-TMPRSS13 mutant re-establishes TMPRSS13 activation. Mutation of R223 alone

(R223Q-TMPRSS13) significantly reduces zymogen cleavage, however not to the level of

catalytically dead TMPRSS13. This indicates that R223 is a preferred stem region cleavage site, but in its absence an alternative site might be employed or that non-cleaved TMPRSS13 has base level proteolytic activity.

4.3.2 Cleavage at R223 is critical for TMPRSS13 amidolytic activity and for shedding into conditioned media

As several TTSP family members are known to harbor extracellular cleavage sites important for shedding into the extracellular milieu (42,234-237), we investigated the potential role of R223 for the release of active TMPRSS13 into the media. HEK293T cells were transfected with EV, WT-TMPRSS13, and mutant TMPRSS13 plasmids. Proteins released from the cells into serum-free media were separated by SDS-PAGE and analyzed by western blotting (**Fig. 11A**) using the α-extra-TMPRSS13 antibody. The SP-domain was detected in the conditioned media from cells transfected with WT, and the single-mutants R191Q, R196Q, and R205Q. Very low levels of the SP-domain were released from R223Q-TMPRSS13 and no detectable SP-domain was observed in conditioned media from RK-TMPRSS13 expressing cells (**Fig. 11A**). Similar to the observation in the cell lysates, reversal of Q223 to R223 in RK-TMPRSS13 led to a rescue of released SP-domain. Notably, a ~55 kDa band was observed in the conditioned media sample from R320Q-transfected cells. As this mutant is locked in its zymogen state, we hypothesize that this shed form results from cleavage at R223, but due to the inability of this mutant to be cleaved at R320, it represents the entire extracellular portion of TMPRSS13 following R223 cleavage. No shed forms were observed in conditioned media from cells expressing catalytically dead S506A-TMPRSS13, likely due to the lack of cleavage at either R223 or R320, thereby prohibiting shedding. Conversely, because WT-TMPRSS13 and the various cleavage mutants harbor a non-mutated zymogen activation site, any shed form of TMPRSS13 resulting from cleavage at R223 is subsequently cleaved at R320, thus allowing for observation of the released SP-domain in the media.

Figure 11: Non-zymogen cleavage of TMPRSS13 allows for shedding of the active serine protease domain
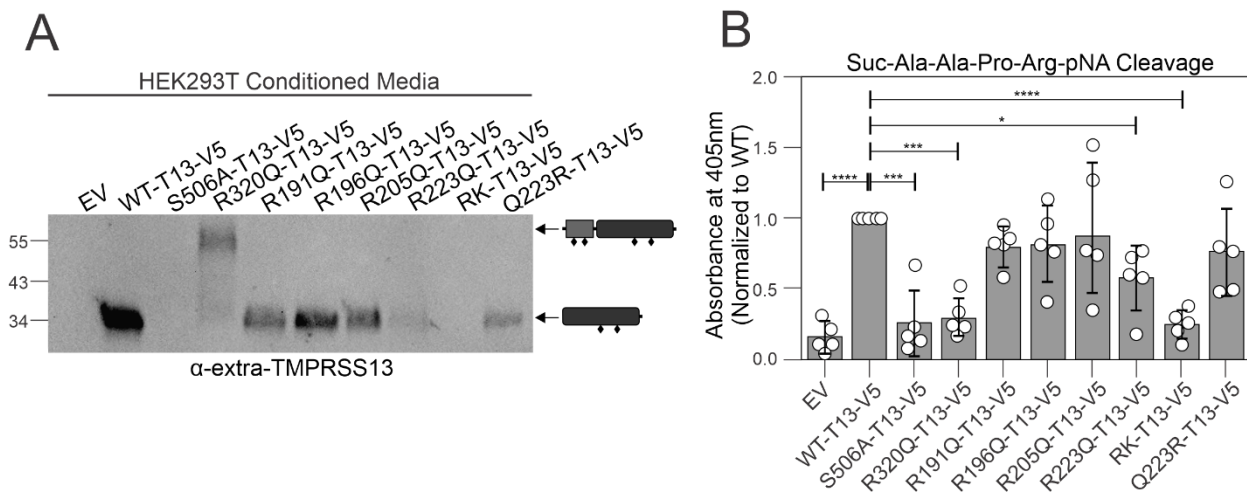
Figure 11. A) HEK293T cells were transfected for 48 hours with empty vector (EV) PCDNA3.1, WT-TMPRSS13 (T13)-V5, S506A-T13-V5, R320Q-T13-V5, R191Q-T13-V5, R196Q-T13-V5, R205Q-T13-V5, R223Q-T13-V5, RK-T13-V5 and Q223R-T13-V5. 24 hours after transfection, cells were serum-starved and conditioned media was collected the following day. Proteins in conditioned media were separated by SDS-PAGE under reducing conditions using 10% gels and analyzed by western blotting. Proteins were detected using the anti-extra-TMPRSS13 antibody. Arrows and schematics to the right of the western blot define the SP domain and SP domain + stem region as detailed in the text. **B)** Conditioned media from transfected HEK293T cells was incubated for 120 minutes at 37 °C with the chromogenic peptide substrate Suc-Ala-Ala-Pro-Arg-pNA (100 µM). Bar graph represents the absorbance at 405 nm after 120 minutes (with absorbance of serum-free DMEM plus substrate (negative control) subtracted), normalized to WT-TMPRSS13. Error bars represent standard deviation. One way ANOVA with Dunnett's multiple comparisons post hoc test was used to determine the significance of the chromogenic substrate cleavage as compared with WT-TMPRSS13. Results for five biological replicates are shown. *$p \leq 0.05$, ***$p \leq 0.001$, ****$p \leq 0.0001$, n.s. not significant.

To verify that the shed SP-domain of TMPRSS13 represents a catalytically active form of the protease, a chromogenic assay to measure amidolytic activity towards a synthetic peptide substrate was employed (47,128). Conditioned media from EV-transfected cells, as well as S506A-TMPRSS13 and R320Q-TMPRSS13 transfected cells showed significantly reduced substrate cleavage as expected when compared to WT-TMPRSS13. Conditioned media harvested from cells transfected with the R223Q and RK ten-site mutants also showed significantly diminished catalytic ability, while reverse mutation of Q223R rescued this loss of

proteolytic activity to a level not significantly different from WT-TMPRSS13 (**Fig. 11B**). Together, these data support the conclusions reached from the western blot analysis of released SP-domain in lysates as a readout of catalytically active TMPRSS13 and suggest that cleavage in the stem region is important for activation and shedding of the protease.

4.3.3 A cleaved form of endogenous TMPRSS13 is detected in human cancer cells

Endogenous TMPRSS13 is expressed in cell lines derived from breast cancer (47,132,182). To examine whether endogenous cleavage fragments were detected in cancer cells, TMPRSS13 expression analysis in control cells and in cells with transient knock-down (KD) using two non-overlapping siRNAs in four different breast cancer cell lines was performed. The cell lines included the estrogen receptor (ER)/progesterone receptor (PR) negative and HER2-postive breast cancer cell line HCC1954 (**Fig. 12A**), the triple negative breast cancer cell lines BT-20 (**Fig. 12B**) and HCC1937 (**Fig. 12C**) and the ER/PR-positive breast cancer cell line MCF-7 (**Fig. 12D**). Proteins from whole cell lysates were separated by SDS-PAGE under reducing conditions followed by western blot analysis using the α-intra-TMPRSS13 antibody. In control cells, a LMW band at ~26 kDa was observed which was not detected in TMPRSS13 KD cells, indicating that it is a TMPRSS13-derived fragment that likely represents the N-terminus fragment of a stem-region cleaved form similar to the one observed in TMPRSS13 transfected HEK293T cells. These observations suggest that endogenous TMPRSS13 is cleaved in its stem region and that the cleavage fragments observed in the HEK293T cell exogenous expression model reflect a biologically relevant post-translational modification.

4.3.4 Cleavage at R223 allows for phosphorylation and cell surface localization of TMPRSS13

TMPRSS13 activity needs to be regulated by co-expression with either of its cognate inhibitors HAI-1 or HAI-2, or rendered inactive by mutagenesis of its active site or zymogen activation site in order to become highly phosphorylated and to efficiently localize to the cell surface (47,182). To explore the importance of stem region cleavage for phosphorylation and cell

Figure 12: Endogenously-expressed TMPRSS13 harbors an additional cleavage site
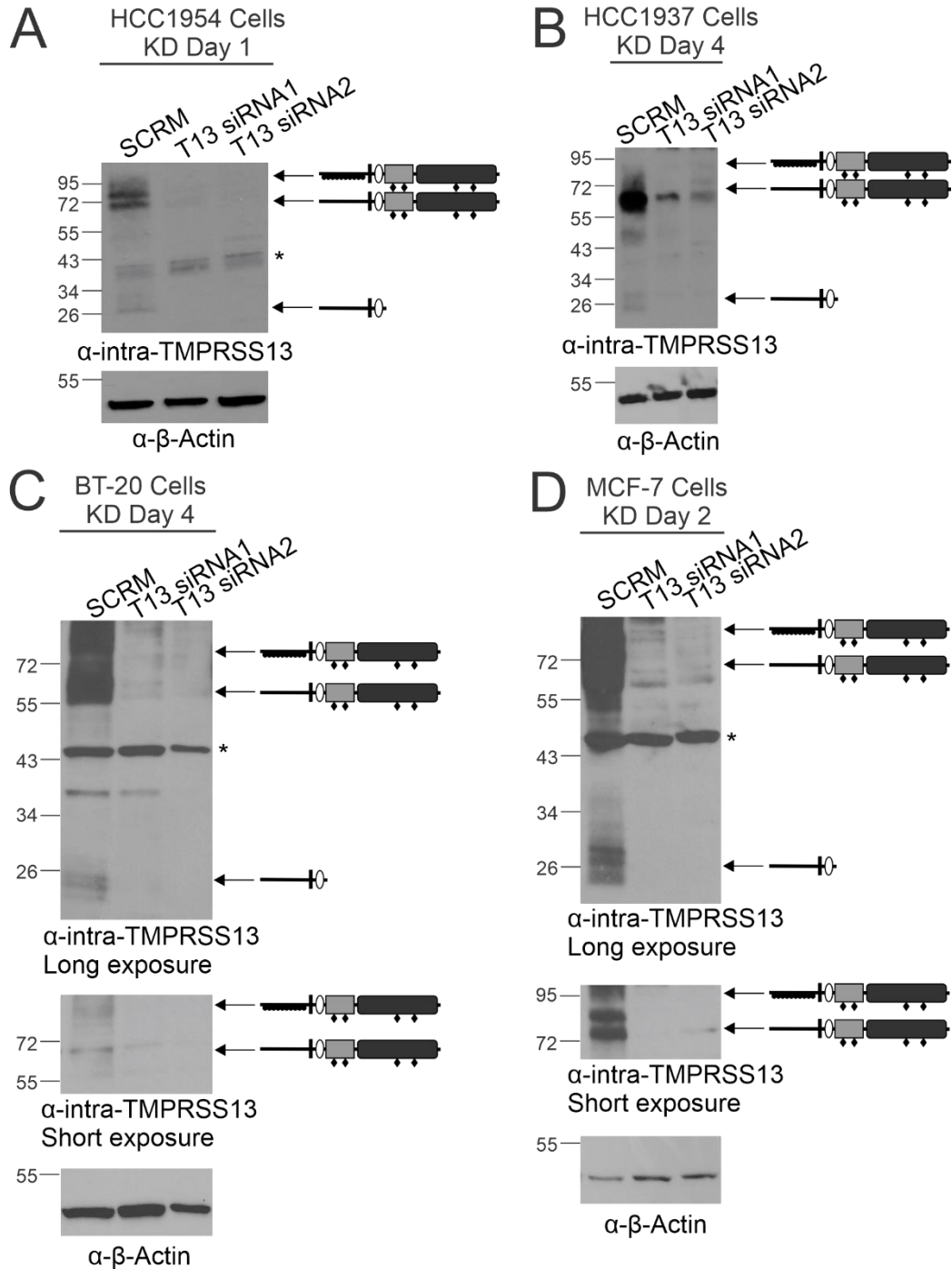
Figure 12. A) HCC1954, **B)** HCC1937, **C)** BT-20, and **D)** MCF-7 cells were treated with two non-overlapping siRNA constructs targeting the TMPRSS13 transcript (siRNA1 and siRNA2) or a %GC matched negative control (scramble, SCRM). On the specified days post-gene knockdown, lysates were harvested and proteins were separated by SDS-PAGE under reducing conditions on 10% gels and analyzed by western blotting. Proteins were detected using anti-intra-

TMPRSS13 or anti-beta-actin antibodies. Arrows and schematics to the right of the western blot indicate the full length-phosphorylated form, full-length non-phosphorylated form, and low-molecular weight form resulting from stem domain cleavage of TMPRSS13, as detailed in the text. Asterisks indicate non-specific bands.

surface localization, respectively, western blot analysis and immunocytochemistry using WT and mutant forms of TMPRSS13 in HEK293T cells was performed. As expected, when WT-TMPRSS13 is co-transfected with HAI-2 or when S506A-TMPRSS13 is co-transfected with empty vector (EV), the HMW phosphorylated form of TMPRSS13 is detected in whole-cell lysates (**Fig. 13**). In contrast, R223Q and RK-TMPRSS13 transfected in the presence or absence of HAI-2 does not lead to detectable levels of the HMW phosphorylated form of TMPRSS13. Notably, in the reverse mutant Q223R, there is a reappearance of the HMW phosphorylated form of TMPRSS13 when co-transfected with HAI-2 (**Fig. 13**), suggesting that cleavage at R223 is important for phosphorylation of TMPRSS13.

Previously published work has indicated a role for phosphorylation in the cell surface localization of TMPRSS13, where the predominant form of TMPRSS13 observed on the cell surface is highly phosphorylated (47,182). Immunofluorescent cell staining was performed to investigate the cell surface localization of the TMPRSS13 cleavage mutants. HEK293T cells were transfected with TMPRSS13 constructs, together with either EV or HAI-2. Nonpermeabilized cells were used (**Fig. 14**) to visualize cell-surface TMPRSS13 only whereas permeabilized cells were used (**Fig. 15**) to co-stain with the endoplasmic reticulum marker, KDEL. Neither TMPRSS13 nor HAI-2 were detected in cells transfected with EV alone (**Fig. 14A** and **Fig. 15A**). In line with previously published data (47,182), WT-TMPRSS13 was not detected at the cell surface in nonpermeabilized cells when co-expressed with EV, while it was detected at the surface localized in the presence of HAI-2 (**Fig. 14B-C** and **Fig. 15B-C**). R223Q and RK-TMPRSS13 were undetectable or detected at very low levels at the cell surface in the presence or absence of HAI-2 (**Fig. 14D-G**), and instead co-localized with KDEL intracellularly (**Fig. 15D-G**) in permeabilized

Figure 13: Cleavage at R223 is critical for TMPRSS13 phosphorylation
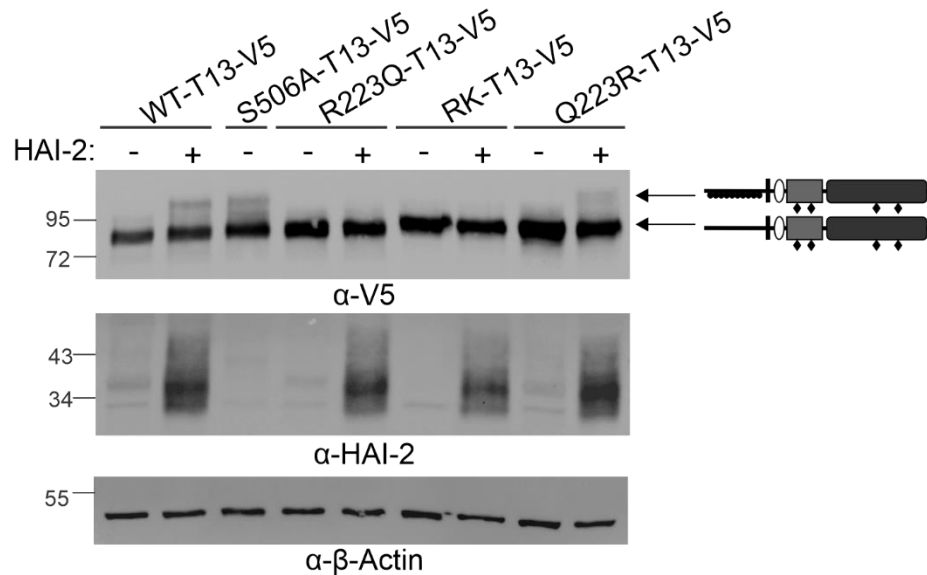
Figure 13. HEK293T cells were transfected for 48 hours with WT-T13-V5, S506A-T13-V5, R223Q-T13-V5, RK-T13-V5 and Q223R-T13-V5 in combination with empty vector (EV) or HAI-2. Proteins in whole cell lysates were separated by SDS-PAGE under reducing conditions using 10% gels and analyzed by western blotting. Proteins were detected using anti-V5, anti-HAI-2, or anti-beta-actin antibodies. Arrows and schematics to the right of the western blot indicate the full length-phosphorylated form and full-length non-phosphorylated form of TMPRSS13 as detailed in the text.

Figure 14: Cell surface localization of TMPRSS13 cleavage mutants
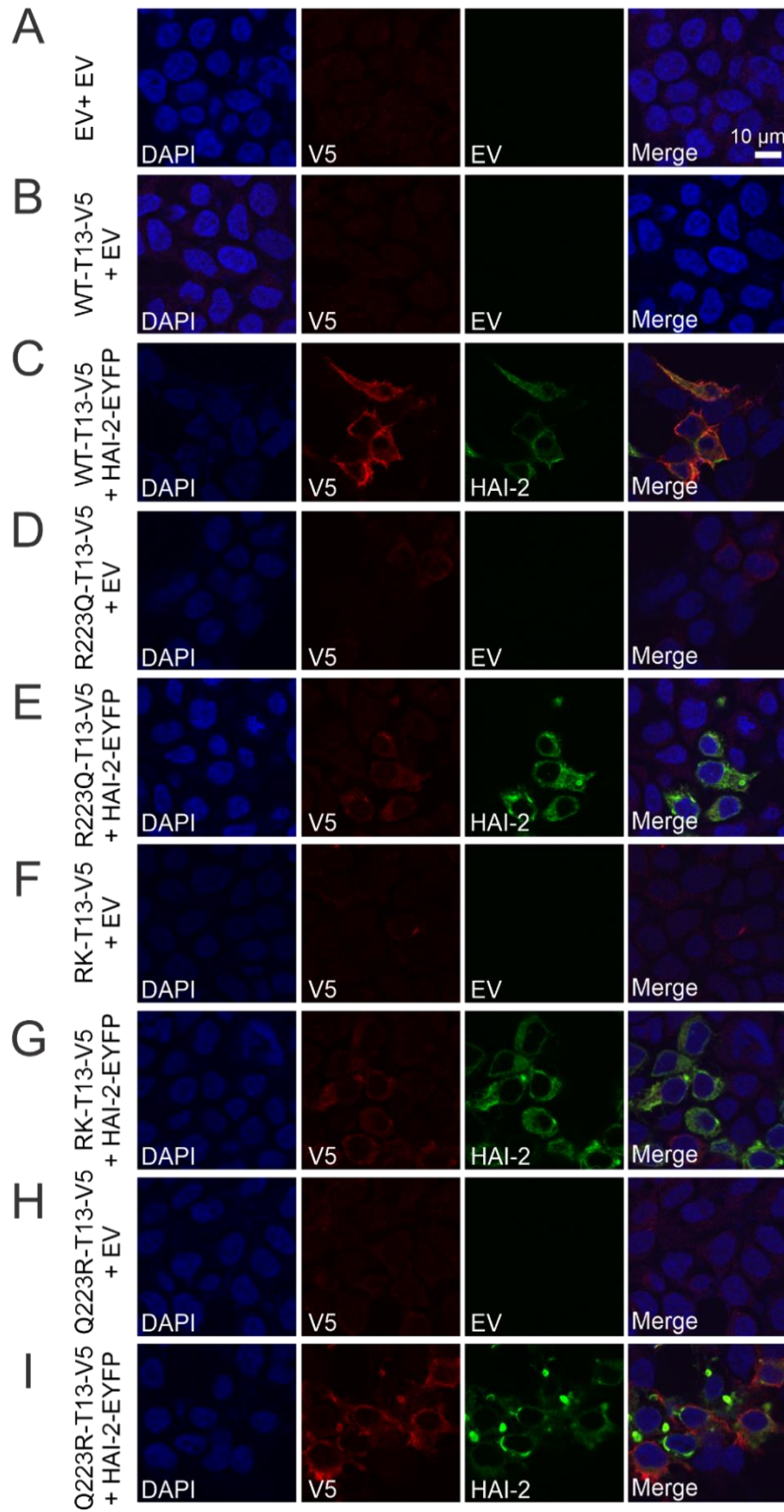
Figure 14: HEK293T cells were plated onto glass coverslips and 24 hours after plating were transfected for 48 hours with **(A)** EV + EV, **(B)** WT-T13-V5 + EV, **(C)** WT-T13-V5 + HAI-2-EYFP,

(D) R223Q-T13-V5 + EV, **(E)** R223Q-T13-V5 + HAI-2-EYFP, **(F)** RK-T13-V5 + EV, **(G)** RK-T13-V5 + HAI-2-EYFP, **(H)** Q223R-T13-V5 + EV, **(I)** Q223R-T13-V5 + HAI-2-EYFP. Cells were fixed onto coverslips and incubated with anti-V5 to detect TMPRSS13. Coverslips were mounted to slides with DAPI-containing mounting media to detect nuclei. Nuclei=blue, panels A-I. TMPRSS13-V5=red, panels A-I. HAI-2-EYFP=green, panels C, E, G, and I. Merged images are shown in panels on the right. Scale bar measures 10 µm.

Figure 15: Abrogation of R223 cleavage retains TMPRSS13 intracellularly
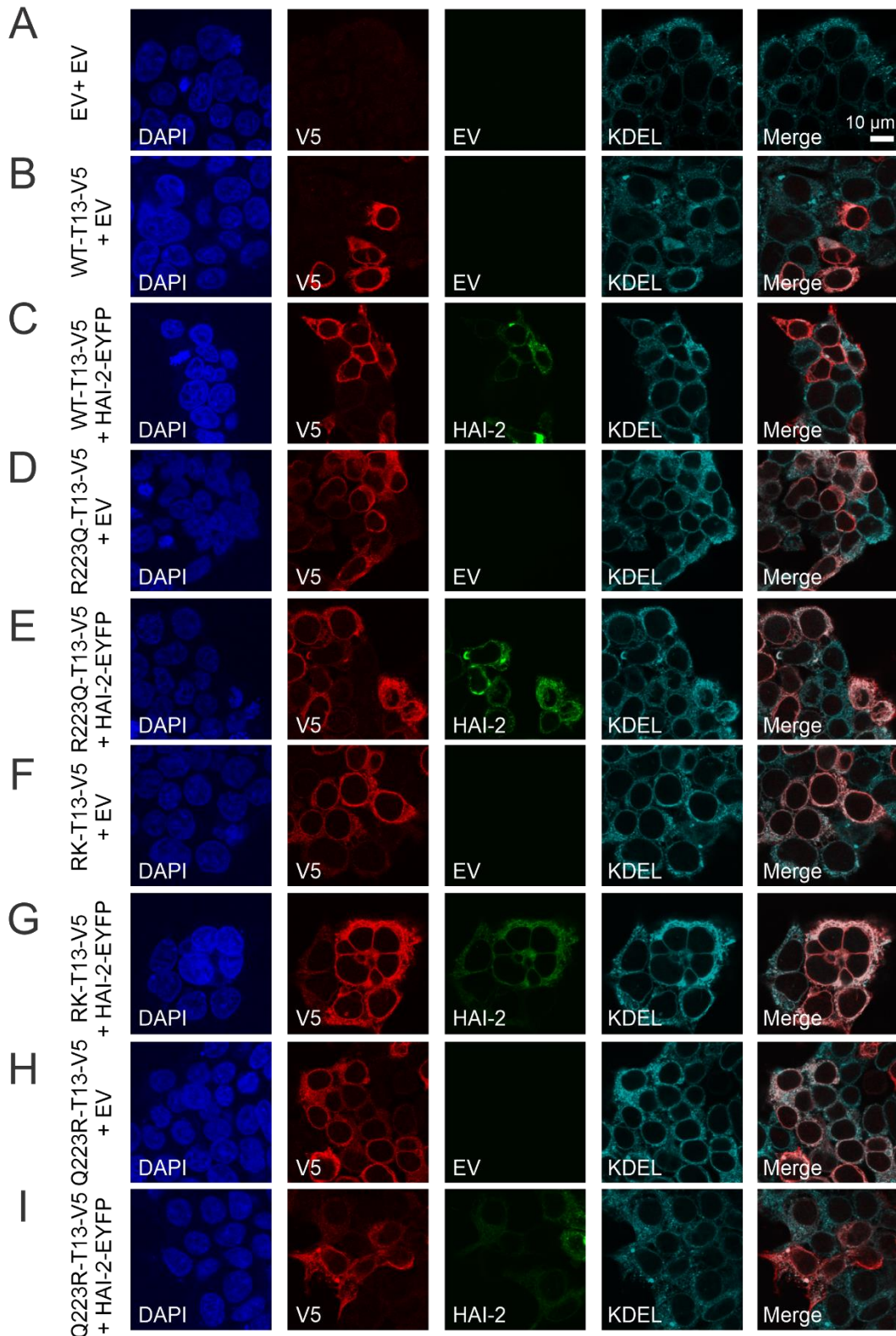
Figure 15: HEK293T cells were plated onto glass coverslips and 24 hours after plating were transfected for 48 hours with **(A)** EV + EV, **(B)** WT-T13-V5 + EV, **(C)** WT-T13-V5 + HAI-2-EYFP,

(D) R223Q-T13-V5 + EV, **(E)** R223Q-T13-V5 + HAI-2-EYFP, **(F)** RK-T13-V5 + EV, **(G)** RK-T13-V5 + HAI-2-EYFP, **(H)** Q223R-T13-V5 + EV, **(I)** Q223R-T13-V5 + HAI-2-EYFP. Cells were fixed onto coverslips, permeabilized, and incubated with anti-V5 to detect TMPRSS13 and anti-KDEL to detect the endoplasmic reticulum (ER). Coverslips were mounted to slides with DAPI-containing mounting media to detect nuclei. Nuclei=blue, panels A-I. TMPRSS13-V5=red, panels A-I. HAI-2-EYFP=green, panels C, E, G, and I. ER (KDEL)=cyan, panels A-I. Merged images of TMPRSS13/KDEL are shown in panels on the right. Scale bar measures 10 µm.

cells. Reversal to an arginine at position 223 (Q223R) led to an increase in cell surface localization in the presence of HAI-2 (**Fig. 14H-I** and **Fig. 15H-I**).

In summary, we report a novel post-transitional mechanism that regulates TMPRSS13 function and cellular localization. Cleavage in the stem region, with R223 being a critical site, depends on an intact TMPRSS13 catalytic triad and affects multiple processes including zymogen activation, amidolytic activity, phosphorylation, and cell surface localization.

4.4 Stem domain cleavage of TMPRSS13 – Discussion

As an ongoing effort to characterize the members of the TTSP family, we performed biochemical and cellular analyses of the hepsin/TMPRSS subfamily member, TMPRSS13.

We identify a novel proteolytic post-translational mechanism for TMPRSS13 that is important for activation/activity of the protease, intracellular phosphorylation, cell-surface localization, and release into the media. R223 in the extracellular TMPRSS13 stem region located between the transmembrane domain and the first site of the N-linked glycosylation at asparagine (N)-250 in the SRCR-domain was identified as a preferred cleavage site. This conclusion was reached based on the observation that a ten-site mutant of the six lysine and four arginine residues from R191 to K232 rendered TMPRSS13 proteolytically inactive, non-phosphorylated, and incapable of cell-surface localization and shedding. Mutation of ten basic residues could potentially lead to conformational changes that may affect function. However, reverse mutation of R223 restored the function of TMPRSS13 for all the assessed functional processes. Furthermore, a single mutation at R223, in the context of the wildtype TMPRSS13 stem region, significantly impaired its proteolytic activity and localization. The R223Q mutant still retained partial activity compared to the ten-site mutant as well as the active site mutant, which may suggest that

cleavage at R223 constitutes a "zymogen-like" state where non-cleaved TMPRSS13 has a basal low level of activity where proteolytic cleavage at R223 leads to a more activated state. Another, less likely possibility is that an alternative cleavage site in close proximity is utilized when R223 is mutated which is not detectable by size difference analysis in western blot experiments. The cleavage at R223 is dependent on TMPRSS13's proteolytic activity since mutation of its catalytic triad serine residue impairs R223 cleavage. The lack of efficient activation and shedding upon mutation of either stem region R223, the zymogen activation site R320, or catalytic serine S506, suggests that these cleavage events regulate activity and functional properties in an interdependent manner. This likely reflects TMPRSS13 autocatalytic cleavage though involvement of a downstream protease activated by TMPRSS13 cannot entirely be ruled out. A direct role of TMPRSS13 activity appears to be the most likely scenario, particularly in HEK293T cells which have been widely used to study multiple TTSPs because they do not express detectable levels of these proteases (47,141,182,210,238-241). In the endogenous expression setting, e.g. in cancer cells, involvement of other proteases cleaving TMPRSS13 in the stem region leading to the fragment observed in breast cancer cells including TTSPs is plausible, because cancer cells express several TTSPs as well as secreted serine proteases (1,38,39,242,243).

Other TTSPs, including matriptase, matriptase-2, and TMPRSS11a, are known to harbor additional cleavage sites apart from their zymogen activation site (42,91,203,234,235,244). In matriptase, the first autolytic event occurs at Gly-149, a residue located within the SEA (sea urchin sperm protein, enterokinase, agrin) domain, which causes the N-terminal fragment and C-terminal fragment of the two-chain zymogen to remain tethered by noncovalent interactions (234,245,246). Following this primary cleavage event, matriptase autoactivates and is subsequently cleaved at R186 between the SEA-domain and the first complement proteases C1r/C1s-urchin embryonic growth factor-bone morphogenetic protein (CUB)-domain for ectodomain shedding in a matriptase-activity dependent manner (234). In contrast to what we observe for TMPRSS13 stem

region cleavage, mutation of the stem region R186 site does not affect matriptase autoactivation (234). Matriptase-2 is also cleaved for ectodomain shedding, as indicated by the presence of soluble fragments in conditioned media of transfected cells (42,91,235,244). It has been shown that matriptase-2 harbors three sites for proteolytic processing: the canonical zymogen activation site at R567, and two sites important for cell surface release of the protease at R404 and R437 (235). Additionally, N-linked glycosylation is a necessary precursor for shedding of matriptase-2 into the media (42). TMPRSS11a undergoes cleavage at a site (R265) in its SP-domain which is dependent on the catalytic activity of TMPRSS11A as well as autoactivation at its zymogen cleavage site at R186 (203).

It is yet unknown whether the N-terminal fragment (NTF) of TMPRSS13 resulting from R223 cleavage has a cellular function. For matriptase, it has been proposed that upon ectodomain shedding, the NTF can be processed further by regulated intramembrane proteolysis which generates an intracellular fragment that can translocate to the nucleus. This fragment can then alter gene expression to induce cancer cell motility and invasiveness (247). As TMPRSS13 has been demonstrated to be cancer promoting in both breast and colorectal cancers by enhancing cell survival and chemoresistance (132,169), it is possible that the N-terminal cleavage fragment of TMPRSS13 could play a role for its pro-oncogenic properties.

In conclusion, this study identifies a new post-translational mechanism critical for cellular activation and localization of TMPRSS13 and provides new insights into the diverse mechanisms involved in regulating TTSP proteolytic functions.

4.5 Materials and methods

4.5.1 Cell lines and culture conditions

HEK293T cells and MCF-7 cells (ATCC, Manassas, VA) were cultured in Dulbecco's modified eagle media (Gibco/Thermo Fisher Scientific) supplemented with 10% fetal bovine serum (FBS) (Atlanta Biologicals, Lawrenceville, GA), 10 units/mL Penicillin and 10 µg/mL streptomycin (Gibco, Life Technologies, Grand Island, NY). BT-20 cells (ATCC) were cultured in

Eagles + NEAA media (Eagle's MEM supplemented with phenol red, with 2 mM L-glutamine and Earle's BSS adjusted to 1.5 g/L sodium bicarbonate, 0.1 mM non-essential amino acids, 1 mM sodium pyruvate, and 10% FBS) supplemented with 10 units/mL penicillin and 10 µg/mL streptomycin (Gibco). Cells were maintained in a humidified incubator at 37 °C with an atmosphere of 5% CO_2. HCC1937 and HCC1954 cells were cultured in RPMI + L-GLUT media (RPMI-1640 media with 2 mM L-glutamine adjusted to contain 1.5 g/L sodium bicarbonate, 4.5 g/L glucose, 10 mM HEPES, 1 mM sodium pyruvate, and 10% FBS) supplemented with 10 units/mL penicillin and 10 µg/mL streptomycin (Gibco).

4.5.2 Western blotting

Cultured human cells were washed 3 times with ice-cold PBS and lysed in-well using ice-cold RIPA buffer (150 mM NaCl; 50 mM Tris/HCl, pH 7.4, 0.1% SDS; 1% NP-40) with protease inhibitor cocktail (Sigma Aldrich, St. Louis, MO) and phosphatase inhibitor cocktail (Sigma Aldrich), and cleared by centrifugation at 12,000 x g at 4°C. Conditioned media samples were obtained following overnight incubation in serum-free media and were subsequently centrifuged at 100 x g for 10 minutes to remove detached cells and supernatant was collected. Protein concentrations in cell lysates were determined using a Pierce BCA Protein Assay Kit (Thermo Fisher Scientific, Waltham, MA). Proteins were separated by SDS-PAGE under reducing conditions using 10% or 4-15% Mini-Protean® gels or Criterion™ TGX midi gels (Bio-Rad) and blotted onto PVDF membranes (Bio-Rad). Membranes were blocked with 5% (w/v) dry milk powder in TBS-T (Tris-buffered saline, 0.1% Tween-20) for 1 hour at room temperature and subsequently incubated overnight at 4 °C in primary antibodies diluted in 5% dry milk powder/TBS-T. Primary antibodies used for western blotting included rabbit anti-TMPRSS13 raised against a recombinant protein fragment corresponding to a region within amino acids 195 and 562 of human TMPRSS13 (anti-extra-TMPRSS13) (PA5-30935, Thermo Fisher Scientific and Life Technologies, Inc); rabbit anti-TMPRSS13 raised against an epitope within the first 60 amino acids of human TMPRSS13 (anti-intra-TMPRSS13) (ab59862, Abcam, Cambridge, MA);

mouse-anti-V5 (R960-25, Thermo Fisher Scientific and Life Technologies, Inc); goat anti-HAI-2 (AF1106, R&D Systems Inc., Minneapolis, MN); and mouse anti-beta-actin (NB600-501, Novus Biologicals, Littleton, CO). Secondary antibodies included horseradish peroxidase conjugated goat anti-rabbit (12-348, Millipore, Billerica, MA), goat anti-mouse (AP181P, Millipore), and rabbit anti-goat (31403, Thermo Fisher Scientific) antibodies. Detection of antibodies was performed using Clarity ECL Western Blotting substrate (Bio-Rad) or Super-Signal West Femto Chemiluminescent Substrate (Pierce, Thermo Fisher Scientific). Chemiluminescent imaging was performed using the ChemiDocMP™ imaging system (Bio-Rad). After detection, PVDF membranes were stripped using Restore™ Western Blot Stripping Buffer (Thermo Fisher Scientific) for 15 minutes at room temperature prior to re-probing with a different primary antibody.

4.5.3 Cloning of full-length TMPRSS13 plasmid constructs

WT-TMPRSS13-V5, S506A-TMPRSS13-V5, and R320Q-TMPRSS13-V5 constructs were generated as previously described (47). Point mutations using WT-TMPRSS13-V5 as a template for R191Q-TMPRSS13-V5, R196Q-TMPRSS13-V5, R205Q-TMPRSS13-V5, and R223Q-TMPRSS13-V5 were generated using the Q5® Site-Directed Mutagenesis Kit (New England Biolabs, Ipswich, MA). The RK-TMPRSS13-V5 mutant plasmid was synthesized by the GenScript company (Piscataway, NJ). Q223R-TMPRSS13-V5 point mutation was generated using the Q5® Site-Directed Mutagenesis Kit using RK-TMPRSS13-V5 as a template. Primers used for R191Q mutagenesis were 5'-CACAGGGATCCAATACAAGGAGCAGAGGGAGAGC-3' and 5'-TGGCCCTGCCAGAACTGG-3'. Primers used for R196Q mutagenesis were 5'-CAAGGAGCAGCAAGAGAGCTGTCC-3' and 5'-TACCTGATCCCTGTGTGG-3'. Primers used for R205Q mutagenesis were 5'-GCACGCTGTTCAATGTGACGGGG-3' and 5'-TTGGGACAGCTCTCCCTC-3'. Primers used for R223Q mutagenesis were 5'-GGGCTGCGTGCAATTTGACTGGGAC-3' and 5'-AGCTCGTCACTCTTCAGC-3'. Primers used for Q223R mutagenesis were 5'-GGGCTGCGTGAGGTTTGACTGGG-3' and 5'-AGCTCGTCACTTTGCAGT-3'. Transformation of all vectors was performed in NEB 5-alpha

Competent E. *coli* cells (New England Biolabs) and positive clones were isolated and amplified using standard techniques. Mutations were verified by DNA sequencing.

4.5.4 Transient transfections with TMPRSS13 expression vectors

Transfections of HEK293T cells were performed using Lipofectamine® LTX reagent with PLUS™ reagent according to the manufacturer's instructions (Invitrogen, Life Technologies, Inc.). Transfection was performed with 500 ng of plasmid DNA for single transfections or 1 µg of DNA total for co-transfections. Vectors included in transfections were pcDNA3.1-TMPRSS13 vectors, empty vector pcDNA3.1, and pcDNA3.1-HAI-2 (227).

4.5.5 Amidolytic activity assay

The assays were performed in 96-well plates in a total reaction volume of 200 µl, in triplicate. 180 µl of conditioned media was incubated at 37 °C for 15 minutes, then the synthetic peptide substrate Suc-Ala-Ala-Pro-Arg-pNA (L-1720) (Bachem, Bubendorf, Switzerland) was added for a final concentration of 100 µM. Serum- and cell-free growth media was used as negative control. Samples were incubated at 37 °C for 120 minutes and changes in absorbance at 405 nm were measured using a Magellan NanoQuant Infinite M200 Pro plate reader (Tecan U.S., Inc., Morrisville, NC).

4.5.6 Knockdown of TMPRSS13 expression in cancer cells

Transient knockdown of TMPRSS13 expression in HCC1954, HCC1937, BT-20 and MCF-7 cells was performed using Lipofectamine® RNAiMAX (Invitrogen, Life Technologies, Inc.) according to manufacturer's instructions. Two non-overlapping Stealth siRNA™ constructs were obtained from Invitrogen, Life Technologies, Inc. (HSS130531, corresponding to siRNA1; HSS130532, corresponding to siRNA2). A %GC-matched negative control (scramble control, SCRM) was used as a non-TMPRSS13-targeting siRNA.

4.5.7 Immunocytochemistry

Cell imaging was performed using HEK293T cells expressing human full-length TMPRSS13 vectors or empty vector pcDNA3.1. HAI-2 was visualized using a vector expressing

a HAI-2-EYFP fusion protein (228). Cells were seeded onto glass coverslips and allowed to grow overnight. Cells were transiently transfected for 48 h, after which media was removed and cells were fixed in Z-FIX (ANATECH LTD, Battle Creek, MI) for 15 min at room temperature. For permeabilized samples, cells were treated with 0.05% Triton X-100 in PBS for 15 min on ice. Cells were then blocked in 5% BSA in PBS for 1 h on ice prior to addition of primary antibodies. After incubation with primary antibodies overnight at 4°C, cells were washed in PBS and secondary Texas Red-conjugated goat anti-mouse and AlexaFluor-647-conjugated goat anti-rabbit antibodies (Invitrogen, Life Technologies, Inc.) were used to detect TMPRSS13-V5 or KDEL. Cells were washed with PBS and mounted with ProLong™ Diamond Antifade Mountant with DAPI (Invitrogen). Confocal images were acquired on the Leica SP5 scope at the Microscopy Imaging and Cytometry Resources Core at Wayne State University School of Medicine. Acquired permeabilized images were pseudo-colored and merged using ImageJ image analysis (229).

4.5.8 Statistical analyses

GraphPad Prism software was used to perform all statistical analyses. For statistical comparison between three or more groups, one-way ANOVA with Dunnett's post-hoc analysis was used. All analyses are representative of at least three biological replicates.

CHAPTER 5: INTRACELLULAR PHOSPHORYLATION OF TMPRSS13

This chapter (Chapter 5) contains preliminary data regarding TMPRSS13 phosphorylation.

5.1 Abstract

TMPRSS13, a member of the hepsin/TMPRSS subfamily of type II transmembrane serine proteases (TTSPs), is the only TTSP family member known to be phosphorylated. The intracellular domain of TMPRSS13 is an intrinsically disordered region that harbors several tandem repeat phosphorylation motifs. At least fifteen serine and threonine residues are phosphorylated throughout the entire intracellular domain of TMPRSS13. Site-directed mutagenesis was used to delete portions of the intracellular domain, as well as to make non-phosphorylatable and phospho-mimetic mutants of TMPRSS13. Utilizing these TMPRSS13 mutants, we show that abrogation of intracellular phosphorylation does not affect the ability of TMPRSS13 to autoactivate or to proteolytically cleave a substrate, prostasin. Furthermore, lack of phosphorylation may not preclude cell surface localization of TMPRSS13, but may be involved in the stability of TMPRSS13 at the cell surface. Future studies will focus on the connection between phosphorylation, cell surface localization, and catalytic deficiency by utilizing a catalytically-dead non-phosphorylatable TMPRSS13 mutant. Additionally, we will investigate the role that phosphorylation of TMPRSS13 plays in its pro-oncogenic activity in breast and colorectal cancers, using mass spectrometry to identify binding partners of phosphorylated TMPRSS13 in cancer cells. These studies will shed light onto the role of the unique post-translational modification of phosphorylation in TMPRSS13 function.

5.2 Intracellular phosphorylation of TMPRSS13 – Introduction

Protein phosphorylation is a post-translational modification by which a phosphate group is enzymatically transferred from an ATP molecule to a serine, threonine, or tyrosine residue on a protein (248,249). While phosphorylation is a crucial process involved in normal cellular physiology, it can be exploited by cancer cells to hyperactivate signaling pathways involved in cell

proliferation, survival, and metastasis (248). TMPRSS13, a member of the hepsin/TMPRSS subfamily of type II transmembrane serine proteases (TTSPs), is highly phosphorylated on serine and threonine residues in its intracellular domain (47). In fact, this phosphorylation renders TMPRSS13 unique among the 17 TTSP family members. The intracellular portion of TMPRSS13 is an intrinsically-disordered region (IDR), meaning that it does not adopt a defined three-dimensional structure (47,250). IDRs are often known to harbor post-translational modifications (PTMs), including phosphorylation (250-252). As TMPRSS13 is the only TTSP known to be phosphorylated, it is plausible that this PTM plays a role in the function of TMPRSS13 in epithelial and/or carcinoma cells. It has been shown that phosphorylation of TMPRSS13 is coupled with the catalytic activity and cell membrane localization of the protease (47). For transfected TMPRSS13 to localize to the surface of HEK293T cells, it needs to either be rendered catalytically inactive by mutation or by co-transfection with one of its endogenous inhibitors, hepatocyte growth factor activator (HAI)-1 or HAI-2. Previous studies have shown that endogenous TMPRSS13 in cancer cells is phosphorylated and is endogenously co-expressed with HAI-1/2 (47,182). TMPRSS13 is also known to be a pro-oncogenic protease in both breast and colorectal cancer (132,169), but the exact role that TMPRSS13 plays in the regulation of oncogenic activity is yet to be elucidated. This chapter aims to establish the role of intracellular phosphorylation in the regulation of TMPRSS13 function and to identify pro-oncogenic signaling pathways to which TMPRSS13 may belong.

5.3 Intracellular phosphorylation of TMPRSS13 – Results

5.3.1 TMPRSS13 is highly phosphorylated in its intracellular domain

TMPRSS13 harbors a long intracellular N-terminal domain, a transmembrane domain, a stem region with a low-density lipoprotein receptor class A (LDLA) and scavenger receptor cysteine rich (SRCR) domain, and a C-terminal serine protease domain (**Fig. 16B, panel I**). It has previously been shown through lambda phosphatase and calf intestinal alkaline phosphatase assays that TMPRSS13 is a phosphorylated protease (47). Furthermore, TMPRSS13

Figure 16: TMPRSS13 is a phosphorylated protease
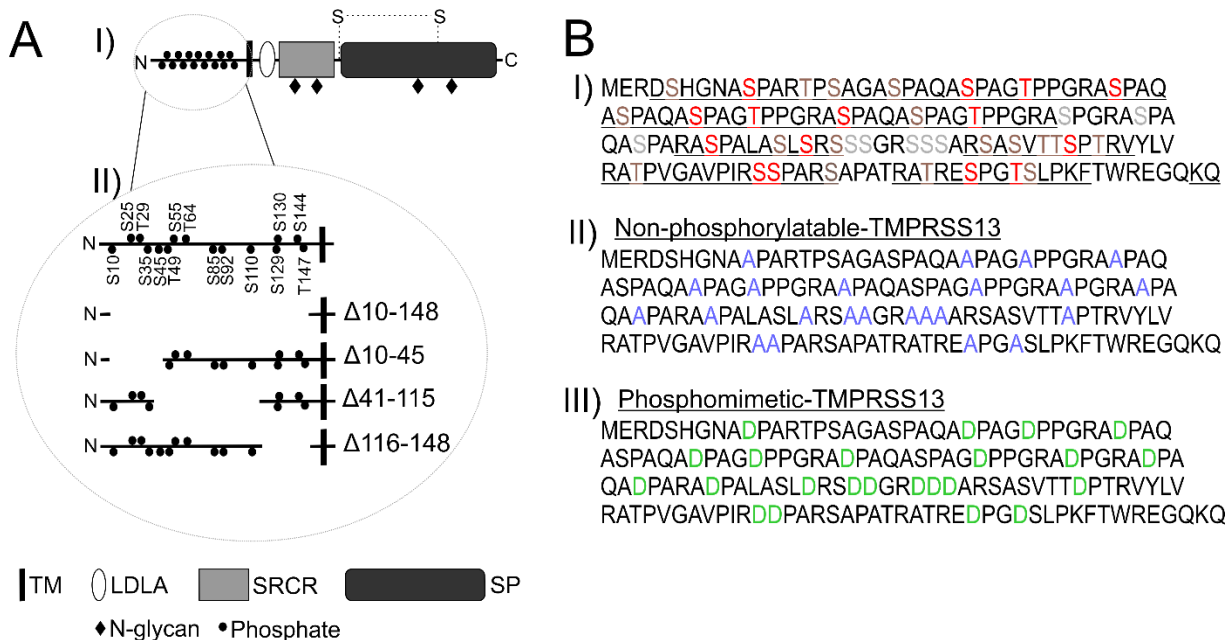
Figure 16: **A)** (I) Schematic representation of TMPRSS13. TM, transmembrane domain; LDLA, low-density lipoprotein receptor class A domain; SRCR, group A scavenger receptor cysteine rich domain; SP, serine protease domain. The disulfide bridge tethering the SP domain to the stem region is denoted with "S-S" and a dashed line. Phosphorylation of the intracellular domain is indicated by filled black circles. N-linked glycosylation sites are indicated by filled black diamonds. (II) Zoomed in intracellular domain with the phosphorylated residues labeled and indicated with filled black circles. Schematics of TMPRSS13 intracellular deletion constructs (Δ10-148, Δ10-45, Δ41-115, Δ116-148) are included. **B)** (I) Sequence of the intracellular domain of TMPRSS13. Phosphorylated serine/threonine residues confirmed by mass spectrometry are in red. Underlined residues indicate the coverage of the intracellular domain by MS. Candidate serine residues not covered by MS but mutated in non-phosphorylatable and phosphomimetic mutants are in gray. Serine/threonine residues covered by MS but not phosphorylated are in brown. (II) Sequence of the intracellular domain of the non-phosphorylatable (NP)-TMPRSS13 mutant. Serine/threonine residues mutated to alanine are in blue. (III) Sequence of the intracellular domain of the phosphomimetic (PM)-TMPRSS13 mutant. Serine/threonine residues mutated to aspartic acid are in green.

phosphorylation occurs when the protease is rendered inactive by mutation (e.g. catalytically-dead or zymogen-locked) or by co-expression with an endogenous inhibitor, the hepatocyte growth factor inhibitor (HAI)-1 or HAI-2 (47). The intracellular domain of TMPRSS13 harbors tandem repeat phosphorylation motifs for different protein kinases (47,127,128). The particular phosphorylated residues, however, have not been determined. Therefore, mass spectrometry was performed to identify phosphorylated residues of the high-molecular weight phosphorylated

form of catalytically-dead TMPRSS13 (and the same region from WT-TMPRSS13). This resulted in the identification of fifteen phosphorylated serine and threonine residues spanning the length of the intracellular domain of TMPRSS13 (**Fig. 16B, panel I**). To elucidate the functional role of phosphorylation of TMPRSS13, intracellular deletion constructs of human full-length TMPRSS13 were made: Δ10-148-TMPRSS13-V5 (deletion of the entire region harboring phosphorylated residues), Δ10-45-TMPRSS13-V5, Δ81-115-TMPRSS13-V5, and Δ116-148-TMPRSS13-V5 (**Fig. 16A, panel II**). Because deleting large portions of TMPRSS13 could potentially interfere with the function and/or the trafficking of the protease, a full-length non-phosphorylatable (NP) TMPRSS13 mutant was also made using site directed mutagenesis. This allows for investigation of the lack of phosphorylation in the context of an intact intracellular domain. For the NP mutant, all serine residues confirmed to be phosphorylated or not covered by prior mass spectrometry were mutated to alanine (**Figure 16B, panel II**). A phosphomimetic TMPRSS13 mutant was also made by site-directed mutagenesis, in which all serine residues confirmed to be phosphorylated or not covered by prior mass spectrometry were mutated to aspartic acid (**Figure 16B, panel III**). Phosphomimetic mutants are used to study the role of constitutive phosphorylation of a protein, as the amino acid substitution mimics a phosphorylated residue (253).

5.3.2 Abrogation of phosphorylation does not affect the enzymatic activity of TMPRSS13

Transfection of WT-TMPRSS13-V5, S506A-TMPRSS13-V5 (catalytically-dead), and TMPRSS13 phospho-mutants into HEK293T cells followed by SDS-PAGE under reducing conditions and western blotting indicated that lack of intracellular phosphorylation does not cause detectable changes for the autoactivation or catalytic ability of TMPRSS13 (**Fig. 17A-C**). As detailed in previous publications (47,182), TMPRSS13 can be detected using an antibody directed against amino acids 195-562 of TMPRSS13 (extracellular; α-extra-TMPRSS13. Catalytically-dead S506A-TMPRSS13 and WT-TMPRSS13 co-expressed with HAI-2 are both highly phosphorylated, as indicated by a high molecular weight (HMW) form of the protease (**Fig. 17A-B, Band 1**). Full-length non-phosphorylated TMPRSS13 migrates as a form ~72 kDa, although

Figure 17: Lack of phosphorylation does not affect the autoactivation or catalytic activity of TMPRSS13
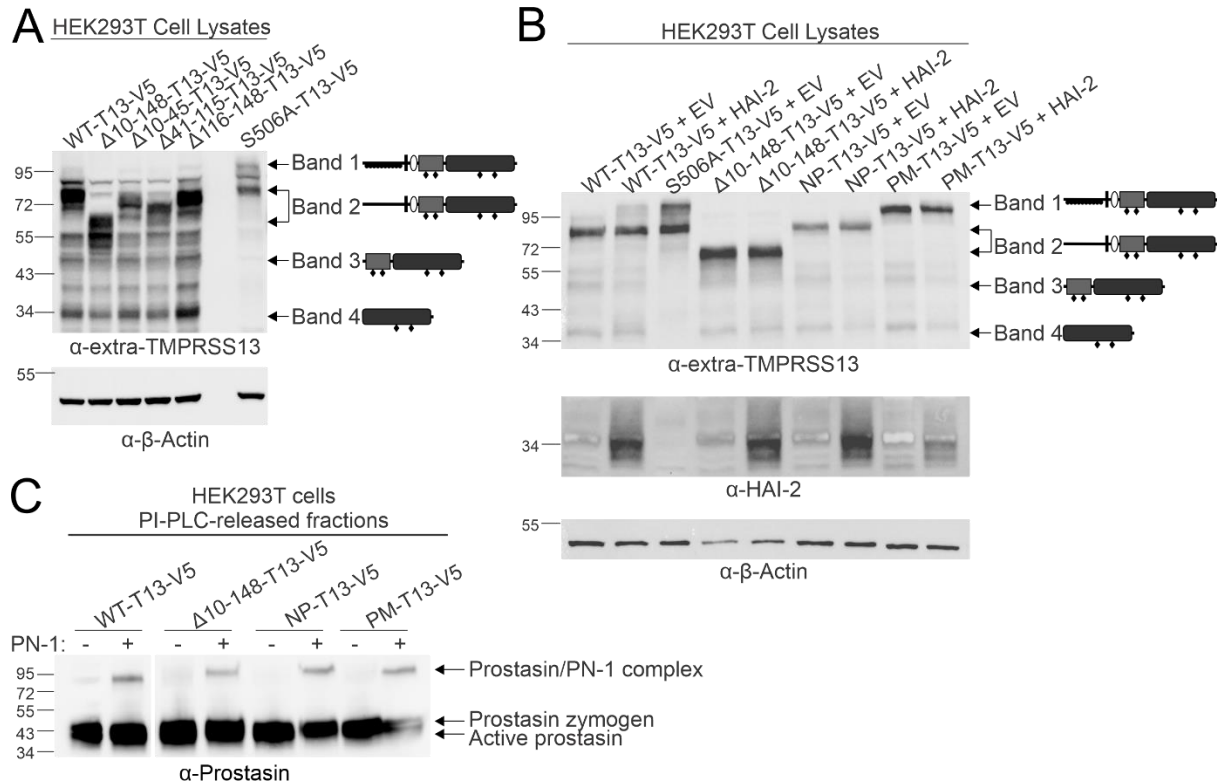
Figure 17: **A)** HEK293T cells were transfected for 48 hours with WT-TMPRSS13 (T13)-V5, Δ10-148-T13-V5, Δ10-45-T13-V5, Δ41-115-T13-V5, Δ116-148-T13-V5 or S506A-T13-V5. Proteins in whole cell lysates were separated by SDS-PAGE under reducing conditions using 4-15% gels and analyzed by western blotting. Proteins were detected using anti-extra-TMPRSS13 or anti-beta-actin antibodies. Arrows and schematics to the right of the western blots define the TMPRSS13 form that is detailed in the text. **B)** HEK293T cells were transfected for 48 hours with WT-TMPRSS13 (T13)-V5, S506A-T13-V5, Δ10-148-T13-V5, non-phosphorylatable (NP)-T13-V5 or phosphomimetic (PM)-T13-V5 along with empty vector (EV) PCDNA3.1 or HAI-2. Proteins in whole cell lysates were separated by SDS-PAGE under reducing conditions using 4-15% gels and analyzed by western blotting. Proteins were detected using anti-extra-TMPRSS13, anti-HAI-2, or anti-beta-actin antibodies. Arrows and schematics to the left of the western blots define the TMPRSS13 form that is detailed in the text. **C)** HEK293T cells were co-transfected with plasmids encoding TMPRSS13 variants and human full-length prostasin. Phosphatidylinositol-specific phospholipase C (PI-PLC) was added to cleave the glycophosphatidylinositol anchor from prostasin and release it into the supernatant. Protease nexin-1 (PN-1) was added (indicated by "+") to form SDS-stable complexes with active prostasin. Proteins were separated by SDS-PAGE under reducing conditions using a 4-15% gel and proteins were detected on western blots using an anti-prostasin antibody. The prostasin zymogen and active forms, as well as the active prostasin/PN-1 complex are indicated with arrows.

its molecular weight is decreased in the TMPRSS13 deletion constructs as portions of the

protease are removed (**Fig. 17A-B, Band 2**). In WT-TMPRSS13, TMPRSS13 intracellular

deletion constructs, as well as NP- and PM-TMPRSS13 mutants, a band ~50 kDa is observed in western blots probed with the α-extra-TMPRSS13, in accordance with data from Chapter 3 indicating that this is a stem region cleavage form of TMPRSS13 (**Fig. 17A-B, Band 3**). Importantly, TMPRSS13 is capable of autoactivation by cleavage at R320, its zymogen activation site. Upon cleavage at this site, the SP domain remains linked to the stem region of the protease by a disulfide bridge which can be disrupted under reducing conditions, and the presence of the released SP domain on a western blot can be used as a readout for autoactivation of the protease. In WT-TMPRSS13, TMPRSS13 deletion constructs, and NP- and PM- TMPRSS13, a band ~36 kDa is observed which is the released SP domain (**Fig. 17A-B, Band 4**). These results indicate that removal of portions of the intracellular domain or mutation of phosphorylated residues of TMPRSS13 does not disrupt the ability of the protease to autoactivate.

To further examine the role of phosphorylation in the proteolytic cleavage of a TMPRSS13 substrate (132,182), HEK293T cells were transfected with WT-TMPRSS13-V5 or TMPRSS13 phospho-mutants plus full-length human prostasin, and cells were treated with phosphatidylinositol-specific phospholipase C (PI-PLC) to release prostasin into the supernatant. As described in Chapter 2, protease nexin (PN)-1, an endogenous inhibitor of prostasin that forms an SDS-stable complex with active prostasin (211), was added to the prostasin-containing supernatants. In western blot analysis, the detection of a band at ~95 kDa corresponding to the active prostasin/PN-1 complex reflects that prostasin has been cleaved and activated by TMPRSS13 (**Fig. 17C**). In this assay, WT-TMPRSS13 is used as a positive control for prostasin activation. Δ10-148-TMPRSS13-V5, NP-TMPRSS13-V5, and PM-TMPRSS13-V5 are all able to cleave and activate prostasin, as indicated by the presence of the active prostasin/PN-1 complex similar to the levels observed with WT-TMPRSS13. These data, combined with the autoactivation data above, suggest that phosphorylation of the intracellular domain of TMPRSS13 is immaterial for its enzymatic activity.

Figure 18: **A)** DLD1 cells or **(C)** MCF-7 cells were treated with cycloheximide for 0, 4, 8, 24 and 48 hours. Proteins in whole cell lysates were separated by SDS-PAGE under reducing conditions using 4-15% gels and analyzed by western blotting. Proteins were detected using anti-intra-TMPRSS13 antibody. Stacked bar graph showing the quantification of ratios of the phosphorylated form to the non-phosphorylated form of **(B)** DLD1 or **(D)** MCF-7 cells from the respective western blots. P-T13, phosphorylated full-length TMPRSS13; FL T13, non-phosphorylated full-length TMPRSS13.

5.3.3 Phosphorylated TMPRSS13 has a longer half-life than non-phosphorylated TMPRSS13

As intracellular phosphorylation of TMPRSS13 does not appear to play a role in catalytic activity of the protease, we chose to investigate the half-life of phosphorylated TMPRSS13 as compared to non-phosphorylated TMPRSS13. It is plausible that phosphorylation could play a role in the stability of TMPRSS13 in the cell. DLD1 colorectal cancer cells and MCF-7 hormone-positive breast cancer cells were treated for 48 hours with cycloheximide to block protein translation. Whole cell lysates were collected and proteins were separated by SDS-PAGE under reducing conditions, following by western blotting using an antibody that detects endogenous TMPRSS13 (anti-intra-TMPRSS13; recognizes amino acids 1-60 in the intracellular domain of

TMPRSS13). While the expression of the full-length non-phosphorylated form of TMPRSS13 decreases over time, the phosphorylated form of TMPRSS13 appears to have a longer half-life; by 48 hours the non-phosphorylated form of TMPRSS13 is nearly completely diminished while the phosphorylated form is still observed (**Fig. 18A-D**). The manner in which this process is occurring is still under investigation, as it is unknown whether the full-length non-phosphorylated form of TMPRSS13 is being turned over and degraded or whether any non-phosphorylated TMPRSS13 is being converted to phosphorylated TMPRSS13 over time.

5.3.4 Cellular localization of NP- and PM-TMPRSS13 mutants

Previous publications have indicated that TMPRSS13, following inactivation by mutation or co-expression with inhibitors, can localize to the cell surface and become phosphorylated (47,182). To examine the role of phosphorylation in the localization of TMPRSS13, immunocytochemistry was performed on HEK293T cells expressing WT-TMPRSS13-V5, NP-TMPRSS13-V5, or PM-TMPRSS13-V5, with or without the co-expression of HAI-2. In non-permeabilized cells expressing only empty vector (EV) PCDNA3.1, no V5 or HAI-2 staining is observed (**Fig. 19A**). As previously demonstrated, WT-TMPRSS13-V5 localizes to the cell surface in the presence, but not the absence, of HAI-2, indicating that it needs to be rendered catalytically inactive in order to localize to the cell membrane (**Fig. 19B-C**). Notably, both NP-TMPRSS13-V5 and PM-TMPRSS13-V5 do not localize to the cell surface when co-expressed with EV, but are observed on the cell surface when co-expressed with HAI-2 (**Fig. 19D-G**). This result was surprising, particularly for the NP-TMPRSS13 mutant, as prior data suggested that inactive, cell surface-localized TMPRSS13 becomes phosphorylated. One possible explanation for these data is that the catalytic inactivity of TMPRSS13 may be more critical than the intracellular phosphorylation for cell surface expression. Both NP-TMPRSS13 and PM-TMPRSS13 mutants have catalytic activity to similar levels as WT-TMPRSS13. In previous studies where TMPRSS13 mutants did not localize to the cell surface in the presence or absence

Figure 19: Cell surface localization of NP- and PM- TMPRSS13 mutants
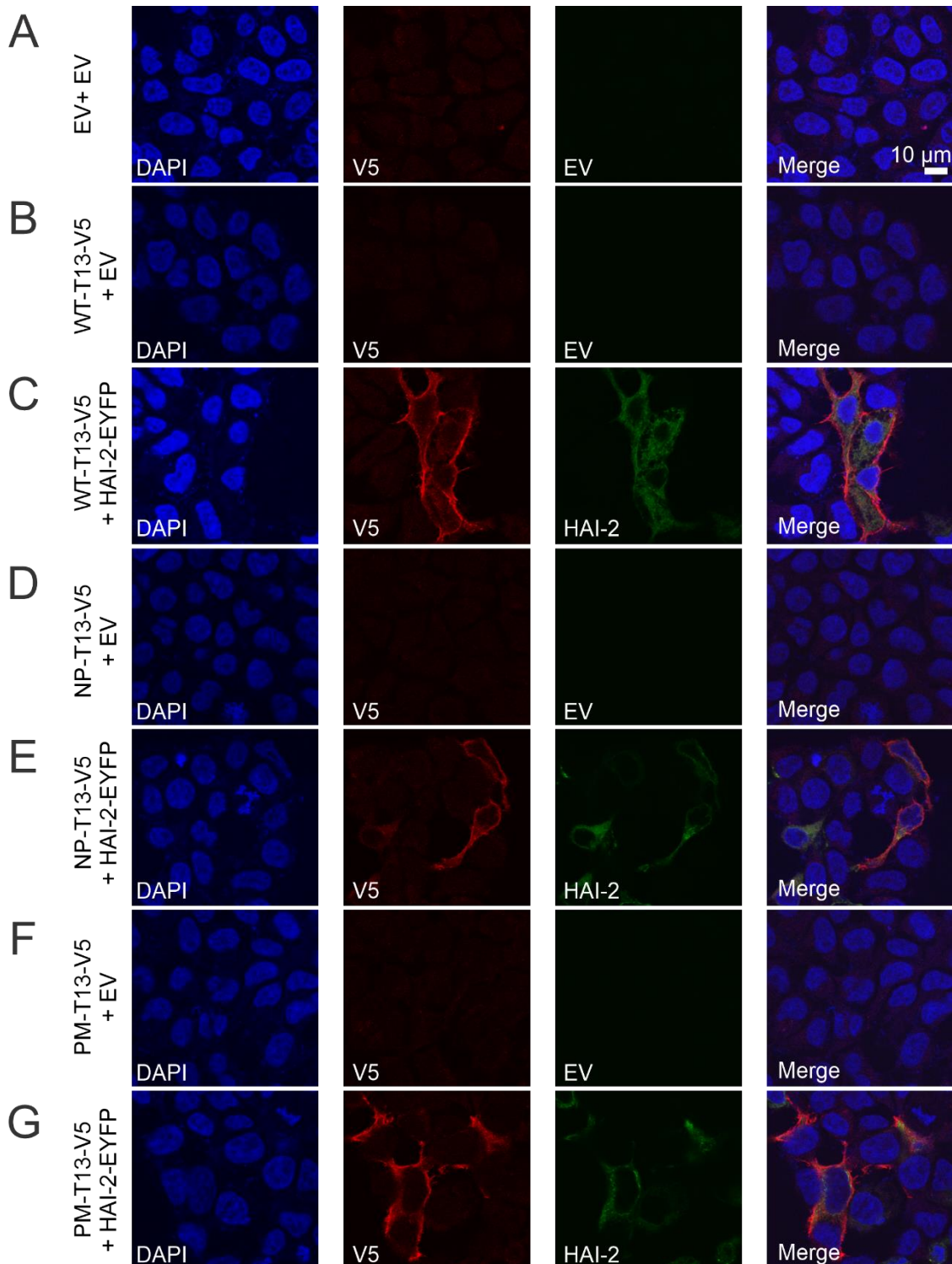
Figure 19: HEK293T cells were plated onto glass coverslips and 24 hours after plating were transfected for 48 hours with **(A)** EV + EV, **(B)** WT-T13-V5 + EV, **(C)** WT-T13-V5 + HAI-2-EYFP, **(D)** NP-T13-V5 + EV, **(E)** NP-T13-V5 + HAI-2-EYFP, **(F)** PM-T13-V5 + EV, and **(G)** PM-T13-V5 + HAI-2-EYFP. Cells were fixed onto coverslips and incubated with anti-V5 to detect TMPRSS13.

Coverslips were mounted to slides with DAPI-containing mounting media to detect nuclei. Nuclei=blue, panels A-G. TMPRSS13-V5=red, panels A-G. HAI-2-EYFP=green, panels C, E, G. Merged images are shown in panels on the right. Scale bar measures 10 µm.

of HAI-2 and did not become phosphorylated, these mutants had significant reductions in the levels of autoactivation and enzymatic activity compared to WT-TMPRSS13 (See **Fig. 2**, **Fig. 4-6**, **Fig. 10-11**, **Fig. 14-15**). These results may indicate that when TMPRSS13 is catalytically active, it can only localize to the cell surface in the presence of HAI-2, and phosphorylation may not be necessary for this process (although phosphorylation may affect stability on the cell surface and/or shedding as well as downstream signaling). Additional studies using a catalytically-dead, non-phosphorylatable TMPRSS13 mutant will seek to further tease apart the roles of intracellular phosphorylation and catalytic activity in the localization of TMPRSS13 (see Section 5.4).

5.4 Intracellular phosphorylation of TMPRSS13 – Discussion and Future Directions

The data presented in Chapters 3-5 indicate that the post-translational modifications of TMPRSS13 play roles in the autoactivation, catalytic ability, shedding, trafficking, and stability of the protease. Furthermore, published work from our lab has shown a pro-oncogenic role for TMPRSS13 in both breast and colorectal cancers. However, there are several characteristics of TMPRSS13 that are yet to be elucidated. It is known that TMPRSS13 is a phosphorylated protease and its phosphorylation is thought to be connected to its enzymatic activity (as catalytic-deficient and HAI-1/2-inhibited TMPRSS13 is highly phosphorylated), cell surface localization, and stability. The kinases responsible for phosphorylating the intracellular domain of TMPRSS13 are yet to be identified, but the intracellular domain of TMPRSS13 harbors many tandem repeat sequences that are sequence motifs for kinases such as CDK5, ERK1/2 and CaM Kinase II (128,254,255). Preliminary experiments treating DLD1 colorectal cancer cells with a broad cyclin-dependent kinase inhibitor (inhibits CDK1, CDK2, CDK5, CDK7, CDK9), roscovitine (256), have shown a dose- and time- dependent increase in TMPRSS13 phosphorylation and ERK1/2 activation (**Fig. 20A-B**). Roscovitine, despite being a kinase inhibitor, has also been shown to activate the MAP kinase pathway, increasing the phosphorylation of ERK1/2 (257,258). There is

Figure 20: Roscovitine treatment of DLD1 cells
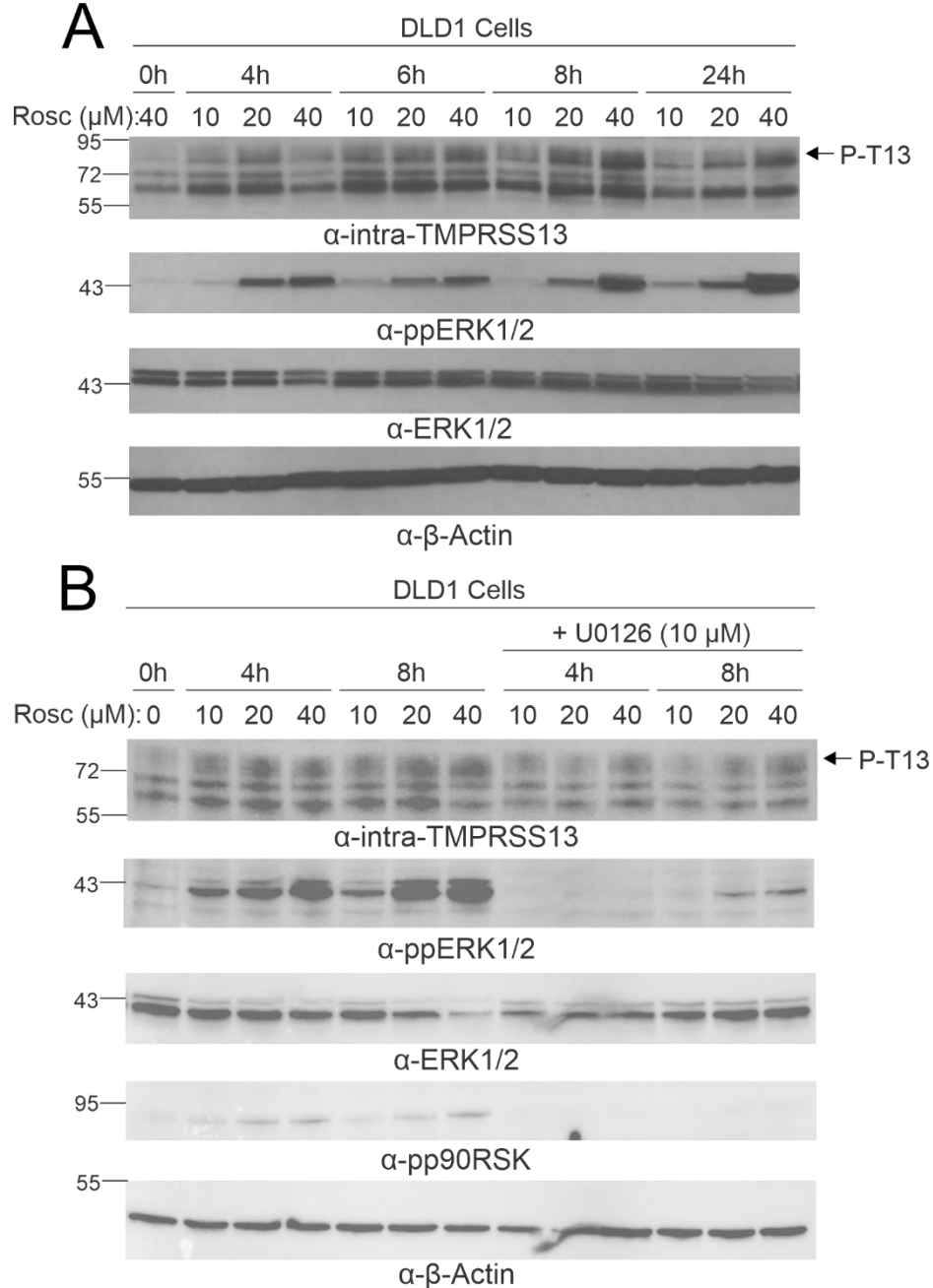
Figure 20: **A)** DLD1 cells were treated for 0-24 hours with varying concentrations (10, 20 or 40 µM) of roscovitine (Rosc). Proteins in whole cell lysates were separated by SDS-PAGE under reducing conditions using 4-15% gels and analyzed by western blotting. Proteins were detected using anti-intra-TMPRSS13, anti-ppERK1/2, anti-ERK1/2 and anti-beta actin antibodies. **B)** DLD1 cells were treated for 0-8 hours with vehicle (DMSO, 0 µM Rosc) or varying concentrations concentrations (10, 20 or 40 µM) of roscovitine. Proteins in whole cell lysates were separated by SDS-PAGE under reducing conditions using 4-15% gels and analyzed by western blotting. Proteins were detected using anti-intra-TMPRSS13, anti-ppERK1/2, anti-ERK1/2 anti-phospho-p90RSK, and anti-beta-actin antibodies. P-T13, phosphorylated full-length TMPRSS13.

a crosstalk between the cyclin dependent kinases and MAP kinases, as CDK5 can phosphorylate and suppress the activity of MEK, the upstream ERK activator (259). Due to this ERK activation upon roscovitine treatment, the MEK1/2 inhibitor U0126 was used alongside roscovitine to block the activation of ERK1/2 induced by treatment with the CDK inhibitor. As roscovitine treatment increased the levels of phosphorylated TMPRSS13, MEK1/2 inhibition reduced the levels of phosphorylated TMPRSS13 to baseline levels (**Fig. 20B**). These experiments suggest a role for the MAP kinase pathway in the phosphorylation of TMPRSS13 in cancer cells, but there are likely other kinases – yet to be determined – also responsible for this phosphorylation event. As the interactions between kinase and substrate tend to be short-lived, future studies will use protein cross-linking followed by immunoprecipitation in order to identify TMPRSS13/kinase interactions. Candidate kinases can also be inhibited alone and in combination both genetically and pharmacologically, using siRNA-mediated gene knockdown and kinase inhibitors. Results from kinase identification studies will also help to gain insight into oncogenic signaling pathways to which TMPRSS13 belongs.

Preliminary investigations are underway to identify binding partners of phosphorylated TMPRSS13 in DLD1 colorectal cancer cells. TMPRSS13 was knocked out in DLD1 cells using CRISPR/Cas9 technology, and knockout cells were subsequently transfected with EV, WT-TMPRSS13-V5 + HAI-2, S506A-TMPRSS13-V5 + EV, and NP-TMPRSS13-V5 + EV. These transfection combinations were chosen as WT-TMPRSS13 becomes highly phosphorylated and localizes to the cell surface in the presence of HAI-2, S506A-TMPRSS13 is highly phosphorylated and localizes to the cell surface in the presence or absence of inhibitors, and NP-TMPRSS13 is not phosphorylated in the presence or absence of HAI-2. Solubilized membranes were isolated from harvested cells and proteins interacting with TMPRSS13 were pulled down using an anti-V5 antibody. Mass spectrometry was performed to identify TMPRSS13-interacting proteins. Notably, six proteins were pulled down in cells transfected with WT-TMPRSS13-V5 + HAI-2 and with S506A-TMPRSS13-V5 + EV, indicating a potential role for interaction specifically with

phosphorylated TMPRSS13. Two proteins, E-cadherin and beta-catenin, were specifically of interest; these proteins are known to interact at the cell membrane and their interaction can mediate cell-cell adhesion and Wnt signaling in cancer (260). Further mass spectrometry studies will also incorporate DLD1 TMPRSS13-KO cells transfected with NP-TMPRSS13-V5 + HAI-2, as the co-expression of NP-TMPRSS13 and HAI-2 allows TMPRSS13 to localize to the cell surface despite its lack of phosphorylation. This will help to elucidate if the interaction of TMPRSS13 and E-cadherin/beta catenin is due to the phosphorylation of TMPRSS13 or if the interaction is due to the cell surface localization of the protease.

To disentangle the roles of phosphorylation and enzymatic activity in the cellular localization of TMPRSS13, catalytically-dead, non-phosphorylatable and phosphomimetic mutants of TMPRSS13 were made using site-directed mutagenesis of the catalytic serine residue (S506A). Resulting V5-tagged plasmids (NP S506A-TMPRSS13-V5 and PM S506A-TMPRSS13-V5) were transfected into HEK293T cells alongside WT-TMPRSS13-V5, S506A-TMPRSS13-V5, NP-TMPRSS13-V5 and PM-TMPRSS13-V5, and proteins in cell lysates were separated by SDS-PAGE. Unlike NP-TMPRSS13 and PM-TMPRSS13, there is no observable released SP domain or extracellular domain following stem domain cleavage in the NP S506A-TMPRSS13 and PM S506A-TMPRSS13 mutants (**Fig. 21**). This confirms an abrogation of autoactivation caused by mutation of the catalytic serine residue in these phospho-mutants. The NP-TMPRSS13 mutant has catalytic activity similar to WT-TMPRSS13, as phosphorylation appears to be inconsequential for activity of TMPRSS13. For this reason, it can be hypothesized that it is the inhibition of catalytic activity by co-expression with HAI-2, rather than the intracellular phosphorylation, that allows for cell surface localization of otherwise enzymatically active TMPRSS13. To test this, NP S506A-TMPRSS13 will be transfected into HEK293T cells with or without co-expression of HAI-2, and cell surface biotinylation as well as immunocytochemistry will be performed to visualize surface proteins. If inactivity – but not phosphorylation – is critical for cell surface localization, NP S506A-TMPRSS13 should be observed on the cell surface with or without co-expression with HAI-2.

Figure 21: Catalytically-dead NP- and PM-TMPRSS13 mutants
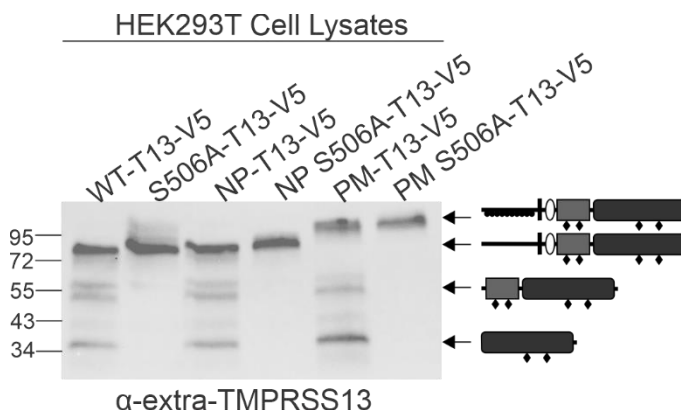
Figure 21: HEK293T cells were transfected for 48 hours with WT-TMPRSS13 (T13)-V5, S506A-T13-V5, NP-T13-V5, NP S506A-T13-V5, PM-T13-V5 or PM S506A-T13-V5. Proteins in whole cell lysates were separated by SDS-PAGE under reducing conditions using 4-15% gels and analyzed by western blotting. Proteins were detected using anti-extra-TMPRSS13 antibody. Arrows and schematics to the right of the western blots define the TMPRSS13 form that is detailed in the text.

In conclusion, elucidating the roles that N-linked glycosylation, stem region cleavage, and intracellular phosphorylation play in the autoactivation, enzymatic activity, and localization of TMPRSS13 gives insight into the function of the protease. These studies may help to identify the pro-oncogenic pathways to which TMPRSS13 belongs, and may also aid in the development of TMPRSS13-specific inhibitors and in understanding the cellular effects of targeting TMPRSS13.

5.5 Materials and methods

5.5.1 Cell lines and culture conditions

HEK293T and MCF7 cells (ATCC, Manassas, VA) were cultured in Dulbecco's modified eagle media (Gibco/Thermo Fisher Scientific) supplemented with 10% fetal bovine serum (FBS) (Atlanta Biologicals, Lawrenceville, GA), 10 units/mL Penicillin and 10 µg/mL streptomycin (Gibco, Life Technologies, Grand Island, NY). DLD1 cells (ATCC) were grown in RPMI 1640 media + L-GLUT media adjusted to contain 10% FBS).

5.5.2 Western blotting

Cultured human cells were washed 3 times with ice-cold PBS and lysed in-well using ice-cold RIPA buffer (150 mM NaCl; 50 mM Tris/HCl, pH 7.4, 0.1% SDS; 1% NP-40) with protease

inhibitor cocktail (Sigma Aldrich, St. Louis, MO) and phosphatase inhibitor cocktail (Sigma Aldrich), and cleared by centrifugation at 12,000 x g at 4°C. Protein concentrations in cell lysates were determined using a Pierce BCA Protein Assay Kit (Thermo Fisher Scientific, Waltham, MA). Proteins were separated by SDS-PAGE under reducing conditions using 10% or 4-15% Mini-Protean® gels or Criterion™ TGX midi gels (Bio-Rad) and blotted onto PVDF membranes (Bio-Rad). Membranes were blocked with 5% (w/v) dry milk powder in TBS-T (Tris-buffered saline, 0.1% Tween-20) for 1 hour at room temperature and subsequently incubated overnight at 4 °C in primary antibodies diluted in 5% dry milk powder/TBS-T. Primary antibodies used for western blotting included rabbit anti-TMPRSS13 raised against a recombinant protein fragment corresponding to a region within amino acids 195 and 562 of human TMPRSS13 (anti-extra-TMPRSS13) (PA5-30935, Thermo Fisher Scientific and Life Technologies, Inc); goat anti-HAI-2 (AF1106, R&D Systems Inc., Minneapolis, MN); rabbit anti-TMPRSS13 raised against an epitope within the first 60 amino acids of human TMPRSS13 (anti-intra-TMPRSS13) (ab59862, Abcam, Cambridge, MA); rabbit anti-ERK1/2 (137F5, Cell Signaling Technology, Danvers, MA); mouse anti-ppERK1/2 (M8159, Sigma Aldrich), rabbit anti-pp90RSK (9344S, Cell Signaling Technology), and mouse anti-beta-actin (NB600-501, Novus Biologicals, Littleton, CO). Secondary antibodies included horseradish peroxidase conjugated goat anti-rabbit (12-348, Millipore, Billerica, MA), goat anti-mouse (AP181P, Millipore), and rabbit anti-goat (31403, Thermo Fisher Scientific) antibodies. Detection of antibodies was performed using Clarity ECL Western Blotting substrate (Bio-Rad) or Super-Signal West Femto Chemiluminescent Substrate (Pierce, Thermo Fisher Scientific). Chemiluminescent imaging was performed using the ChemiDocMP™ imaging system (Bio-Rad). After detection, PVDF membranes were stripped using Restore™ Western Blot Stripping Buffer (Thermo Fisher Scientific) for 15 minutes at room temperature prior to re-probing with a different primary antibody.

5.5.3 Cloning of full-length TMPRSS13 plasmid constructs

WT-TMPRSS13-V5, S506A-TMPRSS13-V5, and R320Q-TMPRSS13-V5 constructs were generated as previously described (47). Intracellular deletion mutations using WT-TMPRSS13-V5 or CD-TMPRSS13-V5 as a template were generated using the Q5® Site-Directed Mutagenesis Kit (New England Biolabs, Ipswich, MA). The NP-TMPRSS13-V5 and PM-TMPRSS13-V5 mutant plasmids were synthesized by the GenScript company (Piscataway, NJ). NP S506A-TMPRSS13-V5 and PM-S506A-TMPRSS13-V5 point mutations were generated using the Q5® Site-Directed Mutagenesis Kit using NP-TMPRSS13-V5 and PM-TMPRSS13-V5, respectively, as templates. Primers used for Δ10-147-TMPRSS13-V5 mutagenesis were 5'-CCTGCCCAAGTTCACCTG-3' and 5'- GCATTCCCGTGGCTGTCC-3'. Primers used for Δ10-45-TMPRSS13-V5 mutagenesis were 5'-TCCAGCTGGGACACCTCC-3' and 5'-GCATTCCCGTGGCTGTCC-3'. Primers used for Δ41-115-TMPRSS13-V5 mutagenesis were 5'-CTTGTTAGAGCAACACCAGTG-3' and 5'-AGATGCCTGGGCTGGAGA-3'. Primers used for Δ116-148-TMPRSS13-V5 mutagenesis were 5'-CCTGCCCAAGTTCACCTG-3' and 5'-TACACTCTGGTTGGGGAG-3'. Primers used for NP S506A-TMPRSS13-V5 and PM S506A-TMPRSS13 mutagenesis were 5'-CCAGGGAGACGCTGGGGGGCCTCTTG-3' and 5'-CAGGAGTCTCTGCCCCCA-3'. Transformation of all vectors was performed in NEB 5-alpha Competent E. *coli* cells (New England Biolabs) and positive clones were isolated and amplified using standard techniques. Mutations were verified by DNA sequencing.

5.5.4 Transient transfections with TMPRSS13 expression vectors

Transfections of HEK293T cells were performed using Lipofectamine® LTX reagent with PLUS™ reagent according to the manufacturer's instructions (Invitrogen, Life Technologies, Inc.). Transfection was performed with 500 ng of plasmid DNA for single transfections or 1 µg of DNA total for co-transfections. Vectors included in transfections were pcDNA3.1-TMPRSS13 vectors, empty vector pcDNA3.1, and pcDNA3.1-HAI-2 (227).

5.5.5 Prostasin/PN-1 complex formation assay

Forward transfection of the mammalian expression vector pIRES2-EGFP containing full-length human prostasin cDNA and TMPRSS13 plasmids was performed in HEK293T cells. Transfection was performed with 1 µg of total plasmid DNA for co-transfections per well using Lipofectamine® LTX reagent with PLUS™ reagent according to the manufacturer's instructions (Invitrogen, Life Technologies, Inc.). For phosphatidylinositol-specific phospholipase C (PI-PLC) treatment, washed cells were mechanically lifted from the plates by gentle pipetting, incubated with 1 unit/ml PI-PLC (Sigma-Aldrich) in PBS for 4 h at 4°C, then centrifuged for 10 min at 1000 x g, and the supernatant containing the PI-PLC-released proteins was collected. For complex formation, PN-1 derived from murine sperm (described in (211)) was added for 1 h at 37°C in 50 mM Tris, 100 nM NaCl pH 8.5. Proteins were analyzed by reducing SDS-PAGE and western blot analysis.

5.5.6 Cycloheximide treatment

Cancer cells were seeded 24 hours prior to treatment with 75 µg/ml of cycloheximide (C-1189, AG Scientific) for up to 48 hours. Following treatment, cells were washed three times in PBS and lysed in-well using RIPA buffer.

5.5.7 Roscovitine treatment

Roscovitine (S1153, Selleck Chemicals, Houston, TX) was reconstituted to 10 mM in DMSO. Cancer cells were seeded 24 hours prior to treatment with 0 µM, 10 µM, 20 µM or 40 µM roscovitine for up to 24 hours. For co-treatment with U0126 (S1102, Selleck Chemicals), 10 µM U0126 was added to cells concomitantly with roscovitine and cells were treated for up to 8 hours with the combination. Following treatment, cells were washed three times in PBS and lysed in-well using RIPA buffer.

5.5.8 Immunocytochemistry

Cell imaging was performed using HEK293T cells expressing human full-length TMPRSS13 vectors or empty vector pcDNA3.1. HAI-2 was visualized using a vector expressing

a HAI-2-EYFP fusion protein (228). Cells were seeded onto glass coverslips and allowed to grow overnight. Cells were transiently transfected for 48 h, after which media was removed and cells were fixed in Z-FIX (ANATECH LTD, Battle Creek, MI) for 15 min at room temperature. Cells were then blocked in 5% BSA in PBS for 1 h on ice prior to addition of primary antibodies. After incubation with primary antibodies overnight at 4°C, cells were washed in PBS and secondary Texas Red-conjugated goat anti-mouse antibody (Invitrogen, Life Technologies, Inc.) was used to detect TMPRSS13-V5. Cells were washed with PBS and mounted with ProLong™ Diamond Antifade Mountant with DAPI (Invitrogen). Confocal images were acquired on the Leica SP5 scope at the Microscopy Imaging and Cytometry Resources Core at Wayne State University School of Medicine.

5.5.9 Identification of phosphorylated residues

HEK293T cells were transfected for 48 hours with WT-TMPRSS13 and S506A-TMPRSS13. Proteins in cell lysates were separated by SDS-PAGE and gels were stained with Coomassie blue. A high molecular weight (~95 kDa) band from S506A-TMPRSS13-V5 was excised from the gel, and an equivalent section of the gel was excised for the WT-TMPRSS13-V5 sample. Samples were analyzed for phosphorylated residues by the MS & Proteomics Resource at Yale University.

5.5.10 LC-MS/MS analysis to identify TMPRSS13 binding partners

Protocol was adapted from (261). 24 hours prior to transfection, 2 million HEK293T cells were seeded onto 10 cm dishes (3 dishes per transfection). Cells were subsequently washed and transfected with PCDNA3.1-TMPRSS13 vectors plus empty vector PCDNA3.1 or PCDNA3.1-HAI-2. 48 hours after transfection, cells were washed 3 times with cold PBS then harvested in 750 µl of lysis solution (5mM tris, 2mM EDTA, pH 7.4) plus protease inhibitor cocktail (Sigma Aldrich) per 10 cm dish using a rubber cell scraper. Cells were lysed using a glass homogenizer and lysates were centrifuged at 4 °C for 20 min at 1000 x g. Supernatants were harvested then centrifuged at 4 °C for 20 min at 16000 RPM using a Sorvall RC 5C Plus Ultra-Centrifuge with the

SS-34 fixed-angle rotor. Pellets were resuspended in 500 µl of solubilization buffer (1% octyl-β-D-glucopyranoside (O8001, Sigma-Aldrich), 75 mM Tris, 2 mM EDTA, 5 mM $MgCl_2$, pH 8.0) plus protease inhibitor cocktail for 30 min on ice. Solubilized membranes were incubated with 75 µl of V5-agarose beads (A7345, Sigma Aldrich) at 4 °C overnight. Beads were washed 4 times with 300 µl solubilization buffer without protease inhibitor cocktail, then 4 times with 300 µl of ammonium bicarbonate buffer (20 mM ammonium bicarbonate pH 8.0, prepared in LC-MS grade water). Beads were transferred to low protein-binding tube then washed once more with ammonium bicarbonate buffer then beads were dried and frozen at -80 °C until processing for LC-MS/MS analysis. HPLC and mass spectrometry was performed at the Université de Sherbrooke, QC, Canada. Analysis was performed using MS/MS counts in the Contaminant Repository for Affinity Purification (CRAPome) analysis to compare experimental pulled-down proteins to proteins pulled down in negative control. Venny2.1 and STRING databases were used to visualize results in Venn diagrams or interaction maps, respectively.

REFERENCES

1. Martin, C. E., and List, K. (2019) Cell surface-anchored serine proteases in cancer progression and metastasis. *Cancer Metastasis Rev*

2. López-Otín, C., and Bond, J. S. (2008) Proteases: multifunctional enzymes in life and disease. *J Biol Chem* **283**, 30433-30437

3. Pérez-Silva, J. G., Español, Y., Velasco, G., and Quesada, V. (2016) The Degradome database: expanding roles of mammalian proteases in life and disease. *Nucleic Acids Res* **44**, D351-355

4. Bond, J. S. (2019) Proteases: History, discovery, and roles in health and disease. *J Biol Chem* **294**, 1643-1651

5. Chapman, H. A., Riese, R. J., and Shi, G. P. (1997) Emerging roles for cysteine proteases in human biology. *Annu Rev Physiol* **59**, 63-88

6. Cianni, L., Feldmann, C. W., Gilberg, E., Gütschow, M., Juliano, L., Leitão, A., Bajorath, J., and Montanari, C. A. (2019) Can Cysteine Protease Cross-Class Inhibitors Achieve Selectivity? *J Med Chem* **62**, 10497-10525

7. Verma, S., Dixit, R., and Pandey, K. C. (2016) Cysteine Proteases: Modes of Activation and Future Prospects as Pharmacological Targets. *Front Pharmacol* **7**, 107

8. Mohamed, M. M., and Sloane, B. F. (2006) Cysteine cathepsins: multifunctional enzymes in cancer. *Nat Rev Cancer* **6**, 764-775

9. Olson, O. C., and Joyce, J. A. (2015) Cysteine cathepsin proteases: regulators of cancer progression and therapeutic response. *Nat Rev Cancer* **15**, 712-729

10. Kostoulas, G., Lang, A., Nagase, H., and Baici, A. (1999) Stimulation of angiogenesis through cathepsin B inactivation of the tissue inhibitors of matrix metalloproteinases. *FEBS Lett* **455**, 286-290

11.   Gocheva, V., Zeng, W., Ke, D., Klimstra, D., Reinheckel, T., Peters, C., Hanahan, D., and Joyce, J. A. (2006) Distinct roles for cysteine cathepsin genes in multistage tumorigenesis. *Genes Dev* **20**, 543-556

12.   Van Opdenbosch, N., and Lamkanfi, M. (2019) Caspases in Cell Death, Inflammation, and Disease. *Immunity* **50**, 1352-1364

13.   Ramirez, M. L. G., and Salvesen, G. S. (2018) A primer on caspase mechanisms. *Semin Cell Dev Biol* **82**, 79-85

14.   Shi, Y. (2004) Caspase activation, inhibition, and reactivation: a mechanistic view. *Protein Sci* **13**, 1979-1987

15.   Bao, Q., and Shi, Y. (2007) Apoptosome: a platform for the activation of initiator caspases. *Cell Death Differ* **14**, 56-65

16.   Khokha, R., Murthy, A., and Weiss, A. (2013) Metalloproteinases and their natural inhibitors in inflammation and immunity. *Nat Rev Immunol* **13**, 649-665

17.   Tocchi, A., and Parks, W. C. (2013) Functional interactions between matrix metalloproteinases and glycosaminoglycans. *FEBS J* **280**, 2332-2341

18.   Lorenzen, I., Lokau, J., Korpys, Y., Oldefest, M., Flynn, C. M., Künzel, U., Garbers, C., Freeman, M., Grötzinger, J., and Düsterhöft, S. (2016) Control of ADAM17 activity by regulation of its cellular localisation. *Sci Rep* **6**, 35067

19.   Chalaris, A., Adam, N., Sina, C., Rosenstiel, P., Lehmann-Koch, J., Schirmacher, P., Hartmann, D., Cichy, J., Gavrilova, O., Schreiber, S., Jostock, T., Matthews, V., Häsler, R., Becker, C., Neurath, M. F., Reiss, K., Saftig, P., Scheller, J., and Rose-John, S. (2010) Critical role of the disintegrin metalloprotease ADAM17 for intestinal inflammation and regeneration in mice. *J Exp Med* **207**, 1617-1624

20.   Baumgart, A., Seidl, S., Vlachou, P., Michel, L., Mitova, N., Schatz, N., Specht, K., Koch, I., Schuster, T., Grundler, R., Kremer, M., Fend, F., Siveke, J. T., Peschel, C., Duyster, J.,

and Dechow, T. (2010) ADAM17 regulates epidermal growth factor receptor expression through the activation of Notch1 in non-small cell lung cancer. *Cancer Res* **70**, 5368-5378

21. Winer, A., Adams, S., and Mignatti, P. (2018) Matrix Metalloproteinase Inhibitors in Cancer Therapy: Turning Past Failures Into Future Successes. *Mol Cancer Ther* **17**, 1147-1155

22. Fields, G. B. (2019) The Rebirth of Matrix Metalloproteinase Inhibitors: Moving Beyond the Dogma. *Cells* **8**

23. Puente, X. S., Sanchez, L. M., Gutierrez-Fernandez, A., Velasco, G., and Lopez-Otin, C. (2005) A genomic view of the complexity of mammalian proteolytic systems. *Biochemical Society transactions* **33**, 331-334

24. Di Cera, E. (2009) Serine proteases. *IUBMB Life* **61**, 510-515

25. Blow, D. M., Birktoft, J. J., and Hartley, B. S. (1969) Role of a buried acid group in the mechanism of action of chymotrypsin. *Nature* **221**, 337-340

26. Hedstrom, L. (2002) Serine protease mechanism and specificity. *Chem Rev* **102**, 4501-4524

27. Radisky, E. S., Lee, J. M., Lu, C. J., and Koshland, D. E. (2006) Insights into the serine protease mechanism from atomic resolution structures of trypsin reaction intermediates. *Proc Natl Acad Sci U S A* **103**, 6835-6840

28. Caughey, G. H. (2007) Mast cell tryptases and chymases in inflammation and host defense. *Immunological reviews* **217**, 141-154

29. Netzel-Arnett, S., Hooper, J. D., Szabo, R., Madison, E. L., Quigley, J. P., Bugge, T. H., and Antalis, T. M. (2003) Membrane anchored serine proteases: a rapidly expanding group of cell surface proteolytic enzymes with potential roles in cancer. *Cancer Metastasis Rev* **22**, 237-258

30. Busek, P., Mateu, R., Zubal, M., Kotackova, L., and Sedo, A. (2018) Targeting fibroblast activation protein in cancer - Prospects and caveats. *Frontiers in bioscience (Landmark edition)* **23**, 1933-1968

31. Zi, F., He, J., He, D., Li, Y., Yang, L., and Cai, Z. (2015) Fibroblast activation protein alpha in tumor microenvironment: recent progression and implications (review). *Molecular medicine reports* **11**, 3203-3211

32. Antalis, T. M., Buzza, M. S., Hodge, K. M., Hooper, J. D., and Netzel-Arnett, S. (2010) The cutting edge: membrane-anchored serine protease activities in the pericellular microenvironment. *The Biochemical journal* **428**, 325-346

33. Hooper, J. D., Clements, J. A., Quigley, J. P., and Antalis, T. M. (2001) Type II transmembrane serine proteases. Insights into an emerging class of cell surface proteolytic enzymes. *J Biol Chem* **276**, 857-860

34. Bugge, T. H., Antalis, T. M., and Wu, Q. (2009) Type II transmembrane serine proteases. *The Journal of biological chemistry* **284**, 23177-23181

35. Bugge, T. H., List, K., and Szabo, R. (2007) Matriptase-dependent cell surface proteolysis in epithelial development and pathogenesis. *Frontiers in bioscience : a journal and virtual library* **12**, 5060-5070

36. Szabo, R., and Bugge, T. H. (2008) Type II transmembrane serine proteases in development and disease. *The international journal of biochemistry & cell biology* **40**, 1297-1316

37. Szabo, R., and Bugge, T. H. (2011) Membrane-anchored serine proteases in vertebrate cell and developmental biology. *Annu Rev Cell Dev Biol* **27**, 213-235

38. Murray, A. S., Varela, F. A., and List, K. (2016) Type II transmembrane serine proteases as potential targets for cancer therapy. *Biol Chem* **397**, 815-826

39. Tanabe, L. M., and List, K. (2017) The role of type II transmembrane serine protease-mediated signaling in cancer. *FEBS J* **284**, 1421-1436

40. Antalis, T. M., Bugge, T. H., and Wu, Q. (2011) Membrane-anchored serine proteases in health and disease. *Prog Mol Biol Transl Sci* **99**, 1-50

41. Takeuchi, T., Harris, J. L., Huang, W., Yan, K. W., Coughlin, S. R., and Craik, C. S. (2000) Cellular localization of membrane-type serine protease 1 and identification of protease-activated receptor-2 and single-chain urokinase-type plasminogen activator as substrates. *The Journal of biological chemistry* **275**, 26333-26342

42. Jiang, J., Yang, J., Feng, P., Zuo, B., Dong, N., Wu, Q., and He, Y. (2014) N-glycosylation is required for matriptase-2 autoactivation and ectodomain shedding. *J Biol Chem* **289**, 19500-19507

43. Qiu, D., Owen, K., Gray, K., Bass, R., and Ellis, V. (2007) Roles and regulation of membrane-associated serine proteases. *Biochemical Society transactions* **35**, 583-587

44. Afar, D. E., Vivanco, I., Hubert, R. S., Kuo, J., Chen, E., Saffran, D. C., Raitano, A. B., and Jakobovits, A. (2001) Catalytic cleavage of the androgen-regulated TMPRSS2 protease results in its secretion by prostate and prostate cancer epithelia. *Cancer research* **61**, 1686-1692

45. Guipponi, M., Vuagniaux, G., Wattenhofer, M., Shibuya, K., Vazquez, M., Dougherty, L., Scamuffa, N., Guida, E., Okui, M., Rossier, C., Hancock, M., Buchet, K., Reymond, A., Hummler, E., Marzella, P. L., Kudoh, J., Shimizu, N., Scott, H. S., Antonarakis, S. E., and Rossier, B. C. (2002) The transmembrane serine protease (TMPRSS3) mutated in deafness DFNB8/10 activates the epithelial sodium channel (ENaC) in vitro. *Human molecular genetics* **11**, 2829-2836

46. Andreasen, D., Vuagniaux, G., Fowler-Jaeger, N., Hummler, E., and Rossier, B. C. (2006) Activation of epithelial sodium channels by mouse channel activating proteases (mCAP) expressed in Xenopus oocytes requires catalytic activity of mCAP3 and mCAP2 but not mCAP1. *Journal of the American Society of Nephrology : JASN* **17**, 968-976

47. Murray, A. S., Varela, F. A., Hyland, T. E., Schoenbeck, A. J., White, J. M., Tanabe, L. M., Todi, S. V., and List, K. (2017) Phosphorylation of the type II transmembrane serine

protease, TMPRSS13, in hepatocyte growth factor activator inhibitor-1 and -2-mediated cell-surface localization. *The Journal of biological chemistry* **292**, 14867-14884

48. Oberst, M. D., Williams, C. A., Dickson, R. B., Johnson, M. D., and Lin, C. Y. (2003) The activation of matriptase requires its noncatalytic domains, serine protease domain, and its cognate inhibitor. *The Journal of biological chemistry* **278**, 26773-26779

49. Tseng, I. C., Xu, H., Chou, F. P., Li, G., Vazzano, A. P., Kao, J. P., Johnson, M. D., and Lin, C. Y. (2010) Matriptase activation, an early cellular response to acidosis. *The Journal of biological chemistry* **285**, 3261-3270

50. Godiksen, S., Soendergaard, C., Friis, S., Jensen, J. K., Bornholdt, J., Sales, K. U., Huang, M., Bugge, T. H., and Vogel, L. K. (2013) Detection of active matriptase using a biotinylated chloromethyl ketone peptide. *PloS one* **8**, e77146

51. Tamberg, T., Hong, Z., De Schepper, D., Skovbjerg, S., Dupont, D. M., Vitved, L., Schar, C. R., Skjoedt, K., Vogel, L. K., and Jensen, J. K. (2019) Blocking the proteolytic activity of zymogen matriptase with antibody-based inhibitors. *J Biol Chem* **294**, 314-326

52. Inouye, K., Yasumoto, M., Tsuzuki, S., Mochida, S., and Fushiki, T. (2010) The optimal activity of a pseudozymogen form of recombinant matriptase under the mildly acidic pH and low ionic strength conditions. *Journal of biochemistry* **147**, 485-492

53. Friis, S., Tadeo, D., Le-Gall, S. M., Jurgensen, H. J., Sales, K. U., Camerer, E., and Bugge, T. H. (2017) Matriptase zymogen supports epithelial development, homeostasis and regeneration. *BMC biology* **15**, 46

54. Yu, J. X., Chao, L., and Chao, J. (1994) Prostasin is a novel human serine proteinase from seminal fluid. Purification, tissue distribution, and localization in prostate gland. *The Journal of biological chemistry* **269**, 18843-18848

55. Chen, L. M., Skinner, M. L., Kauffman, S. W., Chao, J., Chao, L., Thaler, C. D., and Chai, K. X. (2001) Prostasin is a glycosylphosphatidylinositol-anchored active serine protease. *The Journal of biological chemistry* **276**, 21434-21442

56. Szabo, R., Hobson, J. P., List, K., Molinolo, A., Lin, C. Y., and Bugge, T. H. (2008) Potent inhibition and global co-localization implicate the transmembrane Kunitz-type serine protease inhibitor hepatocyte growth factor activator inhibitor-2 in the regulation of epithelial matriptase activity. *The Journal of biological chemistry* **283**, 29495-29504

57. Chen, Y. W., Wang, J. K., Chou, F. P., Chen, C. Y., Rorke, E. A., Chen, L. M., Chai, K. X., Eckert, R. L., Johnson, M. D., and Lin, C. Y. (2010) Regulation of the matriptase-prostasin cell surface proteolytic cascade by hepatocyte growth factor activator inhibitor-1 during epidermal differentiation. *The Journal of biological chemistry* **285**, 31755-31762

58. Fan, B., Wu, T. D., Li, W., and Kirchhofer, D. (2005) Identification of hepatocyte growth factor activator inhibitor-1B as a potential physiological inhibitor of prostasin. *The Journal of biological chemistry* **280**, 34513-34520

59. Inoue, M., Kanbe, N., Kurosawa, M., and Kido, H. (1998) Cloning and tissue distribution of a novel serine protease esp-1 from human eosinophils. *Biochemical and biophysical research communications* **252**, 307-312

60. Hooper, J. D., Nicol, D. L., Dickinson, J. L., Eyre, H. J., Scarman, A. L., Normyle, J. F., Stuttgen, M. A., Douglas, M. L., Loveland, K. A., Sutherland, G. R., and Antalis, T. M. (1999) Testisin, a new human serine proteinase expressed by premeiotic testicular germ cells and lost in testicular germ cell tumors. *Cancer research* **59**, 3199-3205

61. Tang, T., Kmet, M., Corral, L., Vartanian, S., Tobler, A., and Papkoff, J. (2005) Testisin, a glycosyl-phosphatidylinositol-linked serine protease, promotes malignant transformation in vitro and in vivo. *Cancer research* **65**, 868-878

62. Kempkensteffen, C., Christoph, F., Weikert, S., Krause, H., Kollermann, J., Schostak, M., Miller, K., and Schrader, M. (2006) Epigenetic silencing of the putative tumor suppressor gene testisin in testicular germ cell tumors. *Journal of cancer research and clinical oncology* **132**, 765-770

63. Manton, K. J., Douglas, M. L., Netzel-Arnett, S., Fitzpatrick, D. R., Nicol, D. L., Boyd, A. W., Clements, J. A., and Antalis, T. M. (2015) Hypermethylation of the 5' CpG island of the gene encoding the serine protease Testisin promotes its loss in testicular tumorigenesis. *British journal of cancer* **113**, 1640

64. Lin, C. Y., Wang, J. K., Torri, J., Dou, L., Sang, Q. A., and Dickson, R. B. (1997) Characterization of a novel, membrane-bound, 80-kDa matrix-degrading protease from human breast cancer cells. Monoclonal antibody production, isolation, and localization. *The Journal of biological chemistry* **272**, 9147-9152

65. Kim, M. G., Chen, C., Lyu, M. S., Cho, E. G., Park, D., Kozak, C., and Schwartz, R. H. (1999) Cloning and chromosomal mapping of a gene isolated from thymic stromal cells encoding a new mouse type II membrane serine protease, epithin, containing four LDL receptor modules and two CUB domains. *Immunogenetics* **49**, 420-428

66. Takeuchi, T., Shuman, M. A., and Craik, C. S. (1999) Reverse biochemistry: use of macromolecular protease inhibitors to dissect complex biological processes and identify a membrane-type serine protease in epithelial cancer and normal tissue. *Proceedings of the National Academy of Sciences of the United States of America* **96**, 11054-11061

67. Tanimoto, H., Underwood, L. J., Wang, Y., Shigemasa, K., Parmley, T. H., and O'Brien, T. J. (2001) Ovarian tumor cells express a transmembrane serine protease: a potential candidate for early diagnosis and therapeutic intervention. *Tumour biology : the journal of the International Society for Oncodevelopmental Biology and Medicine* **22**, 104-114

68. Bhatt, A. S., Welm, A., Farady, C. J., Vasquez, M., Wilson, K., and Craik, C. S. (2007) Coordinate expression and functional profiling identify an extracellular proteolytic signaling pathway. *Proceedings of the National Academy of Sciences of the United States of America* **104**, 5771-5776

69. Bignotti, E., Tassi, R. A., Calza, S., Ravaggi, A., Bandiera, E., Rossi, E., Donzelli, C., Pasinetti, B., Pecorelli, S., and Santin, A. D. (2007) Gene expression profile of ovarian

serous papillary carcinomas: identification of metastasis-associated genes. *American Journal of Obstetrics and Gynecology* **196**, 245.e241-245.e211

70. List, K., Bugge, T. H., and Szabo, R. (2006) Matriptase: potent proteolysis on the cell surface. *Molecular medicine (Cambridge, Mass.)* **12**, 1-7

71. List, K., Haudenschild, C. C., Szabo, R., Chen, W., Wahl, S. M., Swaim, W., Engelholm, L. H., Behrendt, N., and Bugge, T. H. (2002) Matriptase/MT-SP1 is required for postnatal survival, epidermal barrier function, hair follicle development, and thymic homeostasis. *Oncogene* **21**, 3765-3779

72. List, K., Kosa, P., Szabo, R., Bey, A. L., Wang, C. B., Molinolo, A., and Bugge, T. H. (2009) Epithelial integrity is maintained by a matriptase-dependent proteolytic pathway. *The American journal of pathology* **175**, 1453-1463

73. Avrahami, L., Maas, S., Pasmanik-Chor, M., Rainshtein, L., Magal, N., Smitt, J., van Marle, J., Shohat, M., and Basel-Vanagaite, L. (2008) Autosomal recessive ichthyosis with hypotrichosis syndrome: further delineation of the phenotype. *Clinical genetics* **74**, 47-53

74. Scharschmidt, T. C., List, K., Grice, E. A., Szabo, R., Renaud, G., Lee, C. C., Wolfsberg, T. G., Bugge, T. H., and Segre, J. A. (2009) Matriptase-deficient mice exhibit ichthyotic skin with a selective shift in skin microbiota. *The Journal of investigative dermatology* **129**, 2435-2442

75. Lee, S. L., Dickson, R. B., and Lin, C. Y. (2000) Activation of hepatocyte growth factor and urokinase/plasminogen activator by matriptase, an epithelial membrane serine protease. *The Journal of biological chemistry* **275**, 36720-36725

76. Forbs, D., Thiel, S., Stella, M. C., Sturzebecher, A., Schweinitz, A., Steinmetzer, T., Sturzebecher, J., and Uhland, K. (2005) In vitro inhibition of matriptase prevents invasive growth of cell lines of prostate and colon carcinoma. *International journal of oncology* **27**, 1061-1070

77. Kilpatrick, L. M., Harris, R. L., Owen, K. A., Bass, R., Ghorayeb, C., Bar-Or, A., and Ellis, V. (2006) Initiation of plasminogen activation on the surface of monocytes expressing the type II transmembrane serine protease matriptase. *Blood* **108**, 2616-2623

78. Ustach, C. V., Huang, W., Conley-LaComb, M. K., Lin, C. Y., Che, M., Abrams, J., and Kim, H. R. (2010) A novel signaling axis of matriptase/PDGF-D/ss-PDGFR in human prostate cancer. *Cancer research* **70**, 9631-9640

79. Sales, K. U., Friis, S., Konkel, J. E., Godiksen, S., Hatakeyama, M., Hansen, K. K., Rogatto, S. R., Szabo, R., Vogel, L. K., Chen, W., Gutkind, J. S., and Bugge, T. H. (2015) Non-hematopoietic PAR-2 is essential for matriptase-driven pre-malignant progression and potentiation of ras-mediated squamous cell carcinogenesis. *Oncogene* **34**, 346-356

80. Camerer, E., Barker, A., Duong, D. N., Ganesan, R., Kataoka, H., Cornelissen, I., Darragh, M. R., Hussain, A., Zheng, Y. W., Srinivasan, Y., Brown, C., Xu, S. M., Regard, J. B., Lin, C. Y., Craik, C. S., Kirchhofer, D., and Coughlin, S. R. (2010) Local protease signaling contributes to neural tube closure in the mouse embryo. *Developmental cell* **18**, 25-38

81. Szabo, R., Rasmussen, A. L., Moyer, A. B., Kosa, P., Schafer, J. M., Molinolo, A. A., Gutkind, J. S., and Bugge, T. H. (2011) c-Met-induced epithelial carcinogenesis is initiated by the serine protease matriptase. *Oncogene* **30**, 2003-2016

82. Zoratti, G. L., Tanabe, L. M., Hyland, T. E., Duhaime, M. J., Colombo, E., Leduc, R., Marsault, E., Johnson, M. D., Lin, C. Y., Boerner, J., Lang, J. E., and List, K. (2016) Matriptase regulates c-Met mediated proliferation and invasion in inflammatory breast cancer. *Oncotarget*

83. Zoratti, G. L., Tanabe, L. M., Varela, F. A., Murray, A. S., Bergum, C., Colombo, E., Lang, J. E., Molinolo, A. A., Leduc, R., Marsault, E., Boerner, J., and List, K. (2015) Targeting matriptase in breast cancer abrogates tumour progression via impairment of stromal-epithelial growth factor signalling. *Nature communications* **6**, 6776

84. Velasco, G., Cal, S., Quesada, V., Sanchez, L. M., and Lopez-Otin, C. (2002) Matriptase-2, a membrane-bound mosaic serine proteinase predominantly expressed in human liver and showing degrading activity against extracellular matrix proteins. *The Journal of biological chemistry* **277**, 37637-37646

85. Hooper, J. D., Campagnolo, L., Goodarzi, G., Truong, T. N., Stuhlmann, H., and Quigley, J. P. (2003) Mouse matriptase-2: identification, characterization and comparative mRNA expression analysis with mouse hepsin in adult and embryonic tissues. *The Biochemical journal* **373**, 689-702

86. Wang, C. Y., Meynard, D., and Lin, H. Y. (2014) The role of TMPRSS6/matriptase-2 in iron regulation and anemia. *Frontiers in pharmacology* **5**, 114

87. Stirnberg, M., and Gutschow, M. (2013) Matriptase-2, a regulatory protease of iron homeostasis: possible substrates, cleavage sites and inhibitors. *Current pharmaceutical design* **19**, 1052-1061

88. Lee, P. (2009) Role of matriptase-2 (TMPRSS6) in iron metabolism. *Acta haematologica* **122**, 87-96

89. Tuhkanen, H., Hartikainen, J. M., Soini, Y., Velasco, G., Sironen, R., Nykopp, T. K., Kataja, V., Eskelinen, M., Kosma, V. M., and Mannermaa, A. (2013) Matriptase-2 gene (TMPRSS6) variants associate with breast cancer survival, and reduced expression is related to triple-negative breast cancer. *International journal of cancer* **133**, 2334-2340

90. Finberg, K. E., Heeney, M. M., Campagna, D. R., Aydinok, Y., Pearson, H. A., Hartman, K. R., Mayo, M. M., Samuel, S. M., Strouse, J. J., Markianos, K., Andrews, N. C., and Fleming, M. D. (2008) Mutations in TMPRSS6 cause iron-refractory iron deficiency anemia (IRIDA). *Nature genetics* **40**, 569-571

91. Silvestri, L., Pagani, A., Nai, A., De Domenico, I., Kaplan, J., and Camaschella, C. (2008) The serine protease matriptase-2 (TMPRSS6) inhibits hepcidin activation by cleaving membrane hemojuvelin. *Cell metabolism* **8**, 502-511

92. Folgueras, A. R., de Lara, F. M., Pendas, A. M., Garabaya, C., Rodriguez, F., Astudillo, A., Bernal, T., Cabanillas, R., Lopez-Otin, C., and Velasco, G. (2008) Membrane-bound serine protease matriptase-2 (Tmprss6) is an essential regulator of iron homeostasis. *Blood* **112**, 2539-2545

93. Ramsay, A. J., Reid, J. C., Velasco, G., Quigley, J. P., and Hooper, J. D. (2008) The type II transmembrane serine protease matriptase-2--identification, structural features, enzymology, expression pattern and potential roles. *Frontiers in bioscience : a journal and virtual library* **13**, 569-579

94. Melis, M. A., Cau, M., Congiu, R., Sole, G., Barella, S., Cao, A., Westerman, M., Cazzola, M., and Galanello, R. (2008) A mutation in the TMPRSS6 gene, encoding a transmembrane serine protease that suppresses hepcidin production, in familial iron deficiency anemia refractory to oral iron. *Haematologica* **93**, 1473-1479

95. Chen, L. M., and Chai, K. X. (2017) Proteolytic cleavages in the extracellular domain of receptor tyrosine kinases by membrane-associated serine proteases. *Oncotarget* **8**, 56490-56505

96. Leytus, S. P., Loeb, K. R., Hagen, F. S., Kurachi, K., and Davie, E. W. (1988) A novel trypsin-like serine protease (hepsin) with a putative transmembrane domain expressed by human liver and hepatoma cells. *Biochemistry* **27**, 1067-1074

97. Tsuji, A., Torres-Rosado, A., Arai, T., Chou, S. H., and Kurachi, K. (1991) Characterization of hepsin, a membrane bound protease. *Biomedica biochimica acta* **50**, 791-793

98. Tsuji, A., Torres-Rosado, A., Arai, T., Le Beau, M. M., Lemons, R. S., Chou, S. H., and Kurachi, K. (1991) Hepsin, a cell membrane-associated protease. Characterization, tissue distribution, and gene localization. *The Journal of biological chemistry* **266**, 16948-16953

99. Vu, T. K., Liu, R. W., Haaksma, C. J., Tomasek, J. J., and Howard, E. W. (1997) Identification and cloning of the membrane-associated serine protease, hepsin, from mouse preimplantation embryos. *The Journal of biological chemistry* **272**, 31315-31320

100. Guipponi, M., Tan, J., Cannon, P. Z., Donley, L., Crewther, P., Clarke, M., Wu, Q., Shepherd, R. K., and Scott, H. S. (2007) Mice deficient for the type II transmembrane serine protease, TMPRSS1/hepsin, exhibit profound hearing loss. *The American journal of pathology* **171**, 608-616

101. Herter, S., Piper, D. E., Aaron, W., Gabriele, T., Cutler, G., Cao, P., Bhatt, A. S., Choe, Y., Craik, C. S., Walker, N., Meininger, D., Hoey, T., and Austin, R. J. (2005) Hepatocyte growth factor is a preferred in vitro substrate for human hepsin, a membrane-anchored serine protease implicated in prostate and ovarian cancers. *The Biochemical journal* **390**, 125-136

102. Kirchhofer, D., Peek, M., Lipari, M. T., Billeci, K., Fan, B., and Moran, P. (2005) Hepsin activates pro-hepatocyte growth factor and is inhibited by hepatocyte growth factor activator inhibitor-1B (HAI-1B) and HAI-2. *FEBS letters* **579**, 1945-1950

103. Moran, P., Li, W., Fan, B., Vij, R., Eigenbrot, C., and Kirchhofer, D. (2006) Pro-urokinase-type plasminogen activator is a substrate for hepsin. *The Journal of biological chemistry* **281**, 30439-30446

104. Owen, K. A., Qiu, D., Alves, J., Schumacher, A. M., Kilpatrick, L. M., Li, J., Harris, J. L., and Ellis, V. (2010) Pericellular activation of hepatocyte growth factor by the transmembrane serine proteases matriptase and hepsin, but not by the membrane-associated protease uPA. *The Biochemical journal* **426**, 219-228

105. Tervonen, T. A., Belitskin, D., Pant, S. M., Englund, J. I., Marques, E., Ala-Hongisto, H., Nevalaita, L., Sihto, H., Heikkila, P., Leidenius, M., Hewitson, K., Ramachandra, M., Moilanen, A., Joensuu, H., Kovanen, P. E., Poso, A., and Klefstrom, J. (2016) Deregulated hepsin protease activity confers oncogenicity by concomitantly augmenting HGF/MET signalling and disrupting epithelial cohesion. *Oncogene* **35**, 1832-1846

106. Lin, B., Ferguson, C., White, J. T., Wang, S., Vessella, R., True, L. D., Hood, L., and Nelson, P. S. (1999) Prostate-localized and androgen-regulated expression of the membrane-bound serine protease TMPRSS2. *Cancer research* **59**, 4180-4184

107. Demichelis, F., Fall, K., Perner, S., Andren, O., Schmidt, F., Setlur, S. R., Hoshida, Y., Mosquera, J. M., Pawitan, Y., Lee, C., Adami, H. O., Mucci, L. A., Kantoff, P. W., Andersson, S. O., Chinnaiyan, A. M., Johansson, J. E., and Rubin, M. A. (2007) TMPRSS2:ERG gene fusion associated with lethal prostate cancer in a watchful waiting cohort. *Oncogene* **26**, 4596-4599

108. Tomlins, S. A., Laxman, B., Dhanasekaran, S. M., Helgeson, B. E., Cao, X., Morris, D. S., Menon, A., Jing, X., Cao, Q., Han, B., Yu, J., Wang, L., Montie, J. E., Rubin, M. A., Pienta, K. J., Roulston, D., Shah, R. B., Varambally, S., Mehra, R., and Chinnaiyan, A. M. (2007) Distinct classes of chromosomal rearrangements create oncogenic ETS gene fusions in prostate cancer. *Nature* **448**, 595-599

109. Tomlins, S. A., Rhodes, D. R., Perner, S., Dhanasekaran, S. M., Mehra, R., Sun, X. W., Varambally, S., Cao, X., Tchinda, J., Kuefer, R., Lee, C., Montie, J. E., Shah, R. B., Pienta, K. J., Rubin, M. A., and Chinnaiyan, A. M. (2005) Recurrent fusion of TMPRSS2 and ETS transcription factor genes in prostate cancer. *Science (New York, N.Y.)* **310**, 644-648

110. Vaarala, M. H., Porvari, K., Kyllonen, A., Lukkarinen, O., and Vihko, P. (2001) The TMPRSS2 gene encoding transmembrane serine protease is overexpressed in a majority of prostate cancer patients: detection of mutated TMPRSS2 form in a case of aggressive disease. *International journal of cancer* **94**, 705-710

111. Kim, T. S., Heinlein, C., Hackman, R. C., and Nelson, P. S. (2006) Phenotypic analysis of mice lacking the Tmprss2-encoded protease. *Molecular and cellular biology* **26**, 965-975

112. Baron, J., Tarnow, C., Mayoli-Nussle, D., Schilling, E., Meyer, D., Hammami, M., Schwalm, F., Steinmetzer, T., Guan, Y., Garten, W., Klenk, H. D., and Bottcher-

Friebertshauser, E. (2013) Matriptase, HAT, and TMPRSS2 activate the hemagglutinin of H9N2 influenza A viruses. *Journal of virology* **87**, 1811-1820

113.   Garten, W., Braden, C., Arendt, A., Peitsch, C., Baron, J., Lu, Y., Pawletko, K., Hardes, K., Steinmetzer, T., and Bottcher-Friebertshauser, E. (2015) Influenza virus activating host proteases: Identification, localization and inhibitors as potential therapeutics. *Eur J Cell Biol* **94**, 375-383

114.   Shin, W. J., and Seong, B. L. (2017) Type II transmembrane serine proteases as potential target for anti-influenza drug discovery. *Expert opinion on drug discovery* **12**, 1139-1152

115.   Lambertz, R. L. O., Gerhauser, I., Nehlmeier, I., Leist, S. R., Kollmus, H., Pohlmann, S., and Schughart, K. (2019) Tmprss2 knock-out mice are resistant to H10 influenza A virus pathogenesis. *The Journal of general virology*

116.   Wilson, S., Greer, B., Hooper, J., Zijlstra, A., Walker, B., Quigley, J., and Hawthorne, S. (2005) The membrane-anchored serine protease, TMPRSS2, activates PAR-2 in prostate cancer cells. *The Biochemical journal* **388**, 967-972

117.   Lucas, J. M., Heinlein, C., Kim, T., Hernandez, S. A., Malik, M. S., True, L. D., Morrissey, C., Corey, E., Montgomery, B., Mostaghel, E., Clegg, N., Coleman, I., Brown, C. M., Schneider, E. L., Craik, C., Simon, J. A., Bedalov, A., and Nelson, P. S. (2014) The androgen-regulated protease TMPRSS2 activates a proteolytic cascade involving components of the tumor microenvironment and promotes prostate cancer metastasis. *Cancer discovery* **4**, 1310-1325

118.   Ko, C. J., Huang, C. C., Lin, H. Y., Juan, C. P., Lan, S. W., Shyu, H. Y., Wu, S. R., Hsiao, P. W., Huang, H. P., Shun, C. T., and Lee, M. S. (2015) Androgen-Induced TMPRSS2 Activates Matriptase and Promotes Extracellular Matrix Degradation, Prostate Cancer Cell Invasion, Tumor Growth, and Metastasis. *Cancer research* **75**, 2949-2960

119. Underwood, L. J., Shigemasa, K., Tanimoto, H., Beard, J. B., Schneider, E. N., Wang, Y., Parmley, T. H., and O'Brien, T. J. (2000) Ovarian tumor cells express a novel multi-domain cell surface serine protease. *Biochimica et biophysica acta* **1502**, 337-350

120. Scott, H. S., Kudoh, J., Wattenhofer, M., Shibuya, K., Berry, A., Chrast, R., Guipponi, M., Wang, J., Kawasaki, K., Asakawa, S., Minoshima, S., Younus, F., Mehdi, S. Q., Radhakrishna, U., Papasavvas, M. P., Gehrig, C., Rossier, C., Korostishevsky, M., Gal, A., Shimizu, N., Bonne-Tamir, B., and Antonarakis, S. E. (2001) Insertion of beta-satellite repeats identifies a transmembrane protease causing both congenital and childhood onset autosomal recessive deafness. *Nature genetics* **27**, 59-63

121. Fasquelle, L., Scott, H. S., Lenoir, M., Wang, J., Rebillard, G., Gaboyard, S., Venteo, S., Francois, F., Mausset-Bonnefont, A. L., Antonarakis, S. E., Neidhart, E., Chabbert, C., Puel, J. L., Guipponi, M., and Delprat, B. (2011) Tmprss3, a transmembrane serine protease deficient in human DFNB8/10 deafness, is critical for cochlear hair cell survival at the onset of hearing. *The Journal of biological chemistry* **286**, 17383-17397

122. Wallrapp, C., Hahnel, S., Muller-Pillasch, F., Burghardt, B., Iwamura, T., Ruthenburger, M., Lerch, M. M., Adler, G., and Gress, T. M. (2000) A novel transmembrane serine protease (TMPRSS3) overexpressed in pancreatic cancer. *Cancer research* **60**, 2602-2606

123. Vuagniaux, G., Vallet, V., Jaeger, N. F., Hummler, E., and Rossier, B. C. (2002) Synergistic activation of ENaC by three membrane-bound channel-activating serine proteases (mCAP1, mCAP2, and mCAP3) and serum- and glucocorticoid-regulated kinase (Sgk1) in Xenopus Oocytes. *The Journal of general physiology* **120**, 191-201

124. Garcia-Caballero, A., Dang, Y., He, H., and Stutts, M. J. (2008) ENaC proteolytic regulation by channel-activating protease 2. *The Journal of general physiology* **132**, 521-535

125. Keppner, A., Andreasen, D., Merillat, A. M., Bapst, J., Ansermet, C., Wang, Q., Maillard, M., Malsure, S., Nobile, A., and Hummler, E. (2015) Epithelial Sodium Channel-Mediated Sodium Transport Is Not Dependent on the Membrane-Bound Serine Protease CAP2/Tmprss4. *PloS one* **10**, e0135224

126. Kuhn, N., Bergmann, S., Kosterke, N., Lambertz, R. L. O., Keppner, A., van den Brand, J. M. A., Pohlmann, S., Weiss, S., Hummler, E., Hatesuer, B., and Schughart, K. (2016) The Proteolytic Activation of (H3N2) Influenza A Virus Hemagglutinin Is Facilitated by Different Type II Transmembrane Serine Proteases. *Journal of virology* **90**, 4298-4307

127. Kim, D. R., Sharmin, S., Inoue, M., and Kido, H. (2001) Cloning and expression of novel mosaic serine proteases with and without a transmembrane domain from human lung. *Biochimica et biophysica acta* **1518**, 204-209

128. Kido, H., and Okumura, Y. (2008) MSPL/TMPRSS13. *Front Biosci* **13**, 754-758

129. Madsen, D. H., Szabo, R., Molinolo, A. A., and Bugge, T. H. (2014) TMPRSS13 deficiency impairs stratum corneum formation and epidermal barrier acquisition. *Biochem J* **461**, 487-495

130. Hashimoto, T., Kato, M., Shimomura, T., and Kitamura, N. (2010) TMPRSS13, a type II transmembrane serine protease, is inhibited by hepatocyte growth factor activator inhibitor type 1 and activates pro-hepatocyte growth factor. *Febs j* **277**, 4888-4900

131. Faller, N., Gautschi, I., and Schild, L. (2014) Functional analysis of a missense mutation in the serine protease inhibitor SPINT2 associated with congenital sodium diarrhea. *PLoS One* **9**, e94267

132. Murray, A. S., Hyland, T. E., Sala-Hamrick, K. E., Mackinder, J. R., Martin, C. E., Tanabe, L. M., Varela, F. A., and List, K. (2020) The cell-surface anchored serine protease TMPRSS13 promotes breast cancer progression and resistance to chemotherapy. *Oncogene* **39**, 6421-6436

133. Okumura, Y., Takahashi, E., Yano, M., Ohuchi, M., Daidoji, T., Nakaya, T., Bottcher, E., Garten, W., Klenk, H. D., and Kido, H. (2010) Novel type II transmembrane serine proteases, MSPL and TMPRSS13, Proteolytically activate membrane fusion activity of the hemagglutinin of highly pathogenic avian influenza viruses and induce their multicycle replication. *J Virol* **84**, 5089-5096

134. Kishimoto, M., Uemura, K., Sanaki, T., Sato, A., Hall, W. W., Kariwa, H., Orba, Y., Sawa, H., and Sasaki, M. (2021) TMPRSS11D and TMPRSS13 Activate the SARS-CoV-2 Spike Protein. *Viruses* **13**

135. Hoffmann, M., Hofmann-Winkler, H., Smith, J. C., Krüger, N., Arora, P., Sørensen, L. K., Søgaard, O. S., Hasselstrøm, J. B., Winkler, M., Hempel, T., Raich, L., Olsson, S., Danov, O., Jonigk, D., Yamazoe, T., Yamatsuta, K., Mizuno, H., Ludwig, S., Noé, F., Kjolby, M., Braun, A., Sheltzer, J. M., and Pöhlmann, S. (2021) Camostat mesylate inhibits SARS-CoV-2 activation by TMPRSS2-related proteases and its metabolite GBPA exerts antiviral activity. *EBioMedicine* **65**, 103255

136. Harbig, A., Mernberger, M., Bittel, L., Pleschka, S., Schughart, K., Steinmetzer, T., Stiewe, T., Nist, A., and Böttcher-Friebertshäuser, E. (2020) Transcriptome profiling and protease inhibition experiments identify proteases that activate H3N2 influenza A and influenza B viruses in murine airway. *J Biol Chem*

137. Laporte, M., Raeymaekers, V., Van Berwaer, R., Vandeput, J., Marchand-Casas, I., Thibaut, H. J., Van Looveren, D., Martens, K., Hoffmann, M., Maes, P., Pöhlmann, S., Naesens, L., and Stevaert, A. (2021) The SARS-CoV-2 and other human coronavirus spike proteins are fine-tuned towards temperature and proteases of the human airways. *PLoS Pathog* **17**, e1009500

138. Yamaoka, K., Masuda, K., Ogawa, H., Takagi, K., Umemoto, N., and Yasuoka, S. (1998) Cloning and characterization of the cDNA for human airway trypsin-like protease. *The Journal of biological chemistry* **273**, 11895-11901

139. Yasuoka, S., Ohnishi, T., Kawano, S., Tsuchihashi, S., Ogawara, M., Masuda, K., Yamaoka, K., Takahashi, M., and Sano, T. (1997) Purification, characterization, and localization of a novel trypsin-like protease found in the human airway. *American journal of respiratory cell and molecular biology* **16**, 300-308

140. Sales, K. U., Hobson, J. P., Wagenaar-Miller, R., Szabo, R., Rasmussen, A. L., Bey, A., Shah, M. F., Molinolo, A. A., and Bugge, T. H. (2011) Expression and genetic loss of function analysis of the HAT/DESC cluster proteases TMPRSS11A and HAT. *PloS one* **6**, e23261

141. Duhaime, M. J., Page, K. O., Varela, F. A., Murray, A. S., Silverman, M. E., Zoratti, G. L., and List, K. (2016) Cell Surface Human Airway Trypsin-Like Protease Is Lost During Squamous Cell Carcinogenesis. *J Cell Physiol* **231**, 1476-1483

142. Chokki, M., Yamamura, S., Eguchi, H., Masegi, T., Horiuchi, H., Tanabe, H., Kamimura, T., and Yasuoka, S. (2004) Human airway trypsin-like protease increases mucin gene expression in airway epithelial cells. *American journal of respiratory cell and molecular biology* **30**, 470-478

143. Liu, C., Li, Q., Zhou, X., Kolosov, V. P., and Perelman, J. M. (2013) Human airway trypsin-like protease induces mucin5AC hypersecretion via a protease-activated receptor 2-mediated pathway in human airway epithelial cells. *Archives of biochemistry and biophysics* **535**, 234-240

144. Iwakiri, K., Ghazizadeh, M., Jin, E., Fujiwara, M., Takemura, T., Takezaki, S., Kawana, S., Yasuoka, S., and Kawanami, O. (2004) Human airway trypsin-like protease induces PAR-2-mediated IL-8 release in psoriasis vulgaris. *The Journal of investigative dermatology* **122**, 937-944

145. Chokki, M., Eguchi, H., Hamamura, I., Mitsuhashi, H., and Kamimura, T. (2005) Human airway trypsin-like protease induces amphiregulin release through a mechanism involving

protease-activated receptor-2-mediated ERK activation and TNF alpha-converting enzyme activity in airway epithelial cells. *The FEBS journal* **272**, 6387-6399

146. Beaufort, N., Leduc, D., Eguchi, H., Mengele, K., Hellmann, D., Masegi, T., Kamimura, T., Yasuoka, S., Fend, F., Chignard, M., and Pidard, D. (2007) The human airway trypsin-like protease modulates the urokinase receptor (uPAR, CD87) structure and functions. *American journal of physiology. Lung cellular and molecular physiology* **292**, L1263-1272

147. Zhang, Z., Hu, Y., Yan, R., Dong, L., Jiang, Y., Zhou, Z., Liu, M., Zhou, T., Dong, N., and Wu, Q. (2017) The Transmembrane Serine Protease HAT-like 4 Is Important for Epidermal Barrier Function to Prevent Body Fluid Loss. *Scientific reports* **7**, 45262

148. Miller, G. S., Zoratti, G. L., Murray, A. S., Bergum, C., Tanabe, L. M., and List, K. (2014) HATL5: a cell surface serine protease differentially expressed in epithelial cancers. *PloS one* **9**, e87675

149. Lang, J. C., and Schuller, D. E. (2001) Differential expression of a novel serine protease homologue in squamous cell carcinoma of the head and neck. *British journal of cancer* **84**, 237-243

150. Zmora, P., Blazejewska, P., Moldenhauer, A. S., Welsch, K., Nehlmeier, I., Wu, Q., Schneider, H., Pohlmann, S., and Bertram, S. (2014) DESC1 and MSPL activate influenza A viruses and emerging coronaviruses for host cell entry. *Journal of virology* **88**, 12087-12097

151. Kawaguchi, T., Qin, L., Shimomura, T., Kondo, J., Matsumoto, K., Denda, K., and Kitamura, N. (1997) Purification and cloning of hepatocyte growth factor activator inhibitor type 2, a Kunitz-type serine protease inhibitor. *The Journal of biological chemistry* **272**, 27558-27564

152. Shimomura, T., Denda, K., Kitamura, A., Kawaguchi, T., Kito, M., Kondo, J., Kagaya, S., Qin, L., Takata, H., Miyazawa, K., and Kitamura, N. (1997) Hepatocyte growth factor

activator inhibitor, a novel Kunitz-type serine protease inhibitor. *The Journal of biological chemistry* **272**, 6370-6376

153. Kataoka, H., Kawaguchi, M., Fukushima, T., and Shimomura, T. (2018) Hepatocyte growth factor activator inhibitors (HAI-1 and HAI-2): Emerging key players in epithelial integrity and cancer. *Pathology international* **68**, 145-158

154. Tseng, I. C., Chou, F. P., Su, S. F., Oberst, M., Madayiputhiya, N., Lee, M. S., Wang, J. K., Sloane, D. E., Johnson, M., and Lin, C. Y. (2008) Purification from human milk of matriptase complexes with secreted serpins: mechanism for inhibition of matriptase other than HAI-1. *American journal of physiology. Cell physiology* **295**, C423-431

155. Lin, C. Y., Anders, J., Johnson, M., and Dickson, R. B. (1999) Purification and characterization of a complex containing matriptase and a Kunitz-type serine protease inhibitor from human milk. *The Journal of biological chemistry* **274**, 18237-18242

156. Oberst, M., Anders, J., Xie, B., Singh, B., Ossandon, M., Johnson, M., Dickson, R. B., and Lin, C. Y. (2001) Matriptase and HAI-1 are expressed by normal and malignant epithelial cells in vitro and in vivo. *The American journal of pathology* **158**, 1301-1311

157. Oberst, M. D., Chen, L. Y., Kiyomiya, K., Williams, C. A., Lee, M. S., Johnson, M. D., Dickson, R. B., and Lin, C. Y. (2005) HAI-1 regulates activation and expression of matriptase, a membrane-bound serine protease. *American journal of physiology. Cell physiology* **289**, C462-470

158. Szabo, R., Hobson, J. P., Christoph, K., Kosa, P., List, K., and Bugge, T. H. (2009) Regulation of cell surface protease matriptase by HAI2 is essential for placental development, neural tube closure and embryonic survival in mice. *Development (Cambridge, England)* **136**, 2653-2663

159. Szabo, R., Molinolo, A., List, K., and Bugge, T. H. (2007) Matriptase inhibition by hepatocyte growth factor activator inhibitor-1 is essential for placental development. *Oncogene* **26**, 1546-1556

160. Fan, B., Brennan, J., Grant, D., Peale, F., Rangell, L., and Kirchhofer, D. (2007) Hepatocyte growth factor activator inhibitor-1 (HAI-1) is essential for the integrity of basement membranes in the developing placental labyrinth. *Dev Biol* **303**, 222-230

161. Tanaka, H., Nagaike, K., Takeda, N., Itoh, H., Kohama, K., Fukushima, T., Miyata, S., Uchiyama, S., Uchinokura, S., Shimomura, T., Miyazawa, K., Kitamura, N., Yamada, G., and Kataoka, H. (2005) Hepatocyte growth factor activator inhibitor type 1 (HAI-1) is required for branching morphogenesis in the chorioallantoic placenta. *Molecular and cellular biology* **25**, 5687-5698

162. Tervonen, T. A., Belitškin, D., Pant, S. M., Englund, J. I., Marques, E., Ala-Hongisto, H., Nevalaita, L., Sihto, H., Heikkilä, P., Leidenius, M., Hewitson, K., Ramachandra, M., Moilanen, A., Joensuu, H., Kovanen, P. E., Poso, A., and Klefström, J. (2016) Deregulated hepsin protease activity confers oncogenicity by concomitantly augmenting HGF/MET signalling and disrupting epithelial cohesion. *Oncogene* **35**, 1832-1846

163. Beckmann, A. M., Maurer, E., Lulsdorff, V., Wilms, A., Furtmann, N., Bajorath, J., Gutschow, M., and Stirnberg, M. (2016) En Route to New Therapeutic Options for Iron Overload Diseases: Matriptase-2 as a Target for Kunitz-Type Inhibitors. *Chembiochem : a European journal of chemical biology* **17**, 595-604

164. Vogel, L. K., Saebo, M., Skjelbred, C. F., Abell, K., Pedersen, E. D., Vogel, U., and Kure, E. H. (2006) The ratio of Matriptase/HAI-1 mRNA is higher in colorectal cancer adenomas and carcinomas than corresponding tissue from control individuals. *BMC cancer* **6**, 176

165. Tsai, W. C., Sheu, L. F., Chao, Y. C., Chen, A., Chiang, H., and Jin, J. S. (2007) Decreased matriptase/HAI-1 ratio in advanced colorectal adenocarcinoma of Chinese patients. *The Chinese journal of physiology* **50**, 225-231

166. Kosa, P., Szabo, R., Molinolo, A. A., and Bugge, T. H. (2012) Suppression of Tumorigenicity-14, encoding matriptase, is a critical suppressor of colitis and colitis-associated colon carcinogenesis. *Oncogene* **31**, 3679-3695

167. Huang, A., Zhou, H., Zhao, H., Quan, Y., Feng, B., and Zheng, M. (2014) TMPRSS4 correlates with colorectal cancer pathological stage and regulates cell proliferation and self-renewal ability. *Cancer Biol Ther* **15**, 297-304

168. Kim, S., Kang, H. Y., Nam, E. H., Choi, M. S., Zhao, X. F., Hong, C. S., Lee, J. W., Lee, J. H., and Park, Y. K. (2010) TMPRSS4 induces invasion and epithelial-mesenchymal transition through upregulation of integrin alpha5 and its signaling pathways. *Carcinogenesis* **31**, 597-606

169. Varela, F. A., Foust, V. L., Hyland, T. E., Sala-Hamrick, K. E., Mackinder, J. R., Martin, C. E., Murray, A. S., Todi, S. V., and List, K. (2020) TMPRSS13 promotes cell survival, invasion, and resistance to drug-induced apoptosis in colorectal cancer. *Sci Rep* **10**, 13896

170. Jin, J. S., Cheng, T. F., Tsai, W. C., Sheu, L. F., Chiang, H., and Yu, C. P. (2007) Expression of the serine protease, matriptase, in breast ductal carcinoma of Chinese women: correlation with clinicopathological parameters. *Histology and histopathology* **22**, 305-309

171. Kang, J. Y., Dolled-Filhart, M., Ocal, I. T., Singh, B., Lin, C. Y., Dickson, R. B., Rimm, D. L., and Camp, R. L. (2003) Tissue microarray analysis of hepatocyte growth factor/Met pathway components reveals a role for Met, matriptase, and hepatocyte growth factor activator inhibitor 1 in the progression of node-negative breast cancer. *Cancer research* **63**, 1101-1105

172. Siddiqui, S. F., Pawelek, J., Handerson, T., Lin, C. Y., Dickson, R. B., Rimm, D. L., and Camp, R. L. (2005) Coexpression of beta1,6-N-acetylglucosaminyltransferase V glycoprotein substrates defines aggressive breast cancers with poor outcome. *Cancer epidemiology, biomarkers & prevention : a publication of the American Association for Cancer Research, cosponsored by the American Society of Preventive Oncology* **14**, 2517-2523

173.   Parr, C., Watkins, G., Mansel, R. E., and Jiang, W. G. (2004) The hepatocyte growth factor regulatory factors in human breast cancer. *Clinical cancer research : an official journal of the American Association for Cancer Research* **10**, 202-211

174.   Hurst, N. J., Jr., Najy, A. J., Ustach, C. V., Movilla, L., and Kim, H. R. (2012) Platelet-derived growth factor-C (PDGF-C) activation by serine proteases: implications for breast cancer progression. *The Biochemical journal* **441**, 909-918

175.   Parr, C., Sanders, A. J., Davies, G., Martin, T., Lane, J., Mason, M. D., Mansel, R. E., and Jiang, W. G. (2007) Matriptase-2 inhibits breast tumor growth and invasion and correlates with favorable prognosis for breast cancer patients. *Clinical cancer research : an official journal of the American Association for Cancer Research* **13**, 3568-3576

176.   Xing, P., Li, J. G., Jin, F., Zhao, T. T., Liu, Q., Dong, H. T., and Wei, X. L. (2011) Clinical and biological significance of hepsin overexpression in breast cancer. *J Investig Med* **59**, 803-810

177.   Pant, S. M., Belitskin, D., Ala-Hongisto, H., Klefstrom, J., and Tervonen, T. A. (2018) Analyzing the Type II Transmembrane Serine Protease Hepsin-Dependent Basement Membrane Remodeling in 3D Cell Culture. *Methods in molecular biology (Clifton, N.J.)* **1731**, 169-178

178.   Damalanka, V. C., Han, Z., Karmakar, P., O'Donoghue, A. J., La Greca, F., Kim, T., Pant, S. M., Helander, J., Klefstrom, J., Craik, C. S., and Janetka, J. W. (2019) Discovery of Selective Matriptase and Hepsin Serine Protease Inhibitors: Useful Chemical Tools for Cancer Cell Biology. *J Med Chem* **62**, 480-490

179.   Rui, X., Li, Y., Jin, F., and Li, F. (2015) TMPRSS3 is a novel poor prognostic factor for breast cancer. *Int J Clin Exp Pathol* **8**, 5435-5442

180.   Luo, P., Lu, G., Fan, L. L., Zhong, X., Yang, H., Xie, R., Lv, Z., Lv, Q. Z., Fu, D., Yang, L. X., and Ma, Y. (2017) Dysregulation of TMPRSS3 and TNFRSF11B correlates with

tumorigenesis and poor prognosis in patients with breast cancer. *Oncol Rep* **37**, 2057-2062

181. Pelkonen, M., Luostari, K., Tengström, M., Ahonen, H., Berdel, B., Kataja, V., Soini, Y., Kosma, V.-M., and Mannermaa, A. (2015) Low expression levels of hepsin and TMPRSS3 are associated with poor breast cancer survival. *BMC cancer* **15**, 431-431

182. Martin, C. E., Murray, A. S., Sala-Hamrick, K. E., Mackinder, J. R., Harrison, E. C., Lundgren, J. G., Varela, F. A., and List, K. (2021) Posttranslational modifications of serine protease TMPRSS13 regulate zymogen activation, proteolytic activity, and cell surface localization. *J Biol Chem* **297**, 101227

183. Antalis, T. M., Buzza, M. S., Hodge, K. M., Hooper, J. D., and Netzel-Arnett, S. (2010) The cutting edge: membrane-anchored serine protease activities in the pericellular microenvironment. *Biochem J* **428**, 325-346

184. Zoratti, G. L., Tanabe, L. M., Varela, F. A., Murray, A. S., Bergum, C., Colombo, É., Lang, J. E., Molinolo, A. A., Leduc, R., Marsault, E., Boerner, J., and List, K. (2015) Targeting matriptase in breast cancer abrogates tumour progression via impairment of stromal-epithelial growth factor signalling. *Nat Commun* **6**, 6776

185. List, K., Szabo, R., Molinolo, A., Sriuranpong, V., Redeye, V., Murdock, T., Burke, B., Nielsen, B. S., Gutkind, J. S., and Bugge, T. H. (2005) Deregulated matriptase causes ras-independent multistage carcinogenesis and promotes ras-mediated malignant transformation. *Genes Dev* **19**, 1934-1950

186. Sales, K. U., Friis, S., Abusleme, L., Moutsopoulos, N. M., and Bugge, T. H. (2015) Matriptase promotes inflammatory cell accumulation and progression of established epidermal tumors. *Oncogene* **34**, 4664-4672

187. Kanemaru, A., Yamamoto, K., Kawaguchi, M., Fukushima, T., Lin, C. Y., Johnson, M. D., Camerer, E., and Kataoka, H. (2017) Deregulated matriptase activity in oral squamous

cell carcinoma promotes the infiltration of cancer-associated fibroblasts by paracrine activation of protease-activated receptor 2. *Int J Cancer* **140**, 130-141

188. Sedghizadeh, P. P., Mallery, S. R., Thompson, S. J., Kresty, L., Beck, F. M., Parkinson, E. K., Biancamano, J., and Lang, J. C. (2006) Expression of the serine protease DESC1 correlates directly with normal keratinocyte differentiation and inversely with head and neck squamous cell carcinoma progression. *Head Neck* **28**, 432-440

189. Vogel, L. K., Saebø, M., Skjelbred, C. F., Abell, K., Pedersen, E. D., Vogel, U., and Kure, E. H. (2006) The ratio of Matriptase/HAI-1 mRNA is higher in colorectal cancer adenomas and carcinomas than corresponding tissue from control individuals. *BMC cancer* **6**, 176

190. Guerrero, K., Wang, Z., Bachvarova, M., Gregoire, J., Renaud, M.-C., Plante, M., and Bachvarov, D. (2012) A novel genome-based approach correlates TMPRSS3 overexpression in ovarian cancer with DNA hypomethylation. *Gynecologic Oncology* **125**, 720-726

191. Kido, H., Okumura, Y., Takahashi, E., Pan, H. Y., Wang, S., Chida, J., Le, T. Q., and Yano, M. (2008) Host envelope glycoprotein processing proteases are indispensable for entry into human cells by seasonal and highly pathogenic avian influenza viruses. *J Mol Genet Med* **3**, 167-175

192. Aebi, M. (2013) N-linked protein glycosylation in the ER. *Biochim Biophys Acta* **1833**, 2430-2437

193. Schoberer, J., Shin, Y. J., Vavra, U., Veit, C., and Strasser, R. (2018) Analysis of Protein Glycosylation in the ER. *Methods Mol Biol* **1691**, 205-222

194. Xu, C., and Ng, D. T. (2015) Glycosylation-directed quality control of protein folding. *Nat Rev Mol Cell Biol* **16**, 742-752

195. Goettig, P. (2016) Effects of Glycosylation on the Enzymatic Activity and Mechanisms of Proteases. *Int J Mol Sci* **17**

196. Zhang, M., Zhao, J., Tang, W., Wang, Y., Peng, P., Li, L., Song, S., Wu, H., Li, C., Yang, C., Wang, X., Zhang, C., and Gu, J. (2016) High Hepsin expression predicts poor prognosis in Gastric Cancer. *Sci Rep* **6**, 36902

197. Sun, S., Wang, L., Zhang, S., Zhang, C., Chen, Y., Wu, Q., and Dong, N. (2020) N-glycan in the scavenger receptor cysteine-rich domain of hepsin promotes intracellular trafficking and cell surface expression. *Int J Biol Macromol* **161**, 818-827

198. Zheng, X., Lu, D., and Sadler, J. E. (1999) Apical sorting of bovine enteropeptidase does not involve detergent-resistant association with sphingolipid-cholesterol rafts. *J Biol Chem* **274**, 1596-1605

199. Wang, H., Li, S., Wang, J., Chen, S., Sun, X. L., and Wu, Q. (2018) N-glycosylation in the protease domain of trypsin-like serine proteases mediates calnexin-assisted protein folding. *Elife* **7**

200. Miyake, Y., Tsuzuki, S., Mochida, S., Fushiki, T., and Inouye, K. (2010) The role of asparagine-linked glycosylation site on the catalytic domain of matriptase in its zymogen activation. *Biochim Biophys Acta* **1804**, 156-165

201. Wang, H., Zhou, T., Peng, J., Xu, P., Dong, N., Chen, S., and Wu, Q. (2015) Distinct roles of N-glycosylation at different sites of corin in cell membrane targeting and ectodomain shedding. *J Biol Chem* **290**, 1654-1663

202. Liao, X., Wang, W., Chen, S., and Wu, Q. (2007) Role of glycosylation in corin zymogen activation. *The Journal of biological chemistry* **282**, 27728-27735

203. Zhang, C., Zhang, Y., Zhang, S., Wang, Z., Sun, S., Liu, M., Chen, Y., Dong, N., and Wu, Q. (2020) Intracellular autoactivation of TMPRSS11A, an airway epithelial transmembrane serine protease. *J Biol Chem* **295**, 12686-12696

204. Gupta, R., and Brunak, S. (2002) Prediction of glycosylation across the human proteome and the correlation to protein function. *Pac Symp Biocomput*, 310-322

205. Maley, F., Trimble, R. B., Tarentino, A. L., and Plummer, T. H. (1989) Characterization of glycoproteins and their associated oligosaccharides through the use of endoglycosidases. *Anal Biochem* **180**, 195-204

206. Tarentino, A. L., Gómez, C. M., and Plummer, T. H. (1985) Deglycosylation of asparagine-linked glycans by peptide:N-glycosidase F. *Biochemistry* **24**, 4665-4671

207. Elder, J. H., and Alexander, S. (1982) endo-beta-N-acetylglucosaminidase F: endoglycosidase from Flavobacterium meningosepticum that cleaves both high-mannose and complex glycoproteins. *Proc Natl Acad Sci U S A* **79**, 4540-4544

208. Wu, J., Chen, S., Liu, H., Zhang, Z., Ni, Z., Chen, J., Yang, Z., Nie, Y., and Fan, D. (2018) Tunicamycin specifically aggravates ER stress and overcomes chemoresistance in multidrug-resistant gastric cancer cells by inhibiting N-glycosylation. *J Exp Clin Cancer Res* **37**, 272

209. Hakulinen, J. K., Hering, J., Brändén, G., Chen, H., Snijder, A., Ek, M., and Johansson, P. (2017) MraY-antibiotic complex reveals details of tunicamycin mode of action. *Nat Chem Biol* **13**, 265-267

210. Friis, S., Uzzun Sales, K., Godiksen, S., Peters, D. E., Lin, C. Y., Vogel, L. K., and Bugge, T. H. (2013) A matriptase-prostasin reciprocal zymogen activation complex with unique features: prostasin as a non-enzymatic co-factor for matriptase activation. *The Journal of biological chemistry* **288**, 19028-19039

211. Chen, L. M., Zhang, X., and Chai, K. X. (2004) Regulation of prostasin expression and function in the prostate. *Prostate* **59**, 1-12

212. White, D. A., and Speake, B. K. (1980) The effect of cycloheximide on the glycosylation of lactating-rabbit mammary glycoproteins. *Biochem J* **192**, 297-301

213. Cherepanova, N., Shrimal, S., and Gilmore, R. (2016) N-linked glycosylation and homeostasis of the endoplasmic reticulum. *Curr Opin Cell Biol* **41**, 57-65

214. Lee, H. S., Qi, Y., and Im, W. (2015) Effects of N-glycosylation on protein conformation and dynamics: Protein Data Bank analysis and molecular dynamics simulation study. *Sci Rep* **5**, 8926

215. Bieberich, E. (2014) Synthesis, Processing, and Function of N-glycans in N-glycoproteins. *Adv Neurobiol* **9**, 47-70

216. Yan, W., Sheng, N., Seto, M., Morser, J., and Wu, Q. (1999) Corin, a mosaic transmembrane serine protease encoded by a novel cDNA from human heart. *J Biol Chem* **274**, 14926-14935

217. Chen, S., Cao, P., Dong, N., Peng, J., Zhang, C., Wang, H., Zhou, T., Yang, J., Zhang, Y., Martelli, E. E., Naga Prasad, S. V., Miller, R. E., Malfait, A. M., Zhou, Y., and Wu, Q. (2015) PCSK6-mediated corin activation is essential for normal blood pressure. *Nat Med* **21**, 1048-1053

218. Chen, S., Wang, H., Li, H., Zhang, Y., and Wu, Q. (2018) Functional analysis of corin protein domains required for PCSK6-mediated activation. *Int J Biochem Cell Biol* **94**, 31-39

219. Gladysheva, I. P., Robinson, B. R., Houng, A. K., Kováts, T., and King, S. M. (2008) Corin is co-expressed with pro-ANP and localized on the cardiomyocyte surface in both zymogen and catalytically active forms. *J Mol Cell Cardiol* **44**, 131-142

220. Skovbjerg, S., Holt-Danborg, L., Nonboe, A. W., Hong, Z., Frost, Á., Schar, C. R., Thomas, C. C., Vitved, L., Jensen, J. K., and Vogel, L. K. (2020) Inhibition of an active zymogen protease: the zymogen form of matriptase is regulated by HAI-1 and HAI-2. *Biochem J* **477**, 1779-1794

221. Kalinska, M., Meyer-Hoffert, U., Kantyka, T., and Potempa, J. (2016) Kallikreins - The melting pot of activity and function. *Biochimie* **122**, 270-282

222. Guo, S., Skala, W., Magdolen, V., Brandstetter, H., and Goettig, P. (2014) Sweetened kallikrein-related peptidases (KLKs): glycan trees as potential regulators of activation and activity. *Biol Chem* **395**, 959-976

223. Ohyama, C., Hosono, M., Nitta, K., Oh-eda, M., Yoshikawa, K., Habuchi, T., Arai, Y., and Fukuda, M. (2004) Carbohydrate structure and differential binding of prostate specific antigen to Maackia amurensis lectin between prostate cancer and benign prostate hypertrophy. *Glycobiology* **14**, 671-679

224. Guo, S., Skala, W., Magdolen, V., Briza, P., Biniossek, M. L., Schilling, O., Kellermann, J., Brandstetter, H., and Goettig, P. (2016) A Single Glycan at the 99-Loop of Human Kallikrein-related Peptidase 2 Regulates Activation and Enzymatic Activity. *J Biol Chem* **291**, 593-604

225. Ihara, S., Miyoshi, E., Ko, J. H., Murata, K., Nakahara, S., Honke, K., Dickson, R. B., Lin, C. Y., and Taniguchi, N. (2002) Prometastatic effect of N-acetylglucosaminyltransferase V is due to modification and stabilization of active matriptase by adding beta 1-6 GlcNAc branching. *J Biol Chem* **277**, 16960-16967

226. Ito, Y., Akinaga, A., Yamanaka, K., Nakagawa, T., Kondo, A., Dickson, R. B., Lin, C. Y., Miyauchi, A., Taniguchi, N., and Miyoshi, E. (2006) Co-expression of matriptase and N-acetylglucosaminyltransferase V in thyroid cancer tissues--its possible role in prolonged stability in vivo by aberrant glycosylation. *Glycobiology* **16**, 368-374

227. Friis, S., Sales, K. U., Schafer, J. M., Vogel, L. K., Kataoka, H., and Bugge, T. H. (2014) The protease inhibitor HAI-2, but not HAI-1, regulates matriptase activation and shedding through prostasin. *The Journal of biological chemistry* **289**, 22319-22332

228. Larsen, B. R., Steffensen, S. D., Nielsen, N. V., Friis, S., Godiksen, S., Bornholdt, J., Soendergaard, C., Nonboe, A. W., Andersen, M. N., Poulsen, S. S., Szabo, R., Bugge, T. H., Lin, C. Y., Skovbjerg, H., Jensen, J. K., and Vogel, L. K. (2013) Hepatocyte growth factor activator inhibitor-2 prevents shedding of matriptase. *Exp Cell Res* **319**, 918-929

229. Schneider, C. A., Rasband, W. S., and Eliceiri, K. W. (2012) NIH Image to ImageJ: 25 years of image analysis. *Nat Methods* **9**, 671-675

230. Szabo, R., and Bugge, T. H. (2020) Membrane-anchored serine proteases as regulators of epithelial function. *Biochem Soc Trans* **48**, 517-528

231. Okumura, Y., Takahashi, E., Yano, M., Ohuchi, M., Daidoji, T., Nakaya, T., Böttcher, E., Garten, W., Klenk, H. D., and Kido, H. (2010) Novel type II transmembrane serine proteases, MSPL and TMPRSS13, Proteolytically activate membrane fusion activity of the hemagglutinin of highly pathogenic avian influenza viruses and induce their multicycle replication. *J Virol* **84**, 5089-5096

232. Chen, M., Chen, L. M., Lin, C. Y., and Chai, K. X. (2010) Hepsin activates prostasin and cleaves the extracellular domain of the epidermal growth factor receptor. *Mol Cell Biochem* **337**, 259-266

233. Friis, S., Tadeo, D., Le-Gall, S. M., Jürgensen, H. J., Sales, K. U., Camerer, E., and Bugge, T. H. (2017) Matriptase zymogen supports epithelial development, homeostasis and regeneration. *BMC Biol* **15**, 46

234. Tseng, C.-C., Jia, B., Barndt, R., Gu, Y., Chen, C.-Y., Tseng, I. C., Su, S.-F., Wang, J.-K., Johnson, M. D., and Lin, C.-Y. (2017) Matriptase shedding is closely coupled with matriptase zymogen activation and requires de novo proteolytic cleavage likely involving its own activity. *PLOS ONE* **12**, e0183507

235. Stirnberg, M., Maurer, E., Horstmeyer, A., Kolp, S., Frank, S., Bald, T., Arenz, K., Janzer, A., Prager, K., Wunderlich, P., Walter, J., and Gütschow, M. (2010) Proteolytic processing of the serine protease matriptase-2: identification of the cleavage sites required for its autocatalytic release from the cell surface. *Biochem J* **430**, 87-95

236. Wang, L., Zhang, C., Sun, S., Chen, Y., Hu, Y., Wang, H., Liu, M., Dong, N., and Wu, Q. (2019) Autoactivation and calpain-1-mediated shedding of hepsin in human hepatoma cells. *Biochem J* **476**, 2355-2369

237. Jiang, J., Wu, S., Wang, W., Chen, S., Peng, J., Zhang, X., and Wu, Q. (2011) Ectodomain shedding and autocleavage of the cardiac membrane protease corin. *J Biol Chem* **286**, 10066-10072

238. Tang, X., Mahajan, S. S., Nguyen, L. T., Beliveau, F., Leduc, R., Simon, J. A., and Vasioukhin, V. (2014) Targeted inhibition of cell-surface serine protease Hepsin blocks prostate cancer bone metastasis. *Oncotarget* **5**, 1352-1362

239. Lanchec, E., Désilets, A., Béliveau, F., Flamier, A., Mahmoud, S., Bernier, G., Gris, D., Leduc, R., and Lavoie, C. (2017) The type II transmembrane serine protease matriptase cleaves the amyloid precursor protein and reduces its processing to β-amyloid peptide. *J Biol Chem* **292**, 20669-20682

240. Bestle, D., Heindl, M. R., Limburg, H., Van Lam van, T., Pilgram, O., Moulton, H., Stein, D. A., Hardes, K., Eickmann, M., Dolnik, O., Rohde, C., Klenk, H. D., Garten, W., Steinmetzer, T., and Böttcher-Friebertshäuser, E. (2020) TMPRSS2 and furin are both essential for proteolytic activation of SARS-CoV-2 in human airway cells. *Life Sci Alliance* **3**

241. Enns, C. A., Jue, S., and Zhang, A. S. (2020) The ectodomain of matriptase-2 plays an important nonproteolytic role in suppressing hepcidin expression in mice. *Blood* **136**, 989-1001

242. Webb, S. L., Sanders, A. J., Mason, M. D., and Jiang, W. G. (2011) Type II transmembrane serine protease (TTSP) deregulation in cancer. *Front Biosci (Landmark Ed)* **16**, 539-552

243. Choi, S. Y., Bertram, S., Glowacka, I., Park, Y. W., and Pöhlmann, S. (2009) Type II transmembrane serine proteases in cancer and viral infections. *Trends Mol Med* **15**, 303-312

244. Mao, P., Wortham, A. M., Enns, C. A., and Zhang, A. S. (2019) The catalytic, stem, and transmembrane portions of matriptase-2 are required for suppressing the expression of the iron-regulatory hormone hepcidin. *J Biol Chem* **294**, 2060-2073

245. Cho, E. G., Kim, M. G., Kim, C., Kim, S. R., Seong, I. S., Chung, C., Schwartz, R. H., and Park, D. (2001) N-terminal processing is essential for release of epithin, a mouse type II membrane serine protease. *J Biol Chem* **276**, 44581-44589

246. Lin, C. Y., Tseng, I. C., Chou, F. P., Su, S. F., Chen, Y. W., Johnson, M. D., and Dickson, R. B. (2008) Zymogen activation, inhibition, and ectodomain shedding of matriptase. *Front Biosci* **13**, 621-635

247. Cho, Y., Kim, S. B., Kim, J., Pham, A. V. Q., Yoon, M. J., Park, J. H., Hwang, K. T., Park, D., Kim, M. G., and Kim, C. (2020) Intramembrane proteolysis of an extracellular serine protease, epithin/PRSS14, enables its intracellular nuclear function. *BMC Biol* **18**, 60

248. Singh, V., Ram, M., Kumar, R., Prasad, R., Roy, B. K., and Singh, K. K. (2017) Phosphorylation: Implications in Cancer. *Protein J* **36**, 1-6

249. BURNETT, G., and KENNEDY, E. P. (1954) The enzymatic phosphorylation of proteins. *J Biol Chem* **211**, 969-980

250. van der Lee, R., Buljan, M., Lang, B., Weatheritt, R. J., Daughdrill, G. W., Dunker, A. K., Fuxreiter, M., Gough, J., Gsponer, J., Jones, D. T., Kim, P. M., Kriwacki, R. W., Oldfield, C. J., Pappu, R. V., Tompa, P., Uversky, V. N., Wright, P. E., and Babu, M. M. (2014) Classification of intrinsically disordered regions and proteins. *Chem Rev* **114**, 6589-6631

251. Iakoucheva, L. M., Radivojac, P., Brown, C. J., O'Connor, T. R., Sikes, J. G., Obradovic, Z., and Dunker, A. K. (2004) The importance of intrinsic disorder for protein phosphorylation. *Nucleic Acids Res* **32**, 1037-1049

252. Koike, R., Amano, M., Kaibuchi, K., and Ota, M. (2020) Protein kinases phosphorylate long disordered regions in intrinsically disordered proteins. *Protein Sci* **29**, 564-571

253. Thorsness, P. E., and Koshland, D. E. (1987) Inactivation of isocitrate dehydrogenase by phosphorylation is mediated by the negative charge of the phosphate. *J Biol Chem* **262**, 10422-10425

254. Amano, M., Hamaguchi, T., Shohag, M. H., Kozawa, K., Kato, K., Zhang, X., Yura, Y., Matsuura, Y., Kataoka, C., Nishioka, T., and Kaibuchi, K. (2015) Kinase-interacting substrate screening is a novel method to identify kinase substrates. *J Cell Biol* **209**, 895-912

255. Carlson, S. M., Chouinard, C. R., Labadorf, A., Lam, C. J., Schmelzle, K., Fraenkel, E., and White, F. M. (2011) Large-scale discovery of ERK2 substrates identifies ERK-mediated transcriptional regulation by ETV3. *Sci Signal* **4**, rs11

256. Cicenas, J., Kalyan, K., Sorokinas, A., Stankunas, E., Levy, J., Meskinyte, I., Stankevicius, V., Kaupinis, A., and Valius, M. (2015) Roscovitine in cancer and other diseases. *Ann Transl Med* **3**, 135

257. Whittaker, S. R., Walton, M. I., Garrett, M. D., and Workman, P. (2004) The Cyclin-dependent kinase inhibitor CYC202 (R-roscovitine) inhibits retinoblastoma protein phosphorylation, causes loss of Cyclin D1, and activates the mitogen-activated protein kinase pathway. *Cancer Res* **64**, 262-272

258. Du, J., Wei, N., Guan, T., Xu, H., An, J., Pritchard, K. A., and Shi, Y. (2009) Inhibition of CDKS by roscovitine suppressed LPS-induced *NO production through inhibiting NFkappaB activation and BH4 biosynthesis in macrophages. *Am J Physiol Cell Physiol* **297**, C742-749

259. Rabhi, N., Desevin, K., Cortez, B. N., Hekman, R., Lin, J. Z., Emili, A., and Farmer, S. R. (2021) The cyclin dependent kinase inhibitor Roscovitine prevents diet-induced metabolic disruption in obese mice. *Sci Rep* **11**, 20365

260. Kourtidis, A., Lu, R., Pence, L. J., and Anastasiadis, P. Z. (2017) A central role for cadherin signaling in cancer. *Exp Cell Res* **358**, 78-85

261. St-Louis, É., Degrandmaison, J., Grastilleur, S., Génier, S., Blais, V., Lavoie, C., Parent, J. L., and Gendron, L. (2017) Involvement of the coatomer protein complex I in the intracellular traffic of the delta opioid receptor. *Mol Cell Neurosci* **79**, 53-63

ABSTRACT

CHARACTERIZING THE POST-TRANSLATIONAL MODIFICATIONS OF THE PRO-ONCOGENIC TYPE II TRANSMEMBRANE SERINE PROTEASE TMPRSS13

by

CARLY ELIZABETH MARTIN

May 2022

Advisor: Dr. Karin List

Major: Cancer Biology

Degree: Doctor of Philosophy

TMPRSS13, a type II transmembrane serine protease discovered at the turn of the century, has recently been shown to be significantly overexpressed in both breast cancer (BCa) and colorectal cancer (CRC), and to mediate chemoresistance in cell lines from both cancer types. Furthermore, loss of TMPRSS13 in a genetic model of mouse mammary carcinoma significantly reduced tumor burden and growth rate, and increased overall tumor-free survival. Its location on the cell surface as well as its low expression in normal breast and colon make TMPRSS13 an attractive candidate as an oncogenic biomarker and therapeutic target in cancer. However, little is currently known about the biochemical characteristics and pro-oncogenic mechanisms of TMPRSS13, which are important to understand in order to develop selective and efficacious inhibitors. TMPRSS13 is post-translationally modified by asparagine (N)-linked glycosylation, autoproteolytic cleavage, and intracellular phosphorylation, all of which are interconnected and play a role in the catalytic activity, zymogen activation and cell surface localization of TMPRSS13. Site-directed mutagenesis of N-glycosylated residues and putative cleavage sites in the extracellular domain of TMPRSS13 has revealed that TMPRSS13 must be glycosylated in its catalytic serine protease (SP) domain and cleaved at arginine (R)-223 – localized in the stem region between the low-density lipoprotein receptor class A domain and the scavenger receptor cysteine rich domain – prior to its autoproteolytic zymogen activation at R320.

Furthermore, abrogation of SP-domain glycosylation or cleavage at R223 precludes phosphorylation of the intracellular domain of TMPRSS13. The latter observation also relates to the intracellular trafficking of TMPRSS13, as highly phosphorylated TMPRSS13 has been observed on the cell surface. Ongoing mass-spectrometry based experiments to discover binding partners of phosphorylated TMPRSS13 will help to reveal the oncogenic signaling pathways in which cell-surface TMPRSS13 plays a role. The overarching goals of our project are to fully understand how the unique biochemical properties of TMPRSS13 contribute to its enzymatic function and to elucidate the pro-oncogenic mechanisms of TMPRSS13.

AUTOBIOGRAPHICAL STATEMENT

CARLY ELIZABETH MARTIN

EDUCATION

Wayne State University School of Medicine, Detroit, MI 2017-2022

Doctor of Philosophy: Cancer Biology

University of Michigan, Ann Arbor, MI 2012-2016

Bachelor of Science: Microbiology

PUBLICATIONS

1. **Martin CE**, Murray AS, Sala-Hamrick KE, Mackinder JR, Harrison EC, Lundgren JG, Varela FA, List K. Posttranslational modifications of serine protease TMPRSS13 regulate zymogen activation, proteolytic activity, and cell surface localization. *J Biol Chem.* 2021 Oct;297(4):101227. doi: 10.1016/j.jbc.2021.101227.
2. Murray AS, Hyland TE, Sala-Hamrick KE, Mackinder JR, **Martin CE**, Tanabe LM, Varela FA, List K. The cell-surface anchored serine protease TMPRSS13 promotes breast cancer progression and resistance to chemotherapy. *Oncogene.* 2020 Oct;39(41):6421-6436. doi: 10.1038/s41388-020-01436-3.
3. Varela FA, Foust VL, Hyland TE, Sala-Hamrick KE, Mackinder JR, **Martin CE**, Murray AS, Todi SV, List K. TMPRSS13 promotes cell survival, invasion, and resistance to drug-induced apoptosis in colorectal cancer. *Sci Rep.* 2020 Aug 17;10(1):13896. doi: 10.1038/s41598-020-70636-4.
4. **Martin CE** and List K. Cell surface-anchored serine proteases in cancer progression and metastasis. *Cancer & Metastasis Reviews.* 2019. doi: 10.1007/s10555-019-09811-7.